National Aerospace University “Kharkiv Aviation Institute”
Ministry of Education and Science of Ukraine

On the rights of the manuscript

HU WENJIE

UDC 621.452.32.03:669.295:621.793.7(043)

DISSERTATION
COLD SPRAYING OF PROTECTIVE AND RESTORATIVE COATING ON PARTS OF AVIATION ENGINEERING MADE OF TITANIUM ALLOYS

Specialty 132 – Materials science

Field of knowledge 13 – Mechanical engineering

Applied for the Doctor of Philosophy degree

The dissertation contains the results of my own research. The use of other authors' ideas, results and texts have references to the relevant source

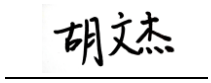
Hu WENJIE

Scientific adviser

Oleksandr SHORINOV, Candidate of Technical Sciences, Associate Professor

Kharkiv – 2024

ABSTRACT

Hu Wenjie. Cold spraying of protective and restorative coatings on parts of aviation engineering made of titanium alloys. – Qualifying scientific work on the rights of the manuscript.

Dissertation submitted for the Doctor of Philosophy degree in the Areas of Knowledge 13 Mechanical Engineering, Specialty 132 Materials Science. – National Aerospace University "Kharkiv Aviation Institute", Kharkiv, 2024.

The dissertation is devoted to the improvement of the technology of cold gas-dynamic spraying of protective and restorative coatings on titanium alloys by establishing the optimal geometry of the spraying nozzles, the laws of influence of gas parameters at the nozzle entrance and powder characteristics on the speed of particles at the moment of impact with the substrate. The object of research is the process of acceleration of powder particles by a supersonic flow in the nozzle channel for cold gas-dynamic spraying and high-speed collision of the particle with the titanium substrate. The subject of the study is the influence of the nozzle geometry, parameters of the cold gas-dynamic spraying process, and powder characteristics on the speed of particles in the flow.

The relevance and necessity of conducting research are determined by the existing problem of extending the life of aviation equipment parts made of titanium alloys. One of the possible ways to maintain the performance of such parts, ensure high operational performance, and increase durability is by developing and improving existing coating methods. The dissertation presents new scientifically based results of theoretical calculations and numerical modeling, which summarize and provide a solution to the most important component of coating application – ensuring the possibility of adhesion of powder particles to the surface with sufficient adhesive strength and further growth of the coating.

The dissertation consists of an abstract, an introduction, four chapters, conclusions and appendices.

The introduction substantiates the relevance and necessity of the chosen direction of research, formulates the goal and task of the research, outlines the scientific novelty and practical significance of the obtained results, and provides information about their approval, publications and the structure of the dissertation work.

The first chapter examines the use of titanium alloys in the aviation and aerospace industries, operational defects, their causes, and possible ways of prevention and elimination. Methods of applying coatings, the place among them of cold gas dynamic spraying, and its advantages and prospects regarding the possibilities of use for obtaining coatings on titanium alloy surfaces are given. Special attention was paid to the analysis of the influence of parameters of cold gas-dynamic spraying on the properties of coatings and the efficiency of the process. An analysis of publications dedicated to the use of technology for spraying wear-resistant coatings on titanium alloys, as well as materials used to restore the worn surfaces of parts from these alloys, was conducted. Based on the results of the analysis, unsolved issues in the field of cold gas-dynamic spraying of coatings on titanium alloys were identified, and ways of solving them and improving the technology were outlined.

In the second chapter, the main equations of gas dynamics are given, which are used to describe the flow in narrowing-expanding nozzles for cold gas dynamic spraying and the calculation of their geometric characteristics. An analysis of the models was performed to find the temperature-velocity characteristics of powder particles in the gas flow in the nozzle channel. The results of the development of a direct supersonic nozzle for spraying are presented, as well as the results of numerical modeling of the influence of the geometric parameters of the nozzle (the diameter of the critical section of the nozzle, its length, the angle of rotation of the axis of the nozzle in the critical section), as well as the material of the powder and the size of the particles on their velocity at the exit from nozzle Using the method of multi-factorial planning of the experiment, the complex influence of gas parameters (pressure and temperature) at the entrance to the nozzle and the diameter of the

powder particles on their velocity at the exit from the nozzle for the selected geometry of the rotary single-channel nozzle was investigated. The regression equation for predicting the speed of particles depending on the studied parameters is obtained, and recommendations for choosing the optimal modes that ensure obtaining the maximum speed of powder particles are given. A rotary nozzle for spraying coatings on interior and hard-to-reach surfaces was developed and studied using numerical simulation. The optimal minimum length of the rotating expanding part of the nozzle was determined to ensure the required speed of the particles at its exit. The simulation results of the influence of the geometric characteristics of this nozzle on the acceleration and speed of the powder particles at the moment of contact with the substrate are given. Dependencies are built and recommendations are given for choosing the radius of rotation of the nozzle, the length of the extended part and the distance of spraying to ensure the maximum values of the velocity of the particles at the moment of contact with the surface of the substrate. A multi-channel rotary nozzle is offered for cold spraying on surfaces of internal and hard-to-reach parts. The effect of particle diameter, pressure of the gas transporting the powder, channel dimensions, recovery coefficient, and powder material on the acceleration and trajectory of particle movement in and out of the nozzle was studied. The results of numerical modeling obtained for determining the speed of particles in the developed rotary nozzle were compared with the values of the critical spraying speed for the studied materials, and conclusions were made regarding the possibility of forming coatings from them.

The third section of the dissertation is devoted to the numerical modeling of the process of high-speed collision of powder particles with the substrate in the process of cold gas-dynamic spraying. For the first time, the use of the criterion Y (the ratio of the depth of the crater in the surface, formed as a result of the collision of a powder particle with it, to the height of the deformed particle) is proposed, which can be used to determine the critical speed of the particle at the moment of collision, necessary for its adhesion to the surface and to predict the possibility of formation adhesive bonds between them. The results of studies of the collision of a

single particle with a surface for homo- and heterogeneous materials in a wide range of particle velocities are given, and recommendations are given for choosing the values of the criterion Y and the corresponding values of the particle velocity for different materials that ensure the formation of bonds and the formation of coatings. The simulation results are compared with the calculated values of the critical speed and the results of other scientists. The process of collision of powder particles of various materials with a titanium surface is considered from the point of view of energy balance for a better understanding of the influence of the particle speed at the time of collision with the substrate on the process of cold gas dynamic spraying. The results of the numerical simulation of the collision of a set of particles of a pure metal powder, as well as a powder mixture, when spraying on a titanium alloy surface are presented.

The fourth chapter provides recommendations for the practical use of the obtained results of the dissertation work, in particular, the geometry of the channels of supersonic nozzles for cold spraying of direct and rotary spraying coatings on the inner surfaces of parts made of titanium alloys, the developed device for feeding powder into the extended part of the nozzle during cold high-pressure spraying, selection of spraying parameters (pressure and temperature of the gas at the entrance to the nozzle, the size of the powder particles), which ensure that the particles achieve the speed values necessary for their adhesion to the surface and the formation of the coating. Recommendations for further studies of the cold gas dynamic spraying process are given.

The scientific novelty of the obtained results is as follows:

1) for the first time, based on the results of numerical modeling, the dependence of the speed of a powder particle at the exit from a profiled single-channel nozzle for spraying on the gas parameters at the nozzle entrance (temperature and pressure), powder characteristics (material and particle size), and geometric characteristics of the nozzle (diameter of the critical section, its length, the angle of rotation of the flow in the critical section, the length of the expanding part of the nozzle, the powder supply point).

2) for the first time, the features of the acceleration and trajectory of the movement of powder particles in the profiled rotating nozzle were determined depending on the temperature and pressure of the main gas flow, the pressure of the transporting flow, the material of the powder and the size of its particles.

3) For the first time, the criterion Y, which is the ratio of the depth of the crater in the surface, formed as a result of the collision of a powder particle with it, to the height of the deformed particle, was applied to assess the possibility of forming connections between them during spraying of homo- and heterogeneous materials.

4) A scientifically based comprehensive approach was further developed, which is based on the use of theoretical calculations and the results of numerical modeling and makes it possible to predict the speed of particles of various powder materials at the exit from the nozzle, which made it possible to obtain and generalize the ways of ensuring the formation of bonds between powder particles and lining.

The practical significance of the obtained results is that the results of the dissertation work can be used in the development of new technical solutions for cold gas-dynamic spraying of protective and restorative coatings on parts of aviation and other equipment made of titanium alloys.

The obtained and generalized results of the research will make it possible to evaluate with high accuracy the influence of various factors, in particular the geometry of the nozzle, spraying parameters, characteristics of the powder material, on the acceleration of powder particles in the channels of the nozzles for spraying, to predict the possibility of the formation of bonds between the powder particles and the substrate, to adjust the composition of the powder mixtures during spraying of coatings on titanium alloys.

The revealed features of the influence of gas parameters, powder characteristics and nozzle geometry on the speed of particles at the exit of the nozzle will expand the understanding of the laws of gas dynamics processes of two-phase flow in supersonic nozzles for cold spraying, which can be used to improve spraying equipment, increase the efficiency of the spraying process and

quality coatings

The developed nozzle and recommendations for the selection of spraying parameters can be used for spraying protective and restorative coatings on internal and hard-to-reach surfaces of parts made of titanium alloys with a diameter of 45 mm and more. Developments are protected by a patent.

The results of the dissertation work can be implemented in research institutions and production and repair enterprises that are engaged in researching the processes of cold spraying and the practical application of technology for the formation of protective and restorative coatings.

Keywords: cold gas dynamic spraying, coating, numerical simulation, supersonic nozzle, optimization, gas flow, high-velocity impact, powder.

АНОТАЦІЯ

Ху Веньцзе. Холодне напилення захисних і відновних покриттів на деталі авіаційної техніки з титанових сплавів – Кваліфікаційна наукова робота на правах рукопису.

Дисертація на здобуття наукового ступеня доктора філософії з галузі знань 13 Механічна інженерія за спеціальністю 132 Матеріалознавсто. – Національний аерокосмічний університет ім. М. Є. Жуковського «Харківський авіаційний інститут», Харків, 2024.

Дисертаційна робота присвячена удосконаленню технології холодного газодинамічного напилювання захисних і відновлювальних покриттів на титанові сплави шляхом встановлення оптимальної геометрії сопел для напилювання, закономірностей впливу параметрів газу на вході в сопло та характеристик порошку на швидкість частинок в момент зіткнення з підкладкою. Об’єктом дослідження є процес прискорення частинок порошку надзвуковим потоком в каналі сопла для холодного газодинамічного напилювання та високошвидкісного зіткнення частинки з титановою підкладкою. Предметом дослідження є закономірності впливу геометрії сопла, параметрів процесу холодного газодинамічного напилювання та характеристик порошку на швидкість частинок в потоці.

Актуальність та необхідність в проведенні досліджень обумовлена існуючою проблемою подовження ресурсу деталей авіаційної техніки, виготовлених з титанових сплавів. Одним з можливих напрямків підтримання працездатності таких деталей, забезпечення високих експлуатаційних показників та підвищення довговічності, є розвиток та удосконалення існуючих способів нанесення покриттів. У дисертаційній роботі представлено нові науково-обґрунтовані результати теоретичних розрахунків і чисельного моделювання, які узагальнюють і забезпечують вирішення найбільш важливої складової нанесення покриттів – забезпечення можливості зчеплення

частинок порошку з поверхнею з достатньою адгезійною міцністю та подальшого зростання покриття.

Дисертація складається з анотації, вступу, чотирьох розділів, висновків і додатків.

У вступі обґрунтовано актуальність і необхідність вибраного напряму досліджень, сформульовано мету й завдання досліджень, викладено наукову новизну й практичне значення отриманих результатів, наведено відомості про їх апробацію, публікації й структуру дисертаційної роботи.

В першому розділі розглянуто використання титанових сплавів в авіаційній та аерокосмічній галузях, експлуатаційних дефектів, причин їх виникнення та можливих шляхів попередження та усунення. Наведено методи нанесення покриттів та місце серед них холодного газодинамічного напилювання, його переваги та перспективи щодо можливостей використання для отримання покриттів на поверхнях з титанових сплавів. Особливу увагу приділено аналізу впливу параметрів холодного газодинамічного напилювання на властивості покриттів та ефективність процесу. Проведено аналіз публікацій присвячених використанню технології для напилювання зносостійких покриттів на титанові сплави, а також матеріалів, які використовуються для відновлення зношених поверхонь деталей з цих сплавів. За результатами проведеного аналізу виділено незакриті питання в області холодного газодинамічного напилювання покриттів на титанові сплави, окреслено шляхи їх вирішення та вдосконалення технології.

В другому розділі наведено основні рівняння газодинаміки, які використовуються для опису потоку в звужувально-розширних соплах для холодного газодинамічного напилювання та розрахунку їх геометричних характеристик. Виконано аналіз моделей, які використовуються для знаходження температурно-швидкісних характеристик частинок порошку в газовому потоці в каналі сопла. Подано результати з розроблення прямого надзвукового сопла для напилювання, а також результати чисельного моделювання впливу геометричних параметрів сопла (діаметру критичного

перетину сопла, його довжини, куту повороту вісі сопла в критичному перетині), а також матеріалу порошку та розміру частинок на їх швидкість на виході з сопла. З використанням методу багатофакторного планування експерименту досліджено комплексний вплив параметрів газу (тиску та температури) на вході в сопло та діаметру частинок порошку на їх швидкість на виході з сопла для обраної геометрії поворотного одноканального сопла. Отримано рівняння регресії для прогнозування швидкості частинок в залежності від досліджуваних параметрів, а також наведено рекомендації щодо вибору оптимальних режимів які забезпечують отримання максимальної швидкості частинок порошку. Розроблено та досліджено з використанням чисельного моделювання поворотне сопло для напилювання покриттів на внутрішні та важкодоступні поверхні. Визначено оптимальну мінімальну довжину поворотної розширної частини сопла для забезпечення необхідної швидкості частинок на виході з нього. Наведено результати моделювання із впливу геометричних характеристик цього сопла на прискорення та швидкість частинок порошку в момент зіткнення з підкладкою. Побудовано залежності та наведено рекомендації щодо вибору радіусу повороту сопла, довжини розширної частини та дистанції напилювання для забезпечення максимальних значень швидкості частинок в момент зіткнення з поверхнею підкладки. Запропоновано багатоканальне поворотне сопло для холодного напилювання на внутрішні та важкодоступні поверхні деталей. Досліджено вплив діаметру частинок, тиску транспортуючого порошок газу, розмірів каналів, коефіцієнт відновлення, матеріалу порошку на прискорення та траєкторію руху частинок в соплі та на виході з нього. Отримані результати чисельного моделювання з визначення швидкості частинок в розробленому поворотному соплі були порівняні з значеннями критичної швидкості напилювання для досліджуваних матеріалів та зроблено висновки щодо можливостей утворення з них покриттів.

Третій розділ дисертаційної роботи присвячено чисельному моделюванню процесу високошвидкісного зіткнення частинок порошку з

підкладкою в процесі холодного газодинамічного напилювання. Вперше запропоновано використання критерію Y (відношення глибини кратеру в поверхні, утворений в результаті зіткнення з нею частинки порошку, до висоти деформованої частинки), який може бути застосований для визначення критичної швидкості частинки в момент зіткнення, необхідної для її зчеплення з поверхнею та прогнозування можливості утворення між ними адгезійних зв'язків. Наведено результати досліджень зіткнення одиничної частинки з поверхнею для гомо- та гетерогенних матеріалів в широкому діапазоні швидкостей частинки та подано рекомендації щодо вибору значень критерію Y та відповідних величин швидкості частинок для різних матеріалів, які забезпечують утворення зв'язків та формування покриттів. Результати моделювання порівняно з розрахунковими значеннями критичної швидкості та результатами інших вчених. Розглянуто процес зіткнення частинок порошку різних матеріалів з титановою поверхнею з точки зору балансу енергії для кращого розуміння впливу швидкості частинки в момент зіткнення з підкладкою на процес холодного газодинамічного напилювання. Наведено результати чисельного моделювання зіткнення множини частинок порошку чистого металу, а також порошкової суміші, при напилюванні на поверхню з титанового сплаву.

В четвертому розділі наведено рекомендації для практичного використання отриманих результатів дисертаційної роботи, зокрема геометрії каналів надзвукових сопел для холодного напилювання прямих та поворотних для напилювання покриттів на внутрішні поверхні деталей з титанових сплавів, розробленого пристрою для подачі порошку в розширну частину сопла при холодному напилюванні високого тиску, вибору параметрів напилювання (тиску та температури газу на вході в сопло, розміру частинок порошку), що забезпечують досягнення частинками значень швидкості, необхідної для їх зчеплення з поверхнею та формування покриття. Наведено рекомендації для подальших досліджень процесу холодного газодинамічного напилювання.

Наукова новизна отриманих результатів полягає в такому:

1) уперше за результатами чисельного моделювання отримано залежності швидкості частинки порошку на виході з спрофільованого одноканального сопла для напилювання від параметрів газу на вході в сопло (температура та тиск), характеристик порошку (матеріал і розмір частинок), та геометричних характеристик сопла (діаметр критичного перерізу, його довжина, кут повороту потоку в критичному перерізі, довжина розширної частини сопла, точки підводу порошку).

2) уперше встановлено особливості прискорення та траєкторії руху частинок порошку в спрофільованому поворотному соплі від температури та тиску основного газового потоку, тиску транспортуючого потоку, матеріалу порошку та розміру його частинок.

3) Уперше застосовано критерій Y, який є відношенням глибини кратеру в поверхні, утворений в результаті зіткнення з нею частинки порошку, до висоти деформованої частинки, для оцінювання можливості утворення між ними зв’язків при напилюванні гомо- та гетерогенних матеріалів.

4) Отримав подальший розвиток науково-обґрунтований комплексний підхід, який базується на використанні теоретичних розрахунків і результатів чисельного моделювання та дає можливість прогнозувати швидкість частинок різних порошкових матеріалів на виході з сопла, що дозволило отримати та узагальнити шляхи забезпечення утворення зв’язків між частинками порошку та підкладкою.

Практична значущість отриманих результатів полягає в тому, що результати, дисертаційної роботи можуть бути використані при розроблені нових технічних рішень з холодного газодинамічного напилювання захисних і відновлювальних покриттів на деталі авіаційної та іншої техніки з титанових сплавів.

Отримані та узагальнені результати досліджень дозволять з високою точністю оцінювати вплив різних чинників, зокрема геометрії сопла, параметрів напилювання, характеристик порошкового матеріалу, на

прискорення частинок порошку в каналах сопел для напилювання, прогнозувати можливість утворення зв’язків між частинками порошку та підкладкою, корегувати склад порошкової суміші при напилювання покриттів на титанові сплави.

Виявлені особливості впливу параметрів газу, характеристик порошків та геометрії сопла на швидкість частинок на виході з сопла, розширять уявлення про закономірності процесів газодинаміки двофазного потоку в надзвукових соплах для холодного напилювання, що може бути використано для вдосконалення обладнання для напилювання, підвищення ефективності процесу напилювання та якості покриттів.

Розроблене сопло та рекомендації щодо вибору параметрів напилювання, можуть бути використані для напилювання захисних і відновлювальних покриттів на внутрішні та важкодоступні поверхні деталей з титанових сплавів діаметром від 45 мм і більше. Розробки захищені патентом.

Результати дисертаційної роботи можуть бути впроваджені в науково-дослідні установи, виробничі та ремонтні підприємства, які займаються дослідженнями процесів холодного газодинамічного напилювання та практичним застосуванням технології для формування захисних і відновлювальних покриттів..

Ключові слова: холодне газодинамічне напилювання, покриття, чисельне моделювання, надзвукове сопло, оптимізація, газовий потік, високошвидкісне зіткнення, порошок.

LIST OF APPLICANT'S PUBLICATION

List of the applicant's publications on the topic of the dissertation

Articles in scientific periodical publications included in category «A» of the List of scientific specialized publications of Ukraine, or in foreign publications indexed in the Web of Science Core Collection and/or Scopus databases:

1.**Wenjie Hu,** O. Shorinov. Optimization of Cold Spraying 90° Rectangu lar Nozzle Technological Parameter via Response Surface Method. Journal of Engineering sciences, 2024, 11(2): F1-F8. DOI: https://doi.org/10.21272/jes.2024.11(2).f1. (**Scopus, Q4**)

2. **Wenjie Hu**, K. Tan, S. Markovych, T. T. Cao, X. L. Liu. Research on the adhesive property of Al+Ti mixed powder deposited on Ti-6Al-4V substrate by CS using Abaqus/Explicit, Metallophysics and Advanced Technologies. 202244(5):613-621. DOI: https://doi.org/10.15407/mfint.44.05.0613.(**Scopus, Q3**)

3. **Wenjie Hu**, Kun Tan, Sergii Markovych, Tingting Cao. Study on structure and technological parameters of multi-channel cold spraying nozzle, Eastern-European Journal of Enterprise Technologies,2021, 5 (113), 6-14. DOI: https://doi.org/10.15587/1729-4061.2021.242707. (**Scopus, Q3**)

4. **Wenjie Hu**, Tan K., S. Markovych, Liu X. L. Study of a Cold Spray Nozzle Throat on Acceleration Characteristics via CFD. Journal of Engineering Sciences, 2021, 8: 19-24. DOI: https://doi.org/10.21272/jes.2021.8(1).f3. (**Scopus, Q4**)

5. **Wenjie Hu**. Effects of different metal particles on cold spray deposition onto Ti-6Al-4V alloy via abaqus/explicit. Journal of Engineering Sciences. 2020, 7:19-25. DOI: 10.21272/jes.2020.7(2).e4. (**Scopus, Q4**)

6. Kun T., **Wenjie Hu**., Yurong W. Optimization of cold spray nozzles based on the response surface methodology. Journal of Engineering Sciences, 2024, 11(1), pp. F1–F11. DOI: https://doi.org/10.21272/jes.2024.11(1).f1. (**Scopus, Q4**)

7. Kun Tan, **Wenjie Hu**, et al. Dimet Laval Nozzle Expansion Section Analysis and Optimization. Journal of Engineering Sciences, 2021, Vol. 8(2): F6-F10.DOI: https://doi.org/10.21272/jes.2021.8(2).f2. (**Scopus, Q4**)

Articles in scientific periodical publications included in the List of scientific specialized publications of Ukraine (category «Б»):

8. **Wenjie Hu**, S. Markovych, Kun Tan, O. Shorinov, Tingting Cao. Research on Wear Resistance Coating of Aircraft Titanium Alloy Parts by Cold Spraying Technology. Aerospace technic and technology. 2020, 6:61-71. DOI: https://doi.org/10.32620/aktt.2020.6.07.

9. **Wenjie Hu,** S. Markovych, Kun Tan, O. Shorinov, Tingting Cao. Surface repair of aircraft titanium alloys by cold spray technology. Aerospace technic and technology. 2020, 3:30-42. DOI:https://doi.org/10.32620/aktt.2020.3.04.

10. **Wenjie Hu**, O. Shorinov. Optimization of particle acceleration parameters of special cold spray nozzles via neural network and genetic algorithm. Aerospace technic and technology. 2024,4:64-70. DOI: 10.32620/aktt.2024.4.08

11. Kun Tan, S. Markovych, **Wenjie Hu**, O. Shorinov, Yurong Wang. Review of manufacturing and repair aircraft and engine parts based on cold spraying technology and additive manufacturing technology. Aerospace technic and technology, 2020, 3:53-70. DOI: https://doi.org/10.32620/aktt.2020.3.06.

12. Kun Tan, S. Markovych, **Wenjie Hu**, O. Shorinov, Yurong Wang. Review of application and research based on cold spray coating materials. Aerospace technic and technology, 2021, 1:47-59. DOI: 10.32620/aktt.2021.1.05.

13. Kun T., **Wenjie Hu**, Oleksandr Shorinov, Yurong W. Muti-paramete coupled optimization of AL6061 coating porosity based on the RSM. Aerosp ace technic and technology, 2024, 3:59-67. DOI: https://doi.org/10.32620/aktt.2 024.3.05.

Scientific works are certified for the approbation of dissertation materials:

14. **Wenjie Hu**, K. Tan, O. Shorinov. Study on Multi-parameter of Cold Spraying Technology via RSM and BP+GA Methods. International Conference on Artificial Intelligence and Advanced Manufacturing, Belgium, Brussels, 2023, pp. 272-278. DOI: https://doi.org/10.1049/icp.2023.2950. (**EI, Scopus**)

15. **Wenjie Hu**, Kun Tan, Sergii Markovych, Tingting Cao. Structural optimization of the special cold spraying nozzle via response surface method.

Conference on Integrated Computer Technologies in Mechanical Engineering – Synergetic Engineering (ICTM’2021), Lecture Notes in Networks and Systems, vol. 367, pp. 110–122, 2022, Kharkiv, Ukraine. DOI: https://doi.org/10.1007/978-3-030-94259-5_11. (**Scopus**)

16. **Wenjie Hu**, K. Tan, S. Markovych, T. T. Cao. A simple method for determining the critical velocity value of cold spraying via SPH, International Conference on Artificial Intelligence and Advanced Manufacturing (AIAM 2021). Manchester, England, 2021, 23-25 oct. pp. 215-221. DOI: https://doi.org/10.1109/AIAM54119.2021.00052.(**Scopus, Engineering Index**)

17. Kun Tan, S. Markovych, **Wenjie Hu**, Yun Wang, O. Shorinov and Yurong Wang. On the Characteristics of Cold Spray Technology and Its Application in Aerospace Industries, IOP Conference Series: Earth and Environmental Science, 2021,719(3), p. 032023. DOI: https://doi.org/10.1088/1755-1315/719/3/032023. (**Scopus**)

18. **Wenjie Hu**, S. Markovych, Kun Tan, O. Shorinov. Deposition of protective and restorative cold spraying coating on aircraft parts made of titanium alloys. 2021 (Topic: The modern problems of engine building, energy and intellectual mechanics - 2021, The open scientific-practical student conference of the Faculty of Aircraft engines (FAE) in National N.E. Zhukovsky Aerospace University "KhAI") https://drive.google.com/file/d/1trS11rljWf1ylXnAkefWSohV8rkH5p28/view

Scientific works that additionally represent the scientific results of the dissertation:

19. Cao Tingting, **Wenjie Hu**. A piston type cold spray device, 2020. (Chinese patent: CN211756622U).
https://xueshu.baidu.com/usercenter/paper/show?paperid=1v0b06y0kv5g06c0e20a0200uy018632&site=xueshu_se

CONTENT

INTRODUCTION 22
CHAPTER 1. OVERVIEW OF TITANIUM ALLOYS IN AIRCRAFT AND CURRENT SITUATION ANALYSIS OF COLD SPRAYING……...28
1.1 Review of titanium alloys in aircraft……..28
1.1.1 The application of titanium alloys in aircraft 28
1.1.2 The urgent problems of aircraft titanium alloys 30
1.2 Overview of traditional surface coating technology..... 30
1.3 The advantages to solve problem onto titanium surface by Cold spraying technology 32
1.3.1 Cold spraying technology 32
1.3.2 Deposition of wear-resistant coating by CS 44
1.3.3 Deposition of the restorative coating..... 50
1.3.4 Additive manufacturing of titanium alloy parts..... 53
1.4 Conclusion of Chapter 1 53
CHAPTER 2. STRUCTURAL AND TECHNOLOGICAL PARAMETER OPTIMIZATION OF THE SPECIAL CS NOZZLE WITH 90° ANGLE 56
2.1 Theoretical study 56
2.1.1 One dimensional steady flow 57
2.1.2 Effect of nozzle section size 57
2.1.3 Mechanical condition of nozzle..... 61
2.1.4 Gas thermodynamic parameter..... 63
2.2 Study of a cold spray nozzle throat structure parameters on acceleration characteristics via CFD..... 63
2.2.1 Determination of geometric model..... 64
2.2.2 The parameter details of numerical simulation 66
2.2.3 Structure parameter factors..... 69
2.2.4 Study on the particle trajectory..... 74
2.2.5 Summary this section..... 78

2.3 Study of the technological parameters on acceleration characteristics by multiple factors analysis 79
2.3.1 Gas temperature 80
2.3.2 Gas pressure 81
2.3.3 Powder diameters 82
2.3.4 Interaction analysis of three factors 82
2.3.5 Summary this section 88
2.4 Research on the special single-channel cold spraying 90° rectangular nozzle 89
2.4.1 Established the special nozzle 3D initial model 89
2.4.2 Optimal single factor analysis of special nozzle structure 91
2.5 Multi-factor interaction analysis of the special single channel nozzle 98
2.5.1 Mathematical modeling 98
2.5.2 Create high and low code 99
2.5.3Analysis of variance 99
2.5.4 Result of multi-factor interaction 101
2.5.5 Application analysis 103
2.5.6 Summary this section 104
2.6 Research on the special cold spraying muti-channel nozzle 104
2.6.1 Established the multi-channel model method 104
2.6.2 Study on particle trajectory in multi-channel nozzle 106
2.6.3 Analysis of technological parameters 110
2.6.4 Result and discussion 113
2.6.5. Summary this section 115
2.7 Conclusion of Chapter 2 116
CHAPTER 3. SIMULATION RESEARCH ON COLD SPRY DEPOSITION ONTO TITANIUM ALLOY SUBSTRATE 118
3.1 Cold spray deposition characteristics 118
3.2 Deposited process based on ABAQUS 120
3.2.1 the J-Cook plastic model 120

3.2.2 The material state equation 123
3.2.3 Numerical method 123
3.3 New method determination of critical velocity 124
3.3.1 The introduction of principle 125
3.3.2 Determination of critical velocity 125
3.4 Theoretical calculation of critical velocity 129
3.4.1 The detail of theoretical principle 129
3.4.2 Comparison between theory and numerical simulation 130
3.5 Research on deposition of traditional pure metal powder on Ti-6Al-4V substrate 133
3.5.1 Material properties 133
3.5.2 Numerical simulation results 133
3.5.3 Energy analysis 135
3.5.4 Study on multi-particle aluminum collision with Ti-6Al-4V matrix 140
3.6 Research on deposition of mixed metal powders on Ti-6Al-4V substrate 142
3.6.1 Material and methods 142
3.6.2 Result and discussion 143
3.7 Conclusion of chapter 3 146
CHAPTER 4. IMPLEMENTATION RECOMMENDATIONS OF COLD SPRAYING REPAIR TI ALLOY TECHNOLOGICAL, SPECIAL NOZZLE AND OPTIMIZATION METHOD 148
4.1 The recommendations of technological process using cold spraying to repair aircraft titanium parts 148
4.2 Suggestion about implementation of the theoretical results for the special nozzle 148
4.2.1 Summary factors about the special nozzles design under high pressure 149
4.2.2 Recommendations about the technological parameters under high pressure 149
4.2.3 Implementation recommendation of high pressure cold spraying

nozzle for powder injection 150
4.3 Recommended method for CS technical parameter optimization 152
4.3.1 Response surface method 152
4.3.2 BP neural network and GA optimization 152
CONCLUSIONS AND SUGGESTIONS FOR FUTURE WORK 157
REFERENCES 161
APPENDIX A 178
APPENDIX B 184

LIST OF ABBREVIATIONS

CS	Cold Spray
CFD	Computational fluid dynamics
RSM	Response surface method
CEL	Coupled Euler-Lagrange
SPH	Smoothed Particle Hydrodynamics
ALE	Arbitrary Lagrange-Euler
ALLKE	Kinetic energy
ALLSE	Strain energy
ALLFD	Frictional dissipation
ALLVD	Viscous dissipation
ALLAE	Artificial strain energy
ALLPD	Plastic dissipation
ALLIE	Internal energy
LHS	Latin Hypercube Sampling
BP	Back propagation neural network

INTRODUCTION

Reasons for choosing the research topic.

Wear, mechanical damage, and corrosion are the main reasons for the reduction of their resource, the occurrence of failures of the unit and the mechanism as a whole. The increase in maintenance and repair costs stimulates the search for new technical solutions to extend the service life of parts and return them to operation. This problem is especially relevant for parts made of titanium alloys, the use of which for the manufacture of parts of aviation and aerospace equipment is explained by their excellent properties of the material - high specific strength, good corrosion resistance, high heat resistance and other properties. However, existing disadvantages, such as low wear resistance and sensitivity to high temperatures, limit their wide use in industry.

One of the main directions of maintaining the performance of parts made of titanium alloys, increasing the durability and resources of aviation equipment in modern conditions is the improvement of low-cost technological processes of their strengthening at the stage of production and restoration during repair in combination with the use of available and cheap materials with guaranteed high reliability indicators of repaired products. The solution to this problem is limited by the limited use of modern methods of repair and restoration of parts made of titanium alloys.

The technology of cold gas dynamic spraying, in contrast to existing alternative methods of coating, is characterized by relatively low operating temperatures of the process and spraying of powder material without its melting. The absence of structural and phase changes in the coating and substrate materials allows applying durable coatings with minimal porosity to temperature-sensitive materials, in particular titanium alloys, which opens up wide opportunities for introducing the technology into industry. This can be realized under the condition of a deeper study of the processes of cold gas-dynamic spraying, such as the acceleration and heating of particles by the gas flow in the channels of supersonic

nozzles, the processes of contact interaction of solid bodies during high-speed collision, the formation of a coating and its growth, etc. Currently, these issues in relation to the spraying of protective and restorative coatings on titanium alloys have not been sufficiently studied, which explains the urgency of conducting research. The development of cold spraying technology through the improvement of equipment, optimization of spraying modes, selection of powder material will allow to offer new technical solutions and technologies for prolonging the service life of aviation equipment parts made of titanium alloys.

The aim and tasks of the research. The aim of the dissertation is to improve the cold gas dynamic spraying of coatings technology on titanium alloys by establishing the optimal geometry of the spraying nozzles, the regularities of the influence of gas parameters at the nozzle entrance and powder characteristics on the speed of particles at the moment of impact with the substrate.

To reach the aim of the research, the following main tasks are formed and solved:

1) to develop supersonic nozzles for cold gas-dynamic spraying of titanium alloy surface coatings, in particular internal and hard-to-reach surfaces;

2) to establish regularities of the effect of the geometry of the supersonic nozzle for cold spraying on the acceleration of powder particles;

3) to investigate the influence of the parameters of the gas entering the nozzle and the characteristics of the powder material on the speed of its particles in the nozzle channel, at the exit from it, as well as before impact with the substrate;

4) to develop an approach to determine the critical spraying velocity necessary for the formation of bonds between the particles of homogeneous and heterogeneous powders onto the titanium substrate, and the subsequent growth of the coating layer;

5) to investigate the features of the high-speed interaction of particles of homogeneous and heterogeneous powders with a titanium substrate and the influence of temperature and speed of particles at the moment of collision on this process;

6) to develop recommendations for improving the technology of cold spraying of protective and restorative coatings on titanium alloys.

The **object** of research is the process of acceleration of powder particles by a supersonic flow in the nozzle channel for cold gas-dynamic spraying and the high-velocity impact of the particle on the titanium substrate.

The **subject** of the research is the influence of the nozzle geometry, the parameters of the cold gas-dynamic spraying process, and powder properties on the velocity of the powder particles in the gas flow.

The research methods. To solve the tasks in the dissertation, the methods of mathematical and numerical modelling were used for designing supersonic nozzles, researching the processes of particle acceleration in the flow and high-velocity impact, designing multi-factorial experiments, regression analysis, and mathematical statistics for optimizing spraying parameters. Optimization methods are based on univariate and multivariate analysis, in particular on the RSM and GA+BPNN methods.

The scientific novelty of the obtained results is as follows:

1) for the first time, based on the results of numerical modelling, the dependence of the speed of a powder particle at the exit from a profiled single-channel nozzle for spraying on the gas parameters at the nozzle entrance (temperature and pressure), powder characteristics (material and particle size), and geometric characteristics of the nozzle (diameter of the critical section).

2) For the first time, the features of the acceleration and trajectory of the movement of powder particles in a special nozzle for rotary parts were established depending on the temperature and pressure of the main gas flow, the pressure of the transporting flow, the material of the powder and the size of its particles.

3) A scientifically based complex approach was further developed, which is based on the use of theoretical calculations and the results of numerical modeling and makes it possible to predict the speed of particles of various powder materials at the exit from the nozzle, which made it possible to obtain and generalize the ways of ensuring the formation of bonds between powder particles and substrate.

Personal contribution of the applicant. The results of the dissertation work were published in 19 articles. Among them 7 articles in scientific periodical publications included in category «A» of the List of scientific specialized publications of Ukraine, or in foreign publications indexed in the Web of Science Core Collection and/or Scopus database; 6 articles in scientific periodical publications included in the List of scientific specialized publications of Ukraine (category «Б»); 5 conference proceedings (4 of them indexed in the Scopus database); and 1 Chinese patent.

All the main results that constitute the essence of the dissertation are obtained by the author personally. Statement of tasks, analysis and interpretation of the main results, and formulation of scientific conclusions are performed together with the supervisor.

In works published in co-authorship, the acquirer owns the following:

- the analysis of the current state of the issue in the field of the use of titanium alloys in the aerospace industry, operational defects, their causes and the possibilities of cold spraying technology to eliminate these defects was performed [1, 4, 169];

- single-channel and multi-channel nozzles for cold spraying were proposed for the first time [74, 81];

- optimization of geometric parameters and modes of cold spraying for special nozzles using RSM and BP+GA methods [116, 124, 170, 171];

- assessment of the critical spraying speed of various powders was performed using the criterion Y proposed for the first time [167];

- the study of the process of spraying powder mixtures on titanium alloys was performed; the use of an intermediate coating is proposed to ensure adhesion between the coating and the titanium alloy substrate [166, 168];

- the analysis of literature on spraying of Ti and other coatings on titanium alloys was performed, and materials that can be sprayed were systematized [85];

- verification of the obtained results was performed; numerical modeling was carried out using optimized modes and developed recommendations [123];

- the construction of a nozzle with a high-pressure supply of powder is proposed, which can improve the throat injection powder pressure problem [79].

Approbation of dissertation materials. The dissertation results were reported and discussed at international and national scientific conferences:

1) International Conference on Mechanical Engineering and Materials (ICMEM2020);

2) Integrated computer technologies in mechanical engineering (ICTM 2021);

3) International Conference on Artificial Intelligence and Advanced Manufacturing (AIAM2021 and AIAM2023);

4) Open scientific and practical student conference of the Faculty of Aviation Engines «Modern problems of engine construction, power engineering and intelligent mechanics», 2020. (Відкрита науково-практична студентська конференція факультету авіаційних двигунів (ФАД) «Сучасні проблеми двигунобудування, енергетики та інтелектуальної механіки»).

The structure and scope of the dissertation. The dissertation consists of an abstract, 4 chapters, conclusions and appendices. The total volume of the dissertation is 186 pages, of which 177 pages are the main text. The dissertation contains 96 figures, 34 tables, 171 references and 2 appendices.

Connection of work with scientific programs, plans, topics. The results of the dissertation obtained by the author were carried out at the Department of Aircraft Engine Production Technology of the National Aerospace University named after M. E. Zhukovsky "Kharkiv Aviation Institute" in the implementation of the state budget research project of the Ministry of Education and Science of Ukraine: "Development of aggregate technology of restoration and repair of aviation (helicopters) parts by cold spraying with post process machining of deposited coatings" (№ ДР 0122U001341, 2022-2023) and "Development of technology and equipment for cold spraying of restorative coatings on aircraft parts" (№ ДР 0124U000553, 2024). This research was funded by the China Scholarship Council (No. 202008100011), under Natural Science Project of Nanchang Institute of Technology (NLZK-22-05): “Optimization of protective and

restorative cold spraying process for aircraft titanium alloy parts"； Science and Technology Project of Jiangxi Provincial Department of Education (GJJ2202721): "Study on protective and restorative cold spraying technology for aircraft titanium alloy parts."

The practical significance of the obtained results is that the obtained results of the dissertation work can be used in the development of new technical solutions for cold gas-dynamic spraying of protective and restorative coatings on parts of aviation and other equipment made of titanium alloys.

The obtained and generalized research results will allow to evaluate with high accuracy the influence of various factors, in particular the geometry of the nozzle, spraying parameters, characteristics of the powder material, on the acceleration of powder particles in the channels of the nozzles for spraying, to predict the possibility of the formation of bonds between the powder particles and the substrate, to adjust the composition of the powder mixtures during spraying of coatings on titanium alloys.

The revealed features of the influence of gas parameters, powder characteristics and nozzle geometry on the speed of particles at the exit of the nozzle will expand the understanding of the laws of gas dynamics processes of two-phase flow in supersonic nozzles for cold spraying, which can be used to improve spraying equipment, increase the efficiency of the spraying process and quality coatings.

The developed nozzle and recommendations for the selection of spraying parameters can be used for spraying protective and restorative coatings on internal and hard-to-reach surfaces of parts made of titanium alloys. An improved powder injection pressure device was proposed for high pressure cold spraying. Developments are protected by a patent.

The results of the dissertation work, can be implemented in research institutions and production and repair enterprises that are engaged in researching the processes of cold spraying and the practical application of technology for the formation of protective and restorative coatings.

CHAPTER 1
OVERVIEW OF TITANIUM ALLOYS IN AIRCRAFT AND CURRENT SITUATION ANALYSIS OF COLD SPRAYING

1.1 Review of titanium alloys in aircraft

1.1.1 The application of titanium alloys in aircraft

Titanium alloys have the advantages of low density, high specific strength and excellent corrosion resistance. So, it is widely used in the field of aerospace. Ti alloys are the main structural material of aircraft parts, including compressor blades, cartridge receivers, black, engine nacelle, thermal baffle and so on. For instance, titanium alloy is used in the F35 for about 27% of the time, and FC-31 fighters for 25 %. America's fourth-generation fighter jet, the F22 engine, uses 41% [1] (Table 1.1), and it is the highest amount of titanium in use. Therefore, titanium alloy has the reputation of "space metal" [2].

Table 1.1 – Mass fraction of titanium alloy used in different planes

State	Aircraft type	Service time	Mass fraction / %
USA	F/A 18E/F	2002	15
USA	F/A 22	2005	41
USA	B787	2011	15
Europe	A350	2013	14
China	FC-31	2016	25
China	J-20	2017	20
USA	F35A	2018	27
Russian	SU-57	2019	18

Table 1.2 – Titanium alloys used in aircraft [3]

Alloy type	Chemical composition	Alloy type	Chemical composition
α (near α) titanium alloy	Pure titanium	β titanium alloy	Ti-6Al-2.75Sn-4Zr 4Mo-0.45Si (Ti-1100)
	Ti-3Al-2.5V		Ti-6Al-6V-2Sn
	Ti-5Al-2.5Sn		Ti-6Al-2Sn-2Cr-2Mo-2Cr-Si
	Ti-8Al-1Mo-1V		Ti-6A1-2Sn-2Zr-6Mo
	Ti-6Al-2Sn-4Zr-2Mo-Si (O.1-0.25)		Ti-5Al-2Sn-2Zr-4Mo-4Cr (TC17)
	Ti-5.5Al-3.5Sn-3Zr-INb-0.25Mo-0.3Si (IMI829)	(α+β) titanium alloy	Ti-13V-11Cr-3Al
	Ti-5.5Al-4Sn-4Zr-0.3Mo-INb-0.5Si-0.006C (IMI834)		Ti-10V-2Fe-3Al
	Ti-5.8Al-4Sn-3.5Zr-0.7Nb-0.5Mo-O.35Si-0.06C (IMI884)		Ti-15V-3Cr-3AI-3Sn
	Ti-6Al-2.75Sn-4Zr 4Mo-0.45Si (Ti-1100)		Ti-15Mo-2.7Nb -3A-0.2Sn (Timetal21S)
			Ti- 3AI-8V-6Cr-4Mo-4Zr (B-C)
			Ti-6Al-4V

There are three types of titanium alloys (table1.2): α,β and (α+β) titanium alloys are widely used in aero-engines [3], among which the α titanium alloys include Ti-3Al-2.5V, Ti-5Al-2.5Sn, Ti-8Al-1Mo-1V, etc, it mainly contains elements such as Al, which can increase the tensile strength and creep stress of the alloy, reduce the density of titanium alloy and improve the specific strength; β titanium alloy include Ti-6Al-2.75Sn-4Zr 4Mo-0.45Si, Ti-6Al-6V-2Sn,

Ti-6Al-2Sn-2Cr-2Mo-2Cr-Si, etc, it has a high enough stable element content to be the preferred structural material for airframes and wings; (α+β) titanium alloy include Ti-6Al-4V, Ti-13V-11Cr-3Al, Ti-10V-2Fe-3Al, Ti-15V-3Cr-3AI-3Sn, etc, its maximum operating temperature is no more than 500°C, and its welding performance and heat resistance are lower than α titanium alloy. Ti-6Al-4V alloy discussed in chapter 3 is a typical α+β titanium alloy, which contains 6% α -stable element aluminum and 4% β -stable element vanadium.

1.1.2 The urgent problems of aircraft titanium alloys

As described in Section 1.1.1, titanium alloys are widely used in aerospace. However, their poor wear resistance limits further application, and Titanium alloys are easy to reactive at high temperatures, have great difficulty in smelting and have high manufacturing costs.

In addition, the application defects in the nautical field are mainly corrosion problems, for example, Ti-5Al-2Sn-2Zr-4Mo-4Cr presents pitting corrosion in the environment of nitric acid and ravine-like corrosion pit in the environment of hydrochloric acid [5], especially in warships, where the corrosion problem is particularly serious. ling

In summary, the defects of titanium alloy include wear, damage, oxidation at high temperatures, corrosion, etc. This chapter mainly discusses the deposition of protective and recovery coatings on titanium alloy surfaces and briefly introduces the additive manufacturing of titanium alloy.

1.2 Overview of traditional surface coating technology

Various protective coating technologies for titanium alloys have emerged (table 1.3). The repair methods of titanium alloy include HVOF [6], HVAF [6], cold spraying [7], laser cladding [8], laser micro-fusion in-situ synthesized technology [9], micro-arc oxidation [10, 11], laser melt injection (LMI) [12], chromium-free dacro

technology [13], supersonic laser deposition [14] (SLD), which is a newly developed material deposition technique that synchronously combines the laser heating with cold spray (CS). And supersonic plasma spray technology [15], which are different from low plasma spray (LPPS).

For Ti-matrix coating, the work [17] research on the wear and corrosion behavior of the Ti-matrix functional gradient layer indicated friction coefficient and wear rate decreased significantly; the value was 0.3…0.5 times of Ti600 substrate. Zhou Heng's research on NiCrAl+YSZ+NiCrAl/Bentonite composite coatings with a thickness of 2mm was prepared by plasma spraying and flame spraying [18] on the surface of Ti40 alloy, Zhang [19] study the effect of TiN/Ti coating structure on equivalent plastic strain of Ti-6Al-4V titanium alloy after impact by ABAQUS, optimize the architecture parameter of TiN/Ti anti-erosion coating. Due to wear resistance of titanium alloy is poor, Cai [20] research on the micro-cracks in fretting wear of Ti-6Al-4V titanium alloy, showed that the increase of load and displacement reduced the binding effect during fretting wear.

In summary, surface coating technology for repair of titanium alloys is an effective method, while the basic coating technology includes thermal spraying technology, such as HVOF (porosity: 1.6%-2%), cold spraying technology (porosity < 0.5 %), plasma spraying technology (porosity: 5%), arc spray (porosity: 10…20 %), etc. Comparative analysis of porosity, cold spraying technology has obvious advantages over other technologies; hence, the next focus is on cold spraying technology.

Table 1.3 – Comparative analysis of some thermal spray coating deposition techniques with CS [16]

Process	**Cold spray**	**HVOF**	**Plasma**	**Arc spray**
Bonding mechanism	Mechanical/ chemical	Mechanical	Metallurgical	Metallurgical

Table 1.3 continuation

Surface finish	< 1 μm	1.3-2 μm Ra	13 μm Ra	2 μm Ra
Surface finish	< 1 μm	1.3-2 μm Ra	13 μm Ra	2 μm Ra
Deposition rate	1…10 kg/h	1…5 kg/h	2…7 kg/h	5…60 kg/h
Deposition efficiency	< 95%	50…70 %	30…60 %	35…65 %
Wear resistance	50 mm^3	27 mm^3	10 mm^3	6 mm^3
Bond strength	30…40 MPa	30…70 MPa	30…55 MPa	20…30 MPa
Corrosion rate	0.25 mpy	3.5 mpy	1 mpy	2 mpy
Porosity	0.15 %	1.6-2 %	5 %	10…20 %
Oxygen content	0.25 %	3 %	9 %	5…15 %
Gas consumption	85 %	45 %	15 %	60 %
Power consumption	5…15 kw	1…2 kw	30…100 kw	5…10 kw
Powder feed rate	25…75 kg/h	25 kg/h	15 kg/h	125…150 kg/h
Spray velocity	At least 500 m/s	750 m/s	500…700 m/s	800 m/s
Feedstock	Metals, polymers, and composites	Metals and ceramics	Metals and ceramics	Metals and ceramics
Typical application	Friction, impact, Abrasion and corrosion	Friction, Abrasion and corrosion	Friction, impact, Abrasion and corrosion	Friction, impact, Abrasion and corrosion

1.3 The advantages to solve problem onto titanium surface by cold spraying technology

1.3.1 Cold spraying technology

Cold Gas Dynamic Spray (CGDS) was first developed by Papyrin [21] et al. in the mid-1980s at the Institute of Theoretical and Applied Mechanics of the Russian Academy of Science in Novosibirsk while working with tracer particles in supersonic wind tunnels [22]. Major innovative development began in the 1950s by Rochevill, using a gas flow at a velocity higher than those obtained with the existing methods at that time. The flow of gas through a nozzle called the De Laval Nozzle produces a

uniform thin coating [23–25]. The deposition during CGDS can be summarized into the molecular attraction between the surface deposit of the particles and the substrates and in-built deposit growth. At a supersonic velocity, particles impact and plastically deform on the substrate. The deformation process results in adhesion to the surface [26–31]. Compared with thermal spraying, since cold spraying is carried out at a lower temperature, the driving force for phase transformation is small, solid particles are not easy to oxidize, and the phenomenon of grain growth does not easily occur.

Because of the advantages of cold spraying [32], researchers [33–34] pay attention to it. Wong [35] indicates that high deposition efficiency (100 %) for titanium and copper. Cold spraying technology can deposit almost any powder materials, including pure metals such as Al [36], Mg [37], Ti, Zn, Cu, Ni, Ag, Co, Fe, Nb [38], Ta [39]; nonmetal such as ceramic, etc; Metallic alloys; composite coating, etc. It can also be directly sprayed mixed powder to deposit wear-resistant coatings; Chen [40] researches that Cu-Al2O3-Graphite Solid-Lubricating coatings are deposited by cold spraying. Results show the Cu-based solid-lubricating coating with 10% Al_2O_3 and 10% cu-coated graphite exhibited the lowest friction coefficient of 0.29.

Protective and restorative coatings on titanium alloy surfaces it is an effective way to reduce the cost of studying the repair of aircraft titanium alloys by coating technology. Through the repair technology of cold spray, which brings great economic benefits. A significant cost to the Department of Defense of the United States supply chain will be mitigated by Cold Spraying technology [4]. This dissertation takes aircraft Ti-6Al-4V alloy as an example and shows it is feasible to repair titanium alloy by cold spraying technology.

1.3.1.1 Cold spraying technological parameters

The cold spraying process has many parameters [41], including Powder size, morphologies and properties, if the powder size is too small (Fig. 1.1), the collision energy is insufficient to form effective deposition [45]

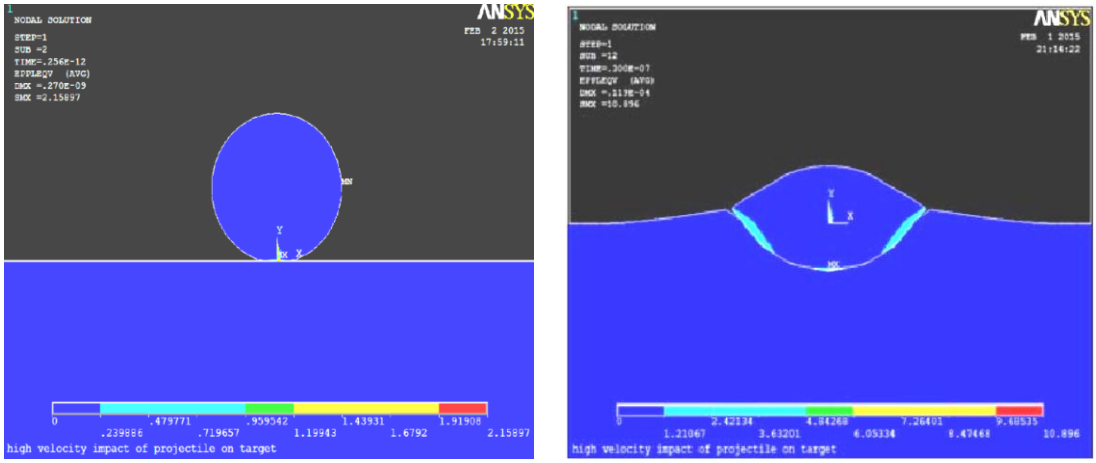

a *b*

a – size of 20 nm; *b* – size of 20 μm

Fig. 1.1. Particle sizes and substrate of plastic strain [45]

In the case of certain powder particles and substrate materials, only when the particle velocity reaches a certain value can the particles collide and deposit on the matrix to form a coating, which is called the critical velocity [42]; otherwise, the particles will produce shot peening or erosion on the matrix. When the particle velocity is less than the critical velocity, the particle is rebounded by the matrix and erodes. When the speed is greater than the critical speed, the coating can be deposited. When the particle velocity is much higher than the critical velocity, the particle erodes the substrate [43]. Compared with other thermal spraying processes, cold spraying mainly depends on the particle kinetic energy, rather than heat, cold and hot spraying powder particles mainly depend on whether form coating powder particles hit the speed of the substrate before, so when particles hit the matrix surface at different speed, the following happens: matrix rebound, deposition on the substrate or through the substrate [44].

Substrate preheating effects on the particle/substrate adhesion, Fig. 1.2 and Fig. 1.3 show that as the substrate temperature increases, decrease particle compression ratio and crater depth go up [46]; substrate surface roughness effects on particle/substrate adhesion; Substrate surface texturing effects on the particle/substrate adhesion; effects of nozzle unit design; characteristic of propellant gas, for instant, adding a small amount of helium to nitrogen can increase the exit

velocity of gases and particles, while avoiding the high cost of using only helium to accelerate [47].

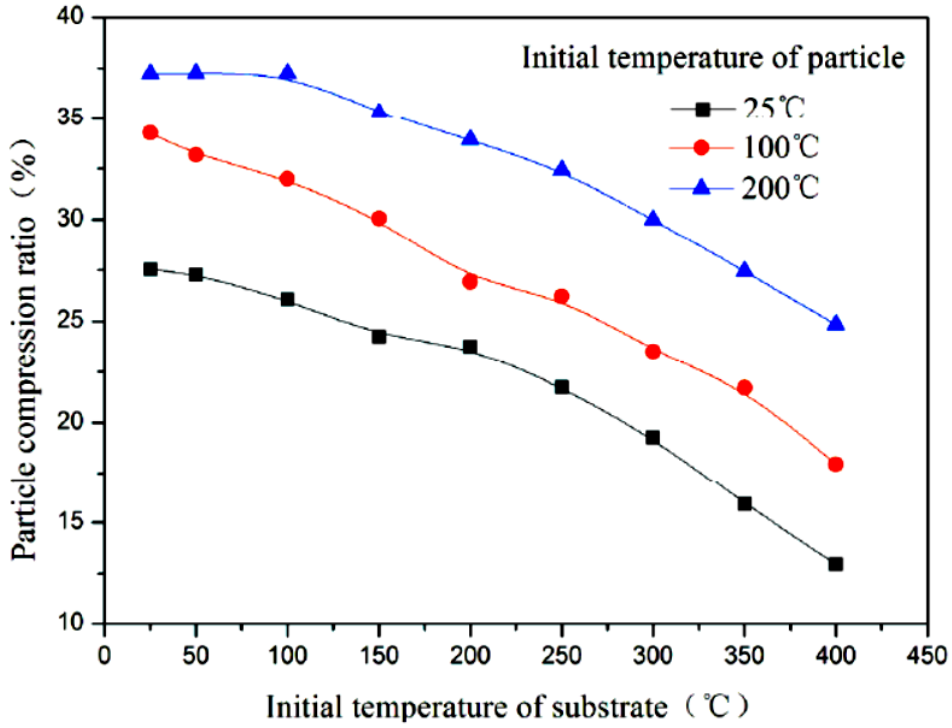

Fig. 1.2. Particle compression rate versus the initial temperature of substrate [46]

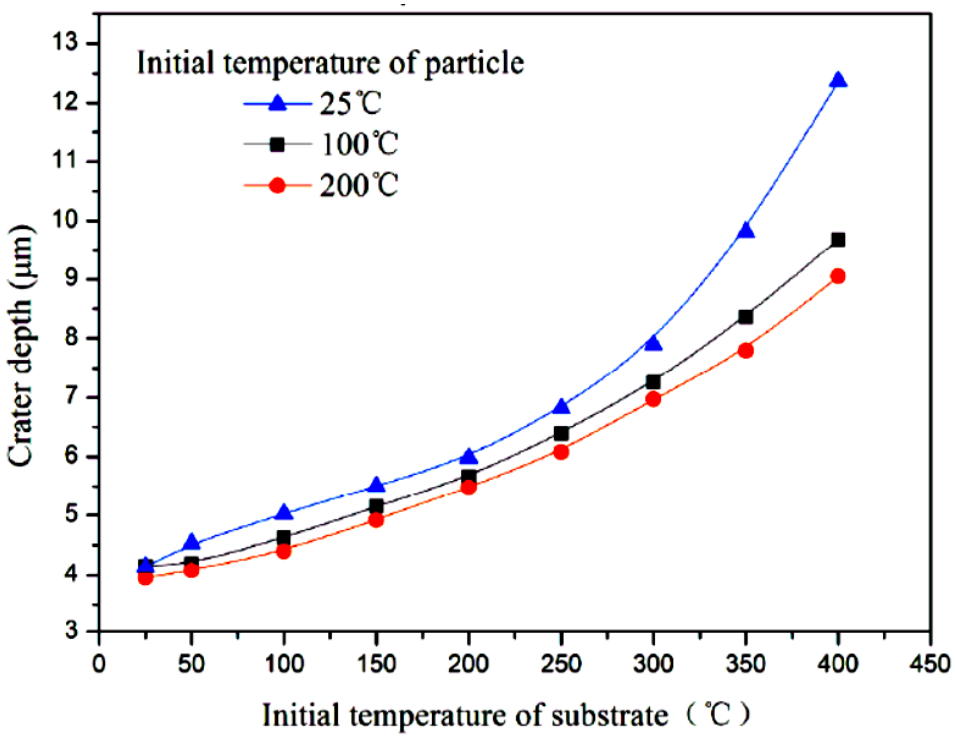

Fig. 1.3. Crater depth of substrate versus the initial temperature of substrate [46]

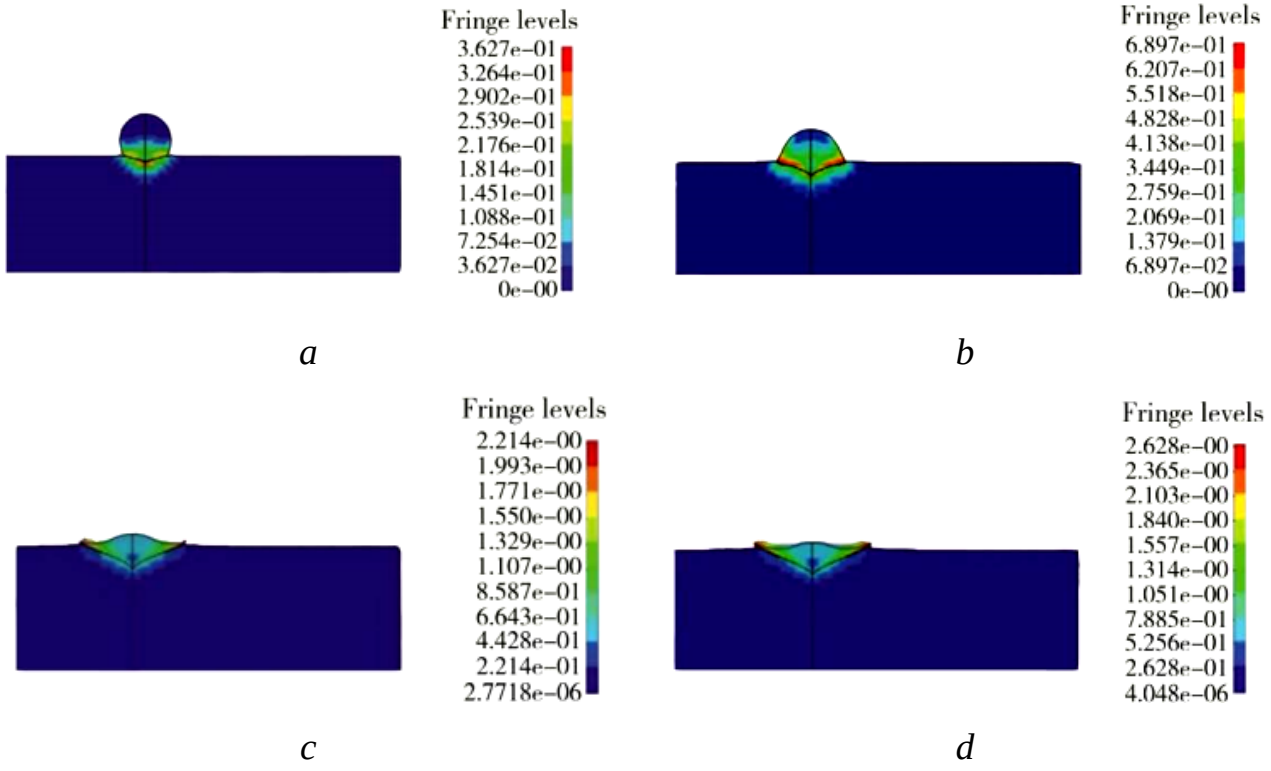

a – 500 m/s; *b* – 600 m/s; *c* – 700 m/s; *d* – 800 m/s

Fig. 1.4. Morphologies of the Ti-6Al-4V after colliding at different speeds [49]

The most important Cold spraying process parameters of titanium are critical velocity and temperature (Table 1.4). Critical velocity can be calculated by numerical simulation [48], beyond the limit of critical velocity, a further increase in particle velocity results in a decrease in deposit porosity. Han's [49] research on morphology characteristics of Ti-6Al-4V particles colliding with the Ti-6Al-4V substrate at different temperatures and velocities (Fig. 1.4) showed that both thickness and density of the coatings prepared increase as gas pressure increases. According to the analysis in Fig. 1.4, particles of 700 m/s and 800 m/s have a very strong plastic deformation, and with the increase of particle velocity, the plastic deformation does not increase significantly, indicating that Ti-6Al-4V particles have effective deposition above 700 m/s.

The work [50] showed that when the deposition efficiency was 50 %, the average velocity of the particle at the nozzle outlet was the critical velocity of the powder particle. The work [51] estimates the critical velocity by this method to be

690 m/s for angular titanium powder. Schmidt [52] reported a critical velocity of around 750 m/s for a 25 μm titanium particle. Wong [53] measured the critical velocity of spherical titanium powder between 505…610 m/s.

Table 1.4 – Details of process parameters

Particle	Ti	Ti	Ti	Ti
Substrate	Ti	Ti	Ti	Ti6A14V
Propellant gas	N_2	N_2	He	He
Particle diameter	29 μm	16-22 μm	16 μm	5-29 μm
Temperature (°C)	300-800	600	600	260
Pressure (MPa)	3.4	2.4	1.5	1.6
Nozzle throat diameter (mm)	-	-	-	3.8
Nozzle length	-	-	-	90 mm
Ref.	[54]	[55]	[56]	[56]

The temperature parameters of Ti and Ti-6Al-4V are as follows in Table 1.4; for different conditions such as particle, substrate, particle diameter, propeller gas, pressure, nozzle throat diameter, etc., the suitable temperature is also different, which ranges from 260 °C to 800 °C.

Other technological parameters, such as stagnation pressure (indoor pressure of spray gun), gas temperature, gas pressure, particle morphology, spray gun structure, spraying distance, angle and powder feeding speed, matrix temperature, etc., can affect the quality and performance of coating by affecting particle speed [57]. This section mainly studies the effects of technological parameters on coating deposition efficiency, porosity, hardness, bonding strength, corrosion performance, wear resistance and other coating properties.

Effect of process parameters on deposition efficiency and porosity.

Porosity is one of the important properties of the coating. The porosity of the coating formed by cold spraying technology is low because the coating is formed by

the stack of deformed particles. The particle speed of cold spraying is high, the deformation is sufficient, and the incomplete overlap between particles is reduced. In addition, the continuous impact of subsequent particles on the earlier coating greatly reduces the porosity of the coating [58]. The change of process parameters affects the particle velocity, and the particle collision velocity directly affects the deposition efficiency of particles. This is because cold spraying mainly relies on the strong plastic deformation caused by the high-speed impact of particles to deposit the coating. The higher the particle velocity is, the more dense and high quality the coating will be formed.

The work [59] studied the cold spraying of aluminium powder on a carbon steel matrix, and the research showed that the stagnation pressure, powder feeding speed and the relative movement speed of the substrate and spray gun had a certain influence on the deposition efficiency and porosity of the coating. Cold spraying aluminum coating, when the stagnation pressure (gun chamber pressure) increases, the porosity of the coating does not increase or slightly increase, but the deposition efficiency of the coating increases sharply. This is mainly because the stagnation pressure is the key factor of whether the particle can reach the critical velocity. Properly increasing the stagnation pressure is conducive to improving the particle velocity, so as to strengthen the impact effect and improve the deposition efficiency of the coating. The deposition efficiency of the coating decreases with the increase of the powder feeding speed. This is because the interaction of particles in the nozzle is enhanced when the powder feeding rate is too high. The particles may melt and bond in the nozzle due to the rising temperature of friction, which affects the velocity of particles in the nozzle and further affects the deposition efficiency. When the relative movement velocity of the substrate and spray gun increases, the deposition efficiency decreases. This is because if the relative movement velocity of the substrate and spray gun is too fast, particles cannot effectively deposit on the substrate to form coating, and the effective deposition time is short, thus affecting the deposition efficiency and porosity of the coating.

The spray distance is directly related to the deposition efficiency because the

size of the spray distance affects the vertical velocity of the sprayed particles when they reach the substrate surface. After the supersonic two-phase flow leaves the nozzle, due to the influence of external factors, the particle velocity will change, and the deposition efficiency can be effectively improved only by selecting the appropriate injection distance. If the spraying distance is too large, the particles cannot reach enough kinetic energy to form the coating, so the deposition efficiency will be reduced. If the injection distance is too small, the particles will be affected by the shock wave forming in the impact area between the matrix and the spray gun, which will reduce the particle velocity and deposition efficiency. The work [60] also found a similar phenomenon. As shown in Figure 2, when the injection distance is less than 60 mm, the deposition efficiency increases with the increase of the injection distance because with the increase of the injection distance, the shock wave gradually weakens, and the particle velocity can be effectively improved. In the range of 60~120 mm, the deposition efficiency can be further improved, because when the gas velocity is higher than the particle velocity, the particle can still accelerate to the critical velocity without being hindered by the shock wave. When the injection distance is greater than 120 mm, the gas velocity is lower than the particle velocity, the particle slows down, and the deposition efficiency decreases significantly.

The work [61] shows that the average particle size and morphology of particles will affect the particle velocity and thus affect the deposition efficiency. Under the same conditions, the velocity of irregular particles is higher than that of spherical particles. For irregularly shaped particles, the particle velocity decreases with the increase in particle size, and the critical velocity also decreases. After pretreatment, the critical velocity of particles decreases. B. Doin et al. [62] also found a similar phenomenon, within the range of average particle size less than 25 μm, the particle distribution was not affected, but the velocity of non-spherical particles was higher than that of spherical particles of the same size. Under the same conditions, the particle velocity decreases with the increase in average particle size. For larger particles, the particle morphology has a significant effect on the particle velocity.

Since the deposition efficiency is directly related to the particle velocity, the higher the particle velocity, the higher the deposition efficiency.

Influence of process parameters on coating hardness and bonding strength.

Hardness and bonding strength are important performance indexes to measure the quality of the coating, which reflects the mechanical properties of the coating. Wang Jiajie and others using the method of cold spraying deposition Cu coating on Q235 steel substrate [63-64], the paper analyses the characteristics of the coating and indicate that the average micro-hardness of Cu coating is higher than the as-cast of pure copper, this is because the high-speed impact happened a lot of Cu particles and matrix is strong plastic deformation and subsequent particle coating too early to have compaction effect, and Cu coating stress is mainly compressive stress. Therefore, the bonding strength has been greatly improved.

The work. shows that with the increase in gas temperature, the binding rate of particles increases, and the coating is denser. This is because increasing the gas temperature can increase the velocity of particles but also can improve its temperature, which is conducive to the plastic deformation of particles more easily; deformation is more sufficient, reducing the incomplete overlap between particles so as to obtain a denser coating.

The work [65] shows that the compactness of the coating increases with the increase of gas pressure, and the bonding strength between the coating and the matrix is also improved. This is because the increase of gas pressure can improve the particle velocity, which is conducive to the plastic deformation of powder. However, if the gas pressure is too large, the powder rebound phenomenon is serious but not conducive to spraying. The work [66] prepared pure copper coating on a stainless-steel substrate by cold spraying technology and tested the hardness with a micrometre. The results showed that the hardness distribution was very uniform, and the average hardness of the coating was higher than that of the as-cast pure copper. This is because the particle's high-speed impact matrix produces strong plastic deformation and causes work hardening so that the coating is hard. The work

[67] studied the effect of different gas pressures on aluminium spray coating hardness, indicating that gas pressure on the hardness of cold sprayed aluminum coatings has a significant effect, low gas pressure under the condition of the coating hardness of the high-pressure coating high hardness, this is due to the low gas pressure, the lower speed of aluminium particles rebound phenomenon, and grain of zi chan at a high speed impact effect, work hardening, is beneficial to improve the hardness of the coating.

The work [68] studied Al-Cu-Mg-Fe-Ni-Sc coating by cold spraying method. After preheating treatment, the hardness of the coating was not improved but softened, which was mainly related to the formation of Al7FeCu2 precipitate, which consumed the Fe matrix, especially the main content of Cu and aluminum alloy. The desired strengthening effect of scandium (Sc) does not overcome softening as the required strengthening phase is reduced. The work [69] also showed a similar phenomenon: Fe coating was prepared on Al substrate by cold spraying, and the hardness of the coating was higher than that of pure Fe. If the Fe coating was heat treated at a lower temperature, the microstructure of the Fe coating did not change significantly, and the microhardness decreased significantly. This is due to the hardening of the coating in the process of cold spraying, the hardness of the coating being higher than that of pure Fe material, and after heat treatment, the hardening effect disappears, so the hardness is significantly reduced.

Influence of technological parameters on other properties of the coating.

Because cold spraying technology is carried out at a lower temperature, the surface coating applied can improve the surface properties of materials, such as wear resistance, corrosion resistance and mechanical properties of materials, and improve the quality of products without changing the structure and properties of materials [70]. Cold spraying coating, compared with thermal spraying coating, has great advantages, such as high-speed impact plastic deformation and avoiding the coating crack and deformation. Because the process is not from molten state volume contraction, it reduces the porosity inclusions, and the coating mainly bears

compressive stress, so the formation of the coating is dense, has low porosity, and the coating is thick and can improve the wear resistance of the matrix.

The work [71] showed that cold spraying technology was used to spray Al-Zn alloy powder onto the magnesium alloy surface to obtain a dense coating. Magnesium alloy with Zn-Al coating had higher wear resistance. The work [72] sprayed Al-al2o3 powder on the AZ91E matrix by cold spraying, and the results showed that the corrosion resistance of Al-al2o3 coating was similar to that of aluminium alloy but significantly better than that of the AZ91E matrix. Cold spraying coating has some other excellent performance, such as the coating can improve fatigue resistance, thermal conductivity, residual stress reduction, etc.

1.3.1.2 The key structure problem statement of the cold spraying system

The critical core component of the cold spraying system is the nozzle. Since the early nozzle structure comes from the rocket tail nozzle, most cold spraying nozzles adopt a circular section [72]. In recent years, researchers have studied different types of nozzles for different applications. However, most researchers focus on straight-line nozzles (connecting lines from nozzle inlet to nozzle outlet center). In paper [73], a nozzle was proposed that can adjust the powder feeding position to improve the deposition efficiency of powder and increase the particle temperature. The powder is mixed in the early stage of the divergent nozzle section to adjust the contact time between powder and fluid. A higher temperature is transmitted to the powder material to obtain the required coating. All of these nozzles are limited by limited space. Therefore, it is necessary to develop a cold spraying nozzle that can meet small space needs and be convenient to operate. In addition, the circular nozzle is inefficient for small rotating parts in practical engineering applications, and the rectangular section nozzle can reflect its advantages [74]. Hence, it is necessary for the square nozzle with a 90° angle to research.

The powder injection port of the cold spraying nozzle will affect the airflow

and affect the powder flow trajectory. The work [75] presents a straight nozzle with the same diameter as the outlet. Although the airflow speed has been improved and powder diffusion has been prevented since the movement track of powder particles has not been studied, the powder may collide with the inner wall of the outlet. The literature [76] presents a hand-held CS gun, and the work [77] researched a short nozzle with a total length of less than 70 mm. It solves the problem that the length is too large to be convenient for spraying, but it can still be further optimized if the diverging section is designed at 90°. The work [78] presents a stepped circle shape, mainly considering the convenience of processing. The fluid analysis results show that the maximum powder velocity is not at the nozzle outlet but at the throat, and the length of the nozzle still limits further application. The work [79] solved the problem of pressure transient imbalance during powder injection but increased the processing difficulty and production cost.

A way to overcome these difficulties is to design the divergence section to be 90°. The work [80] presents the results of the airflow trajectory of the three channels. The parameter field from the nozzle to the substrate is obtained, but the airflow in the nozzle is not uniform, which leads to the low application range of powder particles. This may be because the transient pressure is caused by the pressure of the powder injection port, and the pressure of the gas inlet is unbalanced. The authors suggest that the solution reduces the pressure in the internal channel where the powder is injected. The author has conducted a preliminary study on the nozzle with angle, but the too-long divergence of the nozzle still limits the spray area and makes it challenging to operate [81], so the divergence length needs to be further shortened. All this suggests that it is advisable to research multi-channel cold spraying nozzles. A multi-channel special nozzle is also the focus of this dissertation

1.3.2 Deposition of wear-resistant coating by CS

For the wear resistance of the titanium alloy substrate surface, cold spray technology [82–88] has obvious advantages over thermal spray technology. This is mainly manifested in (1) the low-temperature process of the cold spray process, which is suitable for titanium alloy heat-sensitive materials, (2) high deposition efficiency, (3) low porosity, etc.

Titanium alloy has poor surface wear resistance [89], but it is very expensive and requires long delivery periods, which require repairs such as wear and impact damage during service. Zhang researcher [90] has studied the wear resistance characteristics of titanium alloy. Cold spraying technology stands out among many other technologies because of its low oxidation. The deposit of Ti and titanium alloy coatings by cold spray technology may also protect substrate materials from wear, especially in aggressive environments [91].

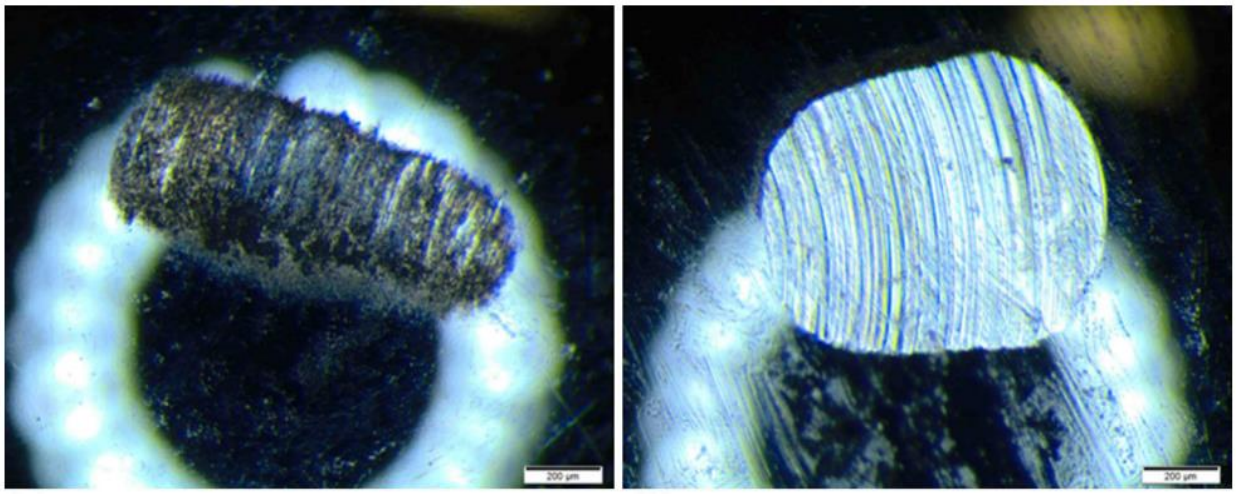

a *b*

a – Ti64 substrate; *b* – Ti coating with a thickness of about 6200 μm.

Fig. 1.5. Optical microscope images showing wear morphologies of counter steel balls tested against [92]

Khun [92] researched Ti coating on a Ti-6Al-4V substrate. The average friction coefficients of the Ti coatings with thicknesses of about 100, 700, 1000, and

6200 μm are about 0.72, 0.74, 0.71, and 0.61, which shows that the Ti-6Al-4V substrate has a larger wear track than the Ti coatings (fig. 1.5), confirming that the Ti coatings have the higher wear resistance. Fig. 1.6 shows the wear topographies and morphologies of the Ti-6Al-4V coating deposits on the Ti-6Al-4V substrate, which is very obvious about abrasive particles in the process of wear [93].

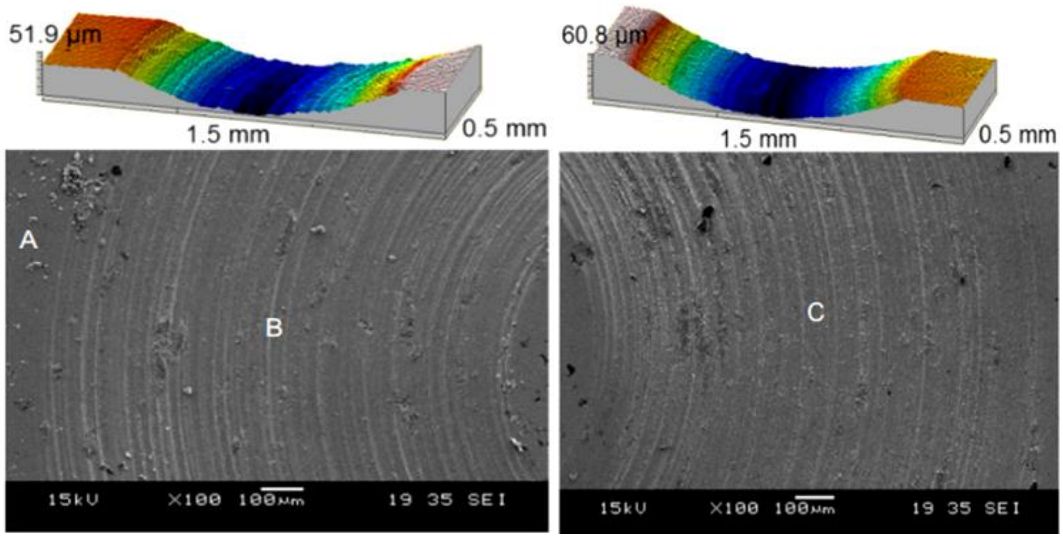

a *b*

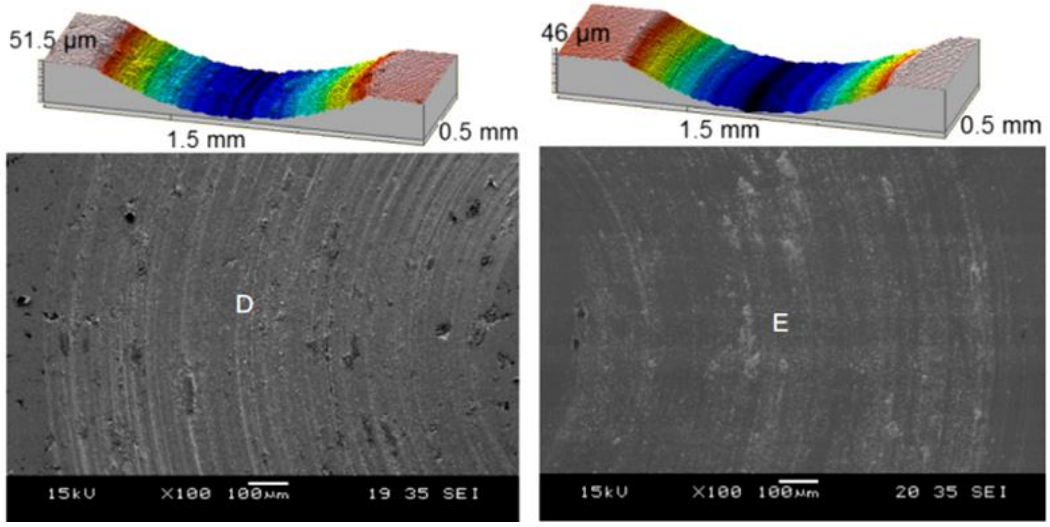

c *d*

a – surface of the first layer; *b* – surface of the second layer; *c* – surface of the third layer; *d* – cross-section

Fig. 1.6. Wear topographies (above) and morphologies (below) of Ti-6Al-4V deposit tested under the same condition [93]

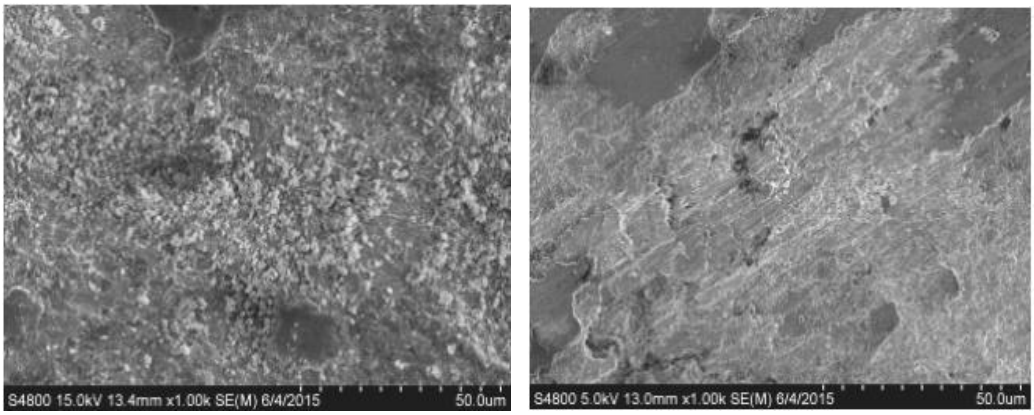

a *b*

a – Ni-cBN (6.2 μm); *b* – Ni-cBN (10 μm)

Fig. 1.7. The morphology of Ni-cBN coatings prepared by different size cBN [94]

Ning [94] prepared Ni-cBN composite coating on Ti-6Al-1.5Cr-2.5Mo-0.5Fe-0.3Si substrate by low-pressure cold spraying. The results showed that the binding strength (58 MPa ± 8 MPa) of Ni-cBN composite coating prepared by larger size cBN (10 μm) was significantly higher than that of the coating prepared by smaller size cBN (6.2 μm) (20 MPa ± 1 MPa), resulting in more severe wear in Fig. 1.7a than in Fig. 1.7b.

Cold spraying technology can also be used in combination with other technologies to produce wear-resistant coatings. Zhang [95] utilized cold spraying technology to prepare the TiAl gradient coating on the surface of titanium alloy by controlling the mixing ratio of aluminium and titanium powder and treating the coating surface with chemical technology to achieve the dual purpose of wear resistance and insulation; the hardness value reached 600HV.

The wear resistance of laser-treated (fig. 3b) Ti-6Al-4V deposit is better than that of the untreated (fig.1.8a) Ti-6Al-4V deposit by laser technology [96]. Li sprayed H13 powder on the surface of titanium alloy to form an H13 coating with a thickness of 50~105 um and then used laser cladding technology to fuse cobalt metal powder on the surface of H13 (Fig. 1.9). Bonding strength of the coating and matrix is up to 55 MPa. Coating thickness is 4.1 mm, hardness reaches 1117.21 $HV_{0.2}$, porosity is 0.61 %, and the friction coefficient is 0.18 [97]

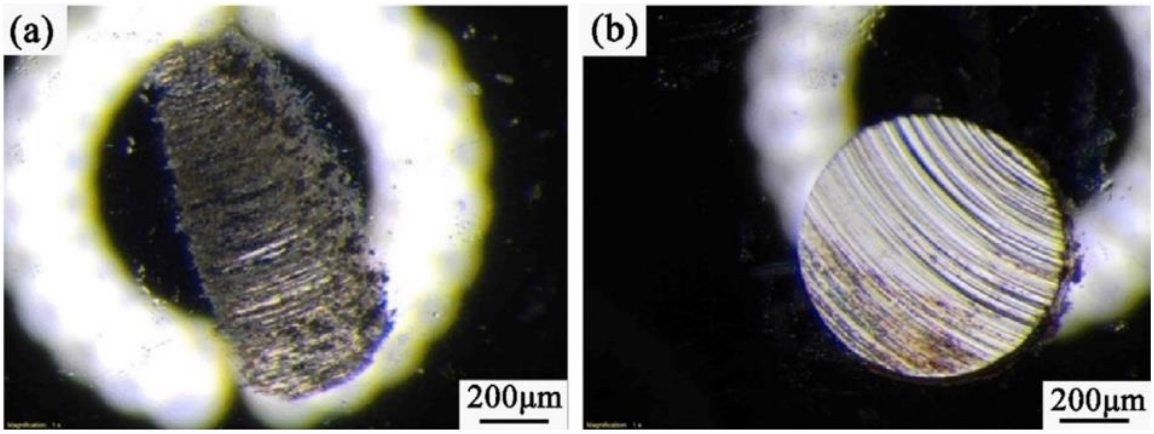

a – without treatment; *b* – treatment with laser of powder 200W [96]

Fig. 1.8. Wear microtopography of 100Cr6 steel balls rubbed on Ti-6Al-4V deposits

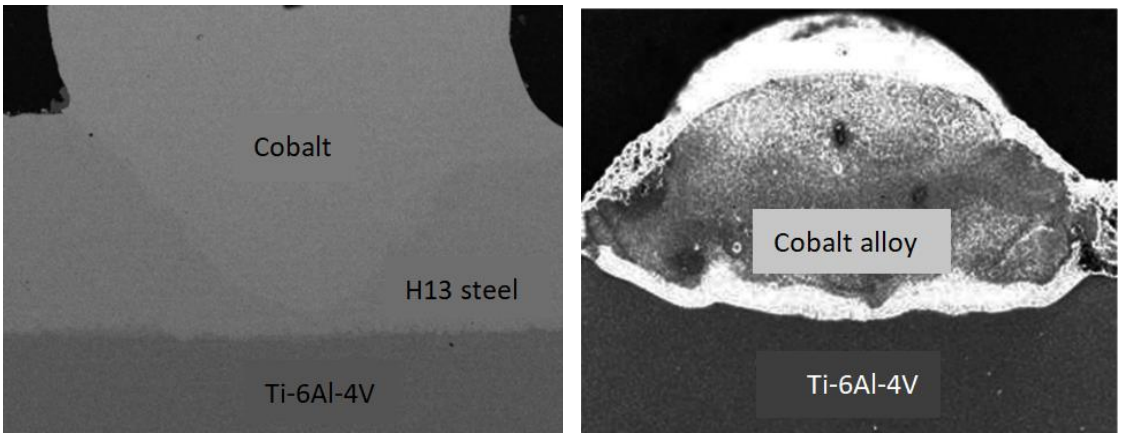

a *b*

a – CS + Cladding technology; *b* – Only Cladding technology

Fig. 1.9. Scanning electron microscope [97]

From the analysis above, different coating materials can be selected for different titanium alloy substrates. Such as Ti-6Al-4V substrate, the average friction coefficients of Ti coatings with thicknesses of 6200 μm are best, up to 0.61; Ti substrate, microhardness of the SiC composite coating was increased to (125 ± 17.75) $HV_{0.3}$; Ti-6Al-1.5Cr-2.5Mo-0.5Fe-0.3Si substrate, binding strength of Ni-cBN composite coating reached (58 MPa ± 8 MPa). However, most studies focus on Ti-6Al-4V matrix materials, and other titanium alloy matrix materials need to be studied.

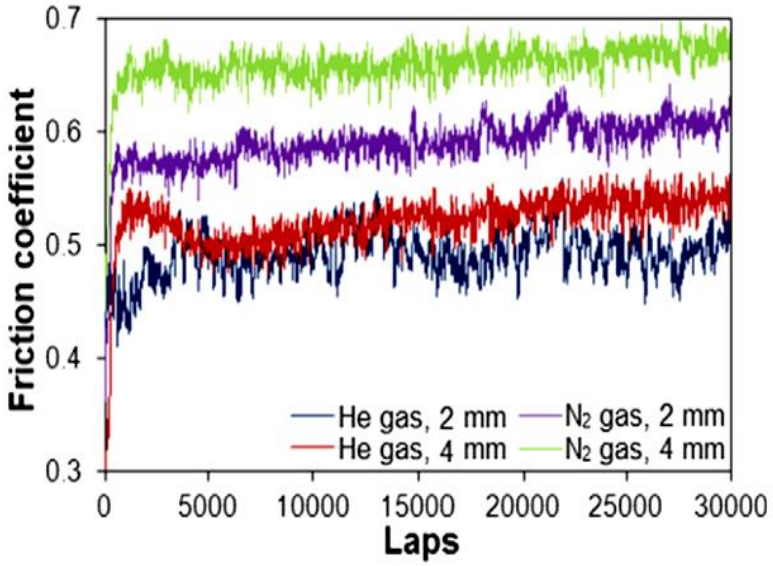

Fig. 1.10. Friction coefficients of Ti-6Al-4V deposits as a function of wear lap. Note that friction coefficients were tested against a 100Cr6 steel ball of 6mm in diameter in circular paths for 30,000 laps at a sliding speed of 3 cm/s under a normal load of 1N [98]

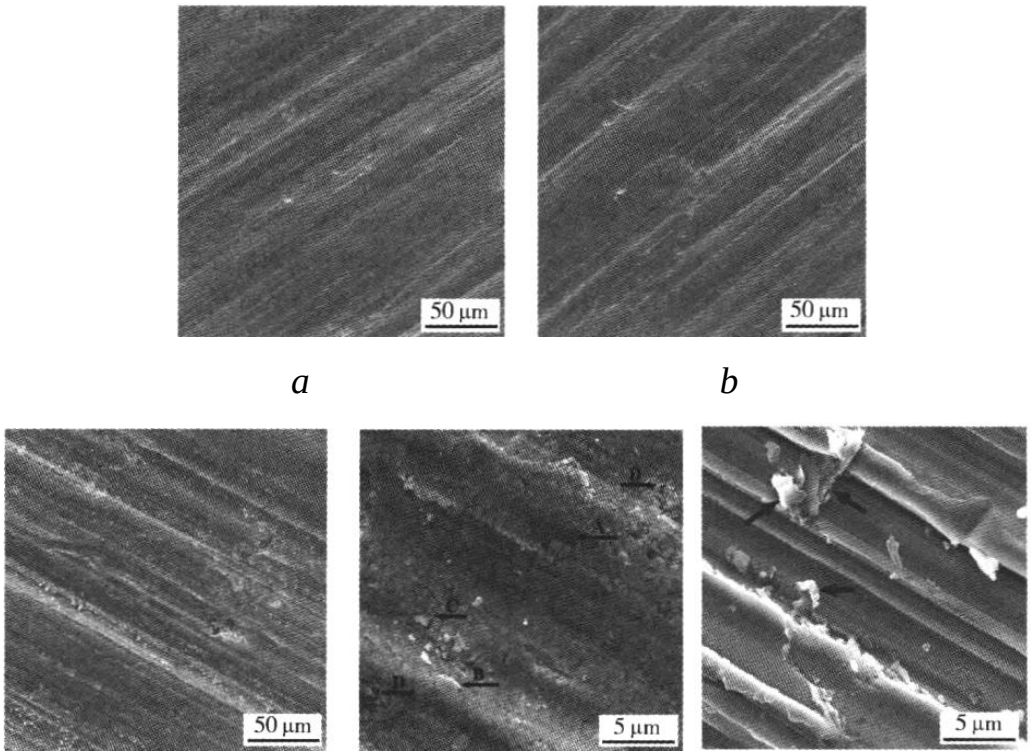

a – WC-12Co; *b* – WC-10Co-4Cr; *c* – WC-17Co; *d* – WC-17Co; *e* – 316L

Fig. 1.11. Worn surface morphologies of cold sprayed multiple dimensioned WC-Co coating and 316L stainless steel [99]

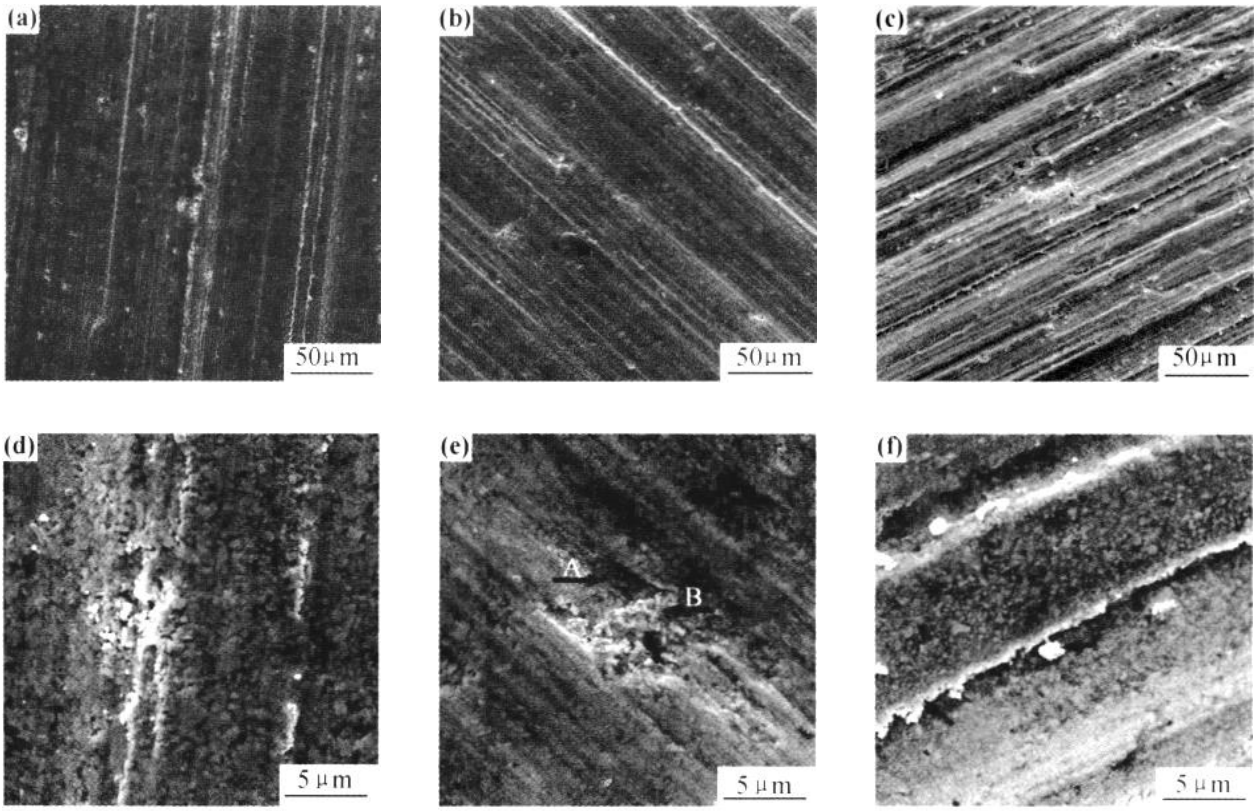

a – micrometer WC-12Co; *b* – nanmeter WC-17Co; *c* – nanometer WC-23Co; *d* – micrometer WC-12Co; *e* – nanmeter WC-17Co; *f* – nanometer WC-23Co.

Fig. 1.12. Wear morphologies of the cold-sprayed WC-Co coatings [100]

Fig. 1.10 shows the friction coefficients of Ti-6Al-4V deposits produced with nitrogen and helium [98]. Obviously, under the same conditions, the friction coefficient of helium gas is lower than that of nitrogen gas, indicating that the friction performance of helium gas as a propellant is better.

Through investigation, WC-Co is a potential wear-resistant coating material of titanium alloy substrate because of its superior wear resistance properties. Wang [99] studied the cold spraying coating experiments of three materials (fig. 1.11): micron WC-12Co, nanometer WC-17Co and WC-23Co, and made a comparative analysis with 316L stainless steel, indicating that WC-Co coating has excellent wear resistance.

Further research on the nanometer WC-Co coating was prepared by cold spraying technology [100] and the wear resistance experiment was conducted on three materials (Fig.1.12): WC-12Co, WC-17Co and WC-23Co. It showed that the

microhardness of WC-17Co was the highest, about 1500HV0.3, and the wear resistance of the coating was the best, which was 11 times that of 316L stainless steel.

1.3.3 Deposition of the restorative coating

Cold spraying is a very good method to repair titanium alloy; the heat effect of the parts is small, compared with other thermal repairs, which has a great advantage, especially for heat-sensitive materials [101].

Jin Lei [102] utilizes Ti-6Al-4V, Ti and Al_2O_3 mixed powder on the damaged surface of Ti-6Al-4V titanium alloy thin wall plate to get the repair coating by cold spray. The repair coating has good characteristics.

Ogawa [103] used Al and its alloy coating to repair parts in the space shuttle solid-fuel rocket boosters and aircraft structures. The United States Army Research Laboratory [104] also used cold spraying technology to repair the magnesium alloy crankcase shell of the helicopter.

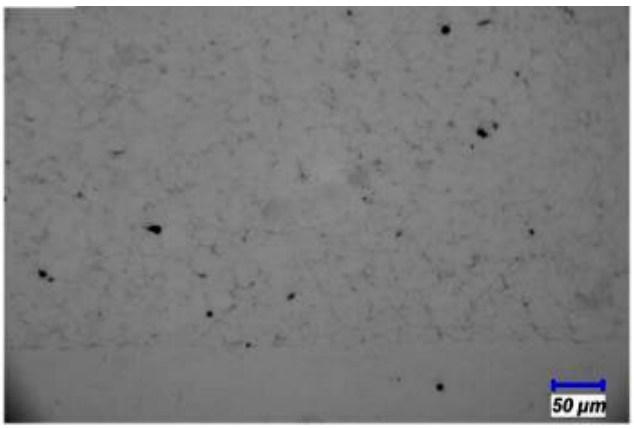

Fig.1.13. Example of Simulated damage repair of Ti-6Al-4V with repair microstructure under an optical microscope [105]

Jean-Louis [104] Pelletier provided a simulation about Ti-6Al-4V coating onto Ti-6Al-4V substrate using low-pressure cold spray. Simulated damage repair was successful, and the coating quality had no major effect. This phenomenon is associated with the high velocity of the particles hitting the substrate and the non-recovery of the dislocations. Such strain hardening increases with the degree

of particle deformation. So, Ti-6Al-4V alloy parts could be repaired efficiently by producing Ti-6Al-4V coating on a machined flat surface or with a 10 to 1 slope (6 degrees) or less. As Fig. 1.13 and Fig. 1.14 show, the interface between the coating and the substrate is very tight. The black dark area is the coating porosities [106]; porosity is found to be 2.69 ± 0.28%.

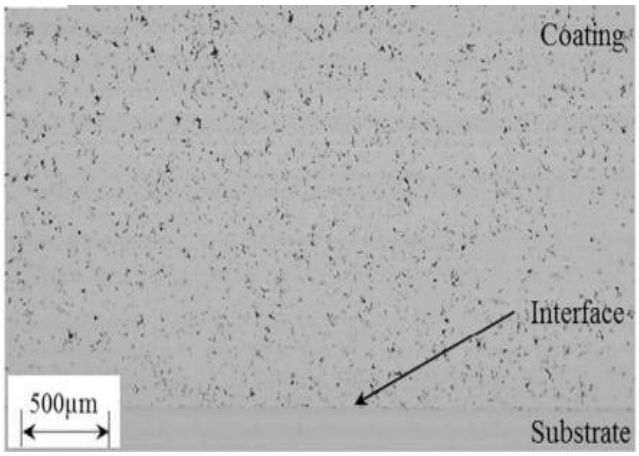

Fig. 1.14. Cold spray deposit, substrate and the interface, and the dark areas in the coating porosities [106]

Cao Congcong's [107] research on Ti-6Al-4V (Fig. 1.15) coating was deposited by cold spray on surfaces of Ti-6Al-4V substrates, showing higher micro-hardness, better-bending property, smooth fractured surface characterized by a brittle fracture with no phase change happened, which confirmed the feasibility of repairing titanium alloy components by cold spray technique.

Ti-6Al-4V particles deposited on Ti-6Al-4V substrate, mainly by mechanical combination, forming a dense coating (Fig. 1.15a). The interface between particles and particles in the coating is closely bonded and mainly combined by metallurgy, with some small pores (Fig. 1.15b).

As Fig. 1.16 shows, the Lagrange finite element method was to observe the obvious mechanical locking at the contact [108] surface between titanium particles and aluminium matrix. This shows that aluminum and titanium materials have good bonding characteristics by cold spraying technology.

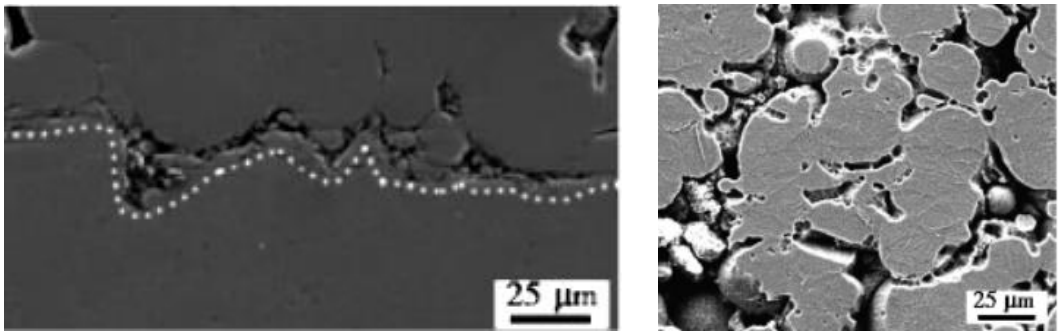

a *b*

a – coating cross-section, *b* – the microstructure

Fig. 1.15. Ti-6Al-4V/Ti-6Al-4V coating [107]

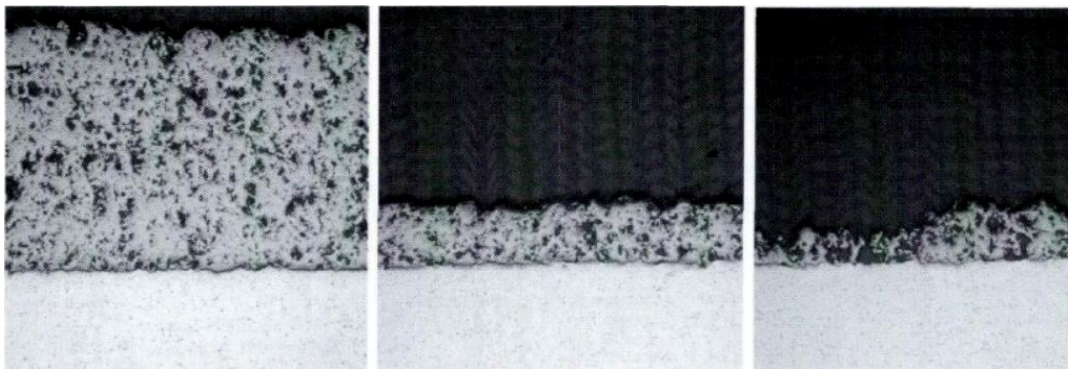

a *b* *c*

a – 90°; *b* – 75°; *c* – 60°

Fig. 1.16. Cross-sectional OM micrographs of the cold-sprayed titanium coating depositing aluminum substrate at different spray angles [108]

Based on the above analysis, it can be concluded that:

1) it has obvious advantages to repair the surface of Ti alloy parts by cold spraying technology;

2) on Ti-6Al-4V substrate, utilize Ti-6Al-4V as cold spraying coating, with an average porosity of 8 % and a hardness of up to 300 MPa. Under the condition of nitrogen temperature of 600 °C and pressure of 3 MPa, TC_4 coating with a porosity of 6.46 %;

3) the repair surface of Ti-6Al-4V titanium alloy can be chosen from the Ti-6Al-4V, Ti, and Al materials mixture, which are mechanically combined with good bonding performance. Repair coating material composition: Ti-6Al-4V is 40%~70%,

Ti is 29%~50%, Al_2O_3 is 1%~10%, the matrix temperature of Ti-6Al-4V titanium alloy is less than 150 °C, the pressure of He work gas is 0.6~1.0 MPa, spraying temperature is 300 °C~600 °C, spraying distance is 10~30 mm. The porosity of the repair coating is 0.1 %, and the hardness of the repair coating reaches 1147 $HV_{0.3}$.

1.3.4 Additive manufacturing of titanium alloy parts

Cold spraying technology has high deposition efficiency, low working temperature and compressive stress of the coating, which can be used to prepare large-thickness coatings. On this basis, at the end of the 20th century, some foreign researchers tried to use cold spraying to manufacture metal components and found that it has great potential in preparing Ti alloy components [109]. At present, with the further development of cold spraying technology, more and more research began to pay attention to the remanufacturing function of cold spraying. Cold spraying is evolving from a surface spraying technology to a new additive manufacturing technology. Jahedi et al. [110] prepared Ti alloy components by cold spraying technology and compared it with several other preparation processes. The results showed that cold spraying Ti alloy components with high efficiency, low oxygen content and excellent mechanical properties can be used for near net forming of Ti alloy. Pattison et al. [111] deposited a variety of metal parts by cold spraying technology. Figure 1.17 shows the Ti-6Al-4V alloy parts prepared by cold spraying. The powder feeding rate is 5 kg/h, which can be formed in a short time [112].

1.4 Conclusion of Chapter 1

This chapter summarizes the application of titanium alloy in the field of aerospace, analyzes the urgent problems of titanium alloy materials, and recommends the methods and principles of cold spraying technology to solve these problems. Finally, in order to facilitate spraying in limited space and convenient operation, the key structural problems of cold spraying technology are stated, and solutions are proposed.

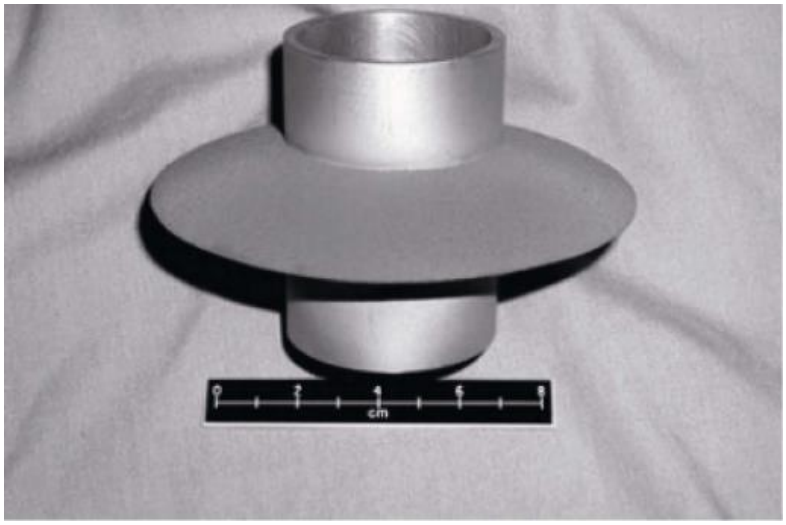

a

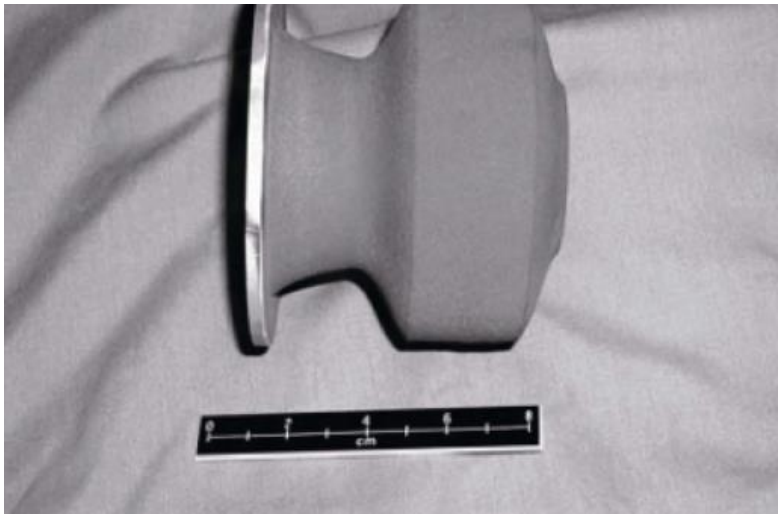

b

a – pipe component; *b* – Axisymmetric parts

Fig. 1.17. Cold-sprayed Ti-6Al-4V components

1. Titanium alloy is a heat-sensitive material, which has poor resistance to abrasive wear for rotating or rubbing aerospace components. Cold spraying technology is suitable for the surface of titanium alloy wear-resistant coating.

2. We can emphasise the group of recommended powders for aircraft titanium alloys by cold spraying, including Ti-6Al-4V, Ti, Al, Al_2O_3, steel, Nickel, etc. Cold spraying technology can be sprayed on almost any material, including Al, Zn, Cu, Ni, Ti, Ag, Co, Fe, Nb, super alloy and high hardness ceramic-metallic coatings, ceramic

coatings and organic coatings.

3. There are few studies on the wear resistance characteristics of titanium alloy substrates using cold spray technology. At present, most researchers only focus on Ti-6Al-4V alloy, and further research is needed for other titanium alloys. Such as the abrasive resistance of Ti-6Al-4V coating sprayed onto the Ti-6Al-4V substrate by CS is better than Ti coating; the main reason is that the porosity of the titanium coating is larger than that of Ti-6Al-4V, hence, reducing porosity is the future research focus of cold spray wear resistant coatings. In addition, the combination of cold spray technology and other technologies, post-treatment of the cold spraying process, is also a future trend that needs to be solved. for example, on Ti-6Al-1.5Cr-2.5Mo-0.5Fe-0.3Si substrate, deposited Ni-cBN composite coating, using the 10 μm size of cBN, the bonding strength is (58 ± 8 MPa) after 600 °C heat treatment conditions.

4. Cermet not only has the toughness, high thermal conductivity and good thermal stability of metal but also has the characteristics of high-temperature resistance, corrosion resistance and wear resistance of ceramics. Cermets are widely used in rockets, missiles, supersonic aircraft shells, and flame nozzles in combustion chambers. The WC-Co in this article is a typical cermet material with a very good surface wear-resistant material， for example， wear- the resistant coating of WC-Co is directly prepared, the microhardness of WC-17Co is the highest, about 1500 $HV_{0.3}$, and wear-resistant performance of a coating is the best, which is 11 times that of 316L stainless steel, however, the porosity of the WC-Co coating directly prepared by cold spraying technology is about 1.2 %, hence, how to reduce the porosity and use it to spray on the titanium alloy surface to obtain the best physical properties is the content of further research.

CHAPTER 2

STRUCTURAL AND TECHNOLOGICAL PARAMETER OPTIMIZATION OF THE SPECIAL CS NOZZLE WITH 90° ANGLE

2.1 Theoretical study

Before designing the special nozzle, some factors that influence gas should be considered, for example, dimensional steady flow, the effect of section size, mechanical condition of the nozzle, gas thermodynamics, etc. Then, consider the case of powder injection. For the special multi-channel nozzle, this dissertation summarizes some of the factors that influence particle collisions to design step by step, as shown in Figure 2.1.

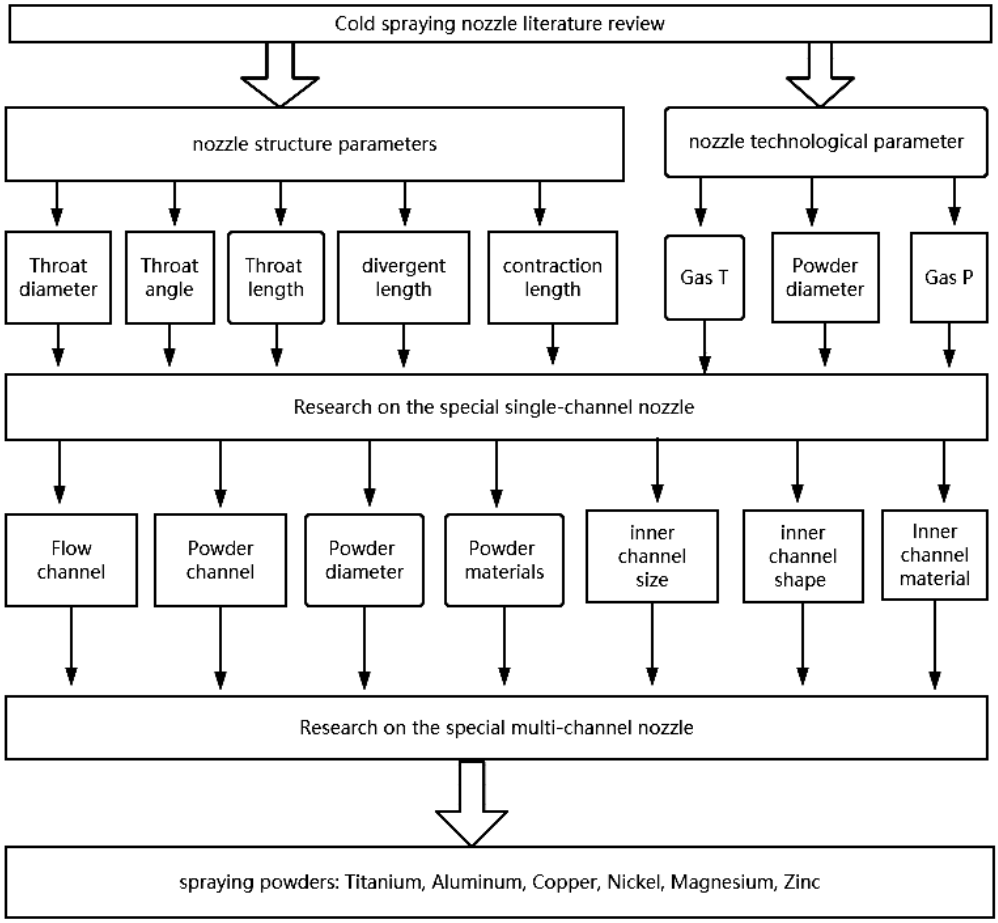

Fig. 2.1. Multi-channel nozzle research idea diagram

2.1.1 One dimensional steady flow

The gas flow in a supersonic nozzle is compressible and non-isentropic. In order to simplify the research process, the gas flow in the nozzle is usually regarded as a one-dimensional steady isentropic flow with a variable cross-section without viscosity and friction. Such flow only needs to pay attention to the factors of cross-section change, ignoring other factors such as gravity. Therefore, this flow is adiabatic and frictionless, and its flow model is shown in Fig. 2.2:

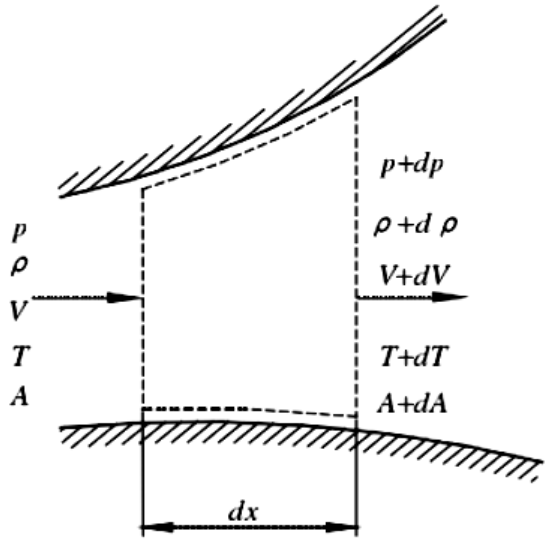

Fig. 2.2. Flow model

$$m = \rho V dV; \tag{2.1}$$

$$dp + \rho V dV = 0; \tag{2.2}$$

$$d(h + 1/2V^2) = 0, \tag{2.3}$$

where ρ – gas density;

P – gas pressure;

A – cross-sectional area;

V – gas velocity.

2.1.2 Effect of nozzle section size

The supersonic nozzle is a channel through which gas velocity increases and

pressure decreases. Fluid in the nozzle can be regarded as one-dimensional moisture flow, and fluid can be regarded as continuous. The continuity equation of flow [113] is as follows:

$$\rho VA = \text{constant} . \tag{2.4}$$

Take the logarithmic differentiation of the continuity equation (2.4), get：

$$\frac{dA}{A} + \frac{d\mathrm{v}}{\mathrm{v}} + \frac{d\rho}{\rho} = 0. \tag{2.5}$$

The non-viscous air flows along the flow in the micro-element pipe and flows through the length of dx. The flow velocity increases from V to V + dV, and the pressure increases from P to P +dp, and the momentum equation in the steady pipe is obtained:

$$\iint_{A_2} \nu_2 \rho \nu_{2\mathrm{n}} \mathrm{d}A - \iint_{A_1} \nu_1 \rho \nu_{2\mathrm{n}} \mathrm{d}A = \Sigma F. \tag{2.6}$$

Differential form of momentum equation:

$$\rho \mathrm{v} d\mathrm{v} = -\mathrm{d}p . \tag{2.7}$$

Introducing the Mach number M=V/c as the characteristic parameter, where the speed of sound $\mathrm{c} = \sqrt{VRT}$, the differential equation can be obtained:

$$\frac{dp}{p} = -\frac{\rho}{p} v dv = -\gamma M^2 \frac{dv}{v} . \tag{2.8}$$

Take the logarithmic differentiation of the isentropic flow equation $P\left(\frac{1}{\rho}\right)^{\mathrm{r}} = \text{constant}$, and work out its differential equation as:

$$\frac{dp}{p} = \gamma \frac{d\rho}{\rho}. \tag{2.9}$$

Take the logarithmic differentiation of the ideal equation of state $\frac{P}{\rho} = RT$, and its differential equation is:

$$\frac{dp}{p} = \frac{d\rho}{\rho} + \frac{dT}{T}. \tag{2.10}$$

According to Equations (2.5), (2.8), (2.9), and (2.10) can be obtained:

$$\frac{dA}{A} = (M^2 - 1)\frac{dv}{v}; \tag{2.11}$$

$$\frac{dp}{p} = -\gamma M^2 \frac{dv}{v}; \tag{2.12}$$

$$\frac{d\rho}{\rho} = -M^2 \frac{dv}{v}; \tag{2.13}$$

$$\frac{dT}{T} = -(\gamma - 1)M^2 \frac{dv}{v}. \tag{2.14}$$

According to Equations (2.12), (2.13) and (2.14), it can be concluded that for one-dimensional steady isentropic flow, gas expands in the nozzle at the subsonic stage and supersonic stage, and the increase of airflow velocity will bring about the decrease of temperature, pressure and density. In turn, the flow is compressed inside the nozzle, resulting in a decrease in gas velocity and an increase in temperature,

pressure, and density. At the same time, it can be concluded that the change of airflow thermodynamic parameters is closely related to Mach number. Since Mach number is closely related to the change of pressure on density, the density of airflow will also change when pressure changes. The above are the basic laws of one-dimensional isometric flow.

In the nozzle, due to dv/ V >0, dp/ P <0, dp/P <0, dT/T<0, it can be seen that the pressure, density and temperature of the gas in the nozzle are constantly decreasing, that is, the airflow in the nozzle experiences the expansion process of decompression, cooling and acceleration. It can be seen from Equation (2.11) that the variation trend of nozzle section is related to the variation trend of velocity and the size of Mach number. Dv/v >0, when Ma < 1, dA/A < 0: this indicates that the variation trend of velocity is opposite to that of nozzle section, and the variation trend of pressure is the same as that of nozzle section, which means that the subsonic section of nozzle section should be gradually reduced. When Ma>1, dA/A>0: this indicates that the variation trend of velocity is the same as that of the cross section, while the variation trend of pressure is opposite to that of the cross section, which means that the cross section of the supersonic section should increase gradually. When Ma=1, dA/A=0: this indicates that the cross section is the maximum or minimum when the airflow speed reaches the speed of sound. However, in the scaled nozzle, the cross section has only a minimum value. Therefore, in order to ensure that the gas accelerates from low speed to sonic speed, it can only be completed at the narrowest part of the nozzle, and the throat diameter remains unchanged.

Hence, to get supersonic airflow through the nozzle to accelerate, you will first need to ensure the nozzle import and export keep enough pressure difference on both ends, the second nozzle section must ensure that the air cooling, decompression, acceleration, the nozzle first to shrink gradually, make the air by the subsonic speed gradually, realize the speed of sound in the throat, and then the nozzle to expand, make the air flow continues to accelerate, supersonic speed is achieved at the nozzle outlet. Therefore, the design of the nozzle should adopt a scaled structure combined with the contraction section and expansion section (as shown in Figure 2.3) to

achieve supersonic flow of gas.

However, in this dissertation, the ultimate goal is to discuss the special nozzle, therefore, in discussing the factors influencing particle collision speed, with common zooming divergent nozzle were studied, and the final special nozzle considering the processing factors, choose inlet with the same size, throat and compressed with Angle, export dilated structure, as shown in Figure 2.4.

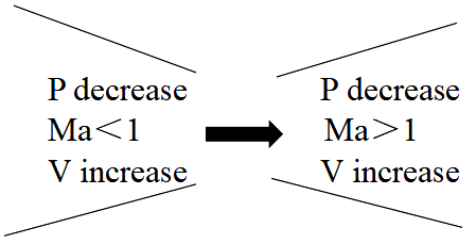

Fig. 2.3. General structure

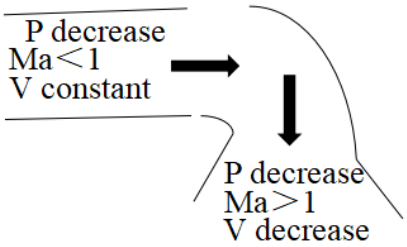

Fig. 2.4. Special structure

2.1.3 Mechanical condition of nozzle

In addition to the geometric conditions, in order to realize the supersonic nozzle flow from subsonic to supersonic transformation, it is necessary to limit the actual pressure (external back pressure) at the nozzle outlet, which is the mechanical conditions of the supersonic nozzle. In order to explore the influence of outlet pressure on the airflow field in a supersonic nozzle, the external pressure Pa at the nozzle outlet is set to be constant, while the stagnation pressure P at the nozzle entrance is variable. With the change of total inlet pressure Po, the outlet gas pressure Pa changes simultaneously. According to the relationship between Pa and Pe, the flow state in the nozzle can be divided into three categories

The optimum expansion state Pe = P.

The complete expansion of the gas in the nozzle is called the optimal state of the nozzle, also known as the design state, as shown in Figure 2.5. The main characteristics of this flow are:

1) the airflow reaches the speed of sound at the throat of the nozzle, Ma = 1; the exit section reaches supersonic speed, Ma > 1.

2) after the air jet nozzle, parallel injection, no expansion or compression phenomenon;

3) the flow speed of external factors (sonic) is lower than the ejection speed of airflow (supersonic), so there is no interference into the nozzle, that is, the flow field in the nozzle will not be interfered by the external environment.

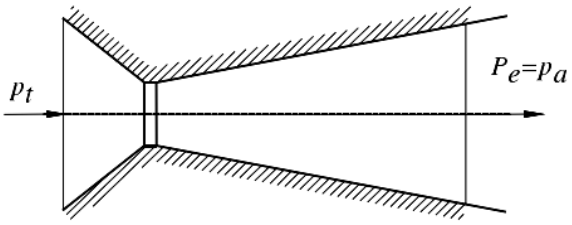

Fig. 2.5. The optimal state of the nozzle

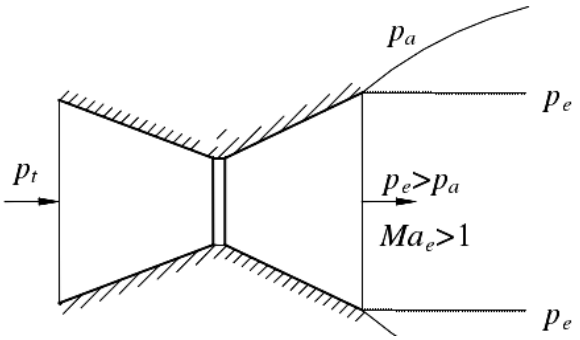

Fig. 2.6. Owe expansion

Under expansion state, Pe > Pa.

When inlet pressure is greater than the best condition of inlet pressure, outlet pressure P, also with the larger, Pe > Pa gas not thoroughly expand, cause the gas energy is not fully functional, which means not efficiently into the kinetic energy of the gas heat, this state is called owe expansion, also means that inflation is not sufficient, as shown in Figure 2.6. The main characteristics of this state are:

1) the gas reaches the critical state at the throat, Ma = 1. It will still reach supersonic speed at the exit, Ma > 1;

2) the gas still expands after ejection of the nozzle until the pressure drops to Pa, which will lead to continuous expansion waves at the outlet of the nozzle:

3) the disturbance of the environmental pressure outside the nozzle is less than

the gas pressure at the nozzle outlet, so it can not reverse into the nozzle.

The overexpansion state, Pe < P.

When the inlet pressure Pa is less than the inlet pressure in the optimal state, the outlet pressure will also decrease, that is, Pe < Pa. Excessive expansion of the gas inside the nozzle is called overexpansion.

2.1.4 Gas thermodynamic parameter

In the process of gas flow, in order to explain the state of a certain position in the flow field, the thermodynamic parameters of this position, such as temperature T, density ρ, pressure P, and mechanical velocity V, are usually given. In gas dynamics, these parameters are called static parameters. If the initial conditions are considered, the problem will be complicated, so a constant entropy stagnation process is assumed. According to this process, the initial velocity of the flow is stagnated to zero, and the thermodynamic parameters after the delay is completed are called stagnation parameters or total parameters, which are the actual stagnation parameters in the flow field. Therefore, in order to facilitate the research and discussion, it is customary to set the stagnation of gas velocity as 0, and then obtain the corresponding stagnation parameters, and take the state after stagnation as the reference state. With the introduction of the above stagnation parameters, the initial conditions will be greatly simplified and stated more clearly.

2.2 Study of a cold spray nozzle throat structure parameters on acceleration characteristics via CFD

In order to study the special nozzle with the final angle, the influence of throat structure parameters on gas and powder acceleration characteristics is discussed by using a common nozzle, especially the throat structure, which will directly determine the special nozzle structure. In addition, because the study of the throat of the nozzle with the angle will directly reduce the total length of the nozzle (the horizontal direction), the spray with the angle will show its advantage. This section discusses the

influence of the throat structure of the conical cold spray nozzle on the acceleration characteristics, including the size, length and angle of the throat.

2.2.1 Determination of geometric model

The initial model (Figure 2.7) is determined by the following formula, then three-dimensional modeling, boundary condition setting and numerical simulation are carried out to study the influence of nozzle throat on the acceleration characteristics.

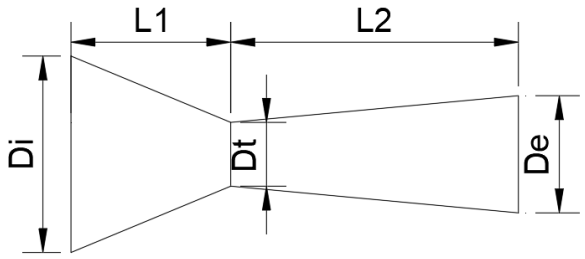

Fig. 2.7. Initial model

$$C = \sqrt{\mathrm{r}RT}\ ; \tag{2.15}$$

$$M\mathrm{a} = \frac{\mathrm{V}}{C}; \tag{2.16}$$

$$M\mathrm{a} = \sqrt{\frac{2}{\gamma\text{-}1}\left[\left(\frac{P_i}{P_e}\right)^{\frac{\gamma-1}{\gamma}}\text{-}1\right]}; \tag{2.17}$$

$$\frac{A_{\mathrm{e}}}{A_{\mathrm{t}}} = \left(\frac{1}{Ma}\right)\left[\left(\frac{2}{\gamma+1}\right)\left(1+\frac{\gamma-1}{2}Ma^2\right)\right]^{(\gamma+1)/[2(\gamma-1)]}; \tag{2.18}$$

$$C_P = \frac{\mathrm{r}R}{\mathrm{r}\text{-}1}; \tag{2.19}$$

$$T_T = T_{\mathrm{i}} + \frac{V_{\mathrm{i}}^2}{2C_P}; \tag{2.20}$$

$$p_T = P_{\mathrm{i}}\left(\frac{T_T}{T_{\mathrm{i}}}\right)^{\frac{\mathrm{r}}{\mathrm{r}\text{-}1}}; \tag{2.21}$$

$$\rho_T = \frac{P_T}{RT_T}; \tag{2.22}$$

$$\mathrm{q_{mcr}} = A_{\mathrm{t}}\left(\frac{2}{\mathrm{r}+1}\right)^{\frac{\mathrm{r}+1}{2\mathrm{r}-2}}(\mathrm{rp_T}\rho_T)^{\frac{1}{2}}; \tag{2.23}$$

$$A_{\mathrm{i}} = \frac{\mathrm{q_{mcr}}}{\rho_{\mathrm{i}}\nu_{\mathrm{i}}}; \tag{2.24}$$

$$L_1 = \left(\frac{D_{\mathrm{i}} - \mathrm{D_t}}{2}\right)\cot\left(\frac{\alpha}{2}\right); \tag{2.25}$$

$$L_2 = \left(\frac{D_{\mathrm{e}} - \mathrm{D_t}}{2}\right)\cot\left(\frac{\beta}{2}\right), \tag{2.26}$$

where C – the ideal speed of sound;

γ – the specific heat ratio of gas;

R – the gas constant;

T – the ambient temperature;

Ma – the Mach number;

Pi – the inlet pressure;

P_t – the throat pressure;

P_e – the outlet pressure;

q_{mcr} – the mass flow rate;

P_T – the stopping pressure;

ρ_T – the stopping density;

T_T – the stopping temperature;

C_P – the specific heat capacity of constant pressure.

The outlet is in direct contact with the atmosphere, $P_e = 1.01\times10^5$ Pa, $V_i = 30$ m/s, this study takes 2…9 mm for numerical simulation.

According to the calculation, the contraction ratio is about 3, the divergence ratio is about 1.84, $D_i = 12.32$ mm. According to the empirical value [114–115], the

Angle of the contraction section (α) is 30°~60°, and the angle of the divergent section (β) is 0°…12°. According to Formulas (2.11) – (2.12), L_1 = 7.21 mm – 15.53 mm and $L_2 \geq$ 17.84 mm can be obtained for the length of the conical cold spray nozzle's diffusion section. Literature shows that the longer the diffusion section is, the faster the acceleration effect is [114]. Hence, L_1=10 mm and L_2=60 mm is taken. Similarly, all parameters are shown in Table 2.1:

Table 2.1 – Cold spray nozzle parameters

Nozzle parameters	Values（mm）							
D_i	6	9	12	15	18	21	24	27
D_t	2	3	4	5	6	7	8	9
D_e	3.68	5.52	7.36	9.2	11.04	12.88	14.72	16.56
L_1	10							
L_2	60							

2.2.2 The parameter details of numerical simulation

Based on the theoretical calculation in Chapter 2, the length of the contraction and expansion parts is determined, but the diameters of the inlet, throat and outlet need further numerical simulation analysis. SolidWorks software is used for 3D modelling. Modelling steps: firstly, the throat is used for modelling, which is helpful for the modelling of the nozzle with angles, and then the contraction and expansion parts are modelled successively. After modelling, the flow simulation module is used for numerical analysis.

In the following numerical simulation process, the influence of turbulence is considered, Because the solid volume fraction of gas-solid two-phase flow in a cold spraying nozzle is less than 10%, it belongs to sparse flow, turbulent and steady flow characteristics are determined by Reynolds number formula $Re = \rho VD/\mu$, where V, ρ and μ are velocity, density and viscosity coefficient of fluid respectively, and D is a

characteristic length. The density of air at room temperature is 1.169 kg/m^3, μ is 18.448, and d is 4mm; when V is supersonic, Reynolds number Re exceeds 2320. Therefore, it is turbulence. The turbulence model adopts the standard K-ε model, which is stable, simple and reliable. Most of the complex turbulence can be solved, and its calculation accuracy is high. Hence, it is widely used in engineering applications. It is based on the turbulent kinetic energy K and adds the dissipation rate equation ε, which is defined as follows:

$$\varepsilon = \mu_{\mathrm{i}}\left(\frac{\partial \mathrm{u}_{\mathrm{i}}}{\partial \mathrm{x}_{\mathrm{j}}}+\frac{\partial \mathrm{u}_{\mathrm{j}}}{\partial \mathrm{x}_{\mathrm{i}}}\right)\frac{\partial \mathrm{u}_{\mathrm{i}}}{\partial \mathrm{x}_{\mathrm{j}}}; \tag{2.27}$$

$$\varepsilon = \frac{\mu}{\rho}\left(\frac{\partial u_i}{\partial x_k}\right)\left(\frac{\partial u_j}{\partial x_k}\right); \tag{2.28}$$

$$\mu_{\mathrm{i}} = \rho C_{\mathrm{u}}\frac{\mathrm{k}^2}{\varepsilon}. \tag{2.29}$$

The transport equation of the standard K-ε model is expressed as follows：

$$\frac{\partial(\rho \mathrm{k})}{\partial \mathrm{t}}+\frac{\partial(\rho \mathrm{k u_i})}{\partial \mathrm{x_i}}=\frac{\partial}{\partial \mathrm{x_j}}\left[\left(\mu+\frac{\mu_{\mathrm{i}}}{\sigma_{\mathrm{k}}}\right)\frac{\partial \mathrm{k}}{\partial \mathrm{x_j}}\right]+G_{\mathrm{k}}+G_{\mathrm{b}}-\rho\varepsilon-Y_M+S_{\mathrm{k}}; \tag{2.30}$$

$$\frac{\partial(\rho \varepsilon)}{\partial \mathrm{t}}+\frac{\partial(\rho \varepsilon \mathrm{u_i})}{\partial \mathrm{x_i}}=\frac{\partial}{\partial \mathrm{x_j}}\left[\left(\mu+\frac{\mu_{\mathrm{i}}}{\sigma_{\varepsilon}}\right)\frac{\partial \varepsilon}{\partial \mathrm{x_j}}\right]+C_{1\varepsilon}\frac{\varepsilon}{\mathrm{k}}\left(G_{\mathrm{k}}+C_{3\varepsilon}G_{\mathrm{b}}\right)-C_{2\varepsilon}\rho\frac{\varepsilon^2}{\mathrm{k}}+S_{\varepsilon}, \tag{2.31}$$

where μ_{i} – turbulence viscosity;

G_{k} – turbulence kinetic energy;

K – generation term generated by average velocity gradient;

G_{b} – turbulence kinetic energy K generation term generated by buoyancy;

$\mathrm{Y_M}$– turbulence pulsation quantity;

$C_{1\varepsilon}$, $C_{2\varepsilon}$, $C_{3\varepsilon}$ – constant;

σ_{k} – Prandtl number of K;

σ_ε – Prandtl number of ε;

s_k and S_ε – user-defined source term.

$C_{1\varepsilon}$ =1.44, $C_{2\varepsilon}$ =1.92, C_u=0.09, σ_ε =1.3, $C_{3\varepsilon}$ are the coefficients related to buoyancy. When the mainstream direction is perpendicular to the gravity direction, $C_{3\varepsilon}$ = 0; when the mainstream direction is parallel to the gravity direction, $C_{3\varepsilon}$ = 1.

For turbulence intensity, it generally refers to the ratio of the root mean square of velocity fluctuation to the average velocity, less than 1 % is low turbulence intensity, and more than 10 % is high turbulence intensity. Calculation formula:

$$I = \frac{0.16}{\sqrt[8]{\mathrm{Re}}}, \tag{2.32}$$

where I – turbulence intensity;

Re – Reynolds number.

Through calculation, the turbulence intensity of this dissertation is 1%-4% (when using SolidWorks/flow, input 2%), and the inner wall conditions are adiabatic and smooth.

If considering the K-ε model, then it uses the turbulent kinetic energy and dissipation rate equation：$K=(UI)^2$, $\varepsilon = \frac{C_u^{0.75} \times k^{1.5}}{I}$, it can be evaluated separately to set the initial value.

The propulsion gas in the simplified nozzle is an ideal non-viscous gas with no heat exchange with the outside world, and the flow can be regarded as a steady isentropic flow. The propelling gas selects air and the internal cavity and excludes the internal non-flowing area. The inlet of the contraction section was selected as the velocity inlet (30 m/s), and the outlet of the expansion section was set as the pressure outlet (0.1 MPa).

2.2.3 Structure parameter factors

A one-dimensional isentropic analytical model is a convenient tool for roughly estimating the flow characteristics inside a cold spraying nozzle; with the rapid development of computer technology, the computational fluid dynamics(CFD) model has attracted more and more attention due to its high prediction accuracy and feasibility of simulating different situations [116].

2.2.3.1 The different lengths of throat

As shown in Fig. 2.8, the effect of throat length on acceleration characteristics was studied with the throat length of 1 mm…15 mm, respectively. Numerical results show that the throat length has little influence on the acceleration characteristic (Figure 2.9); the overall range fluctuates from 533 m/s to 550 m/s, indicating that throat length has little influence on acceleration characteristics, and further discussion on throat diameter is needed.

Set 11 mm throat length and discuss the influence of gas temperature and pressure on outlet velocity, as shown in Fig. 2.10a.

The temperature has a positive influence on the acceleration characteristic. When the temperature is in the range of 800 K…900 K, the outlet velocity reaches the maximum value, and the outlet velocity decreases when the temperature continues to increase. The influence of pressure is further discussed, and the inlet gas temperature is kept at 800 K, as shown in Fig. 2.10b. With the increase of pressure within 1 MPa, the outlet velocity gradually increases significantly, but the increase is small when the pressure exceeds 1 MPa.

The reason for the decrease may be that the supersonic reaches a certain value, which generates shock waves and increases the resistance of gas.

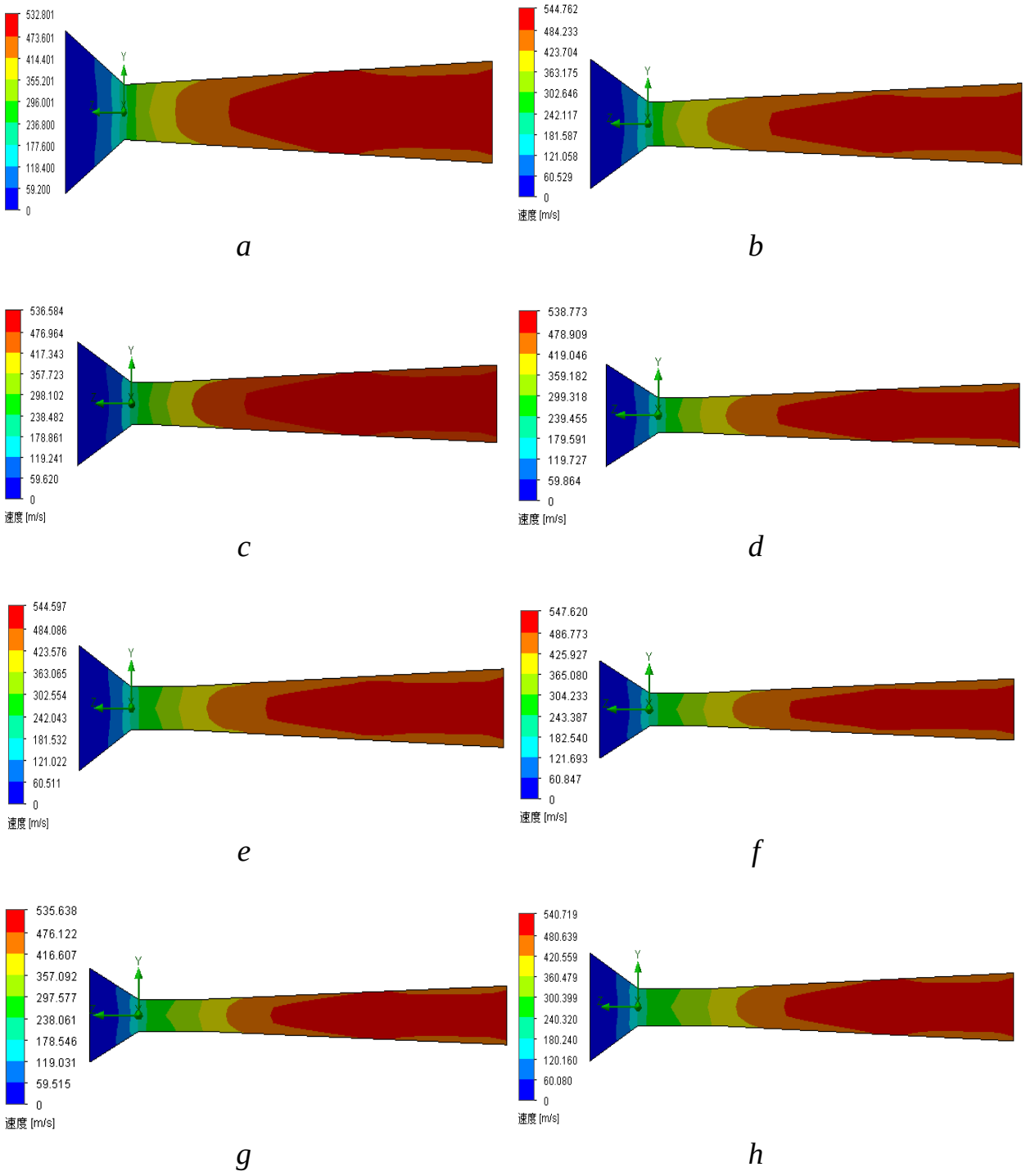

a – 1 mm, V_{max} =532.8 m/s; *b* – 3 mm, V_{max} =544.76 m/s; *c* – 5 mm, V_{max} =536.58 m/s; *d* – 7 mm, V_{max} =538.77 m/s; *e* – 9 mm, V_{max} =544.6 m/s; f – 11 mm, V_{max} =547.62 m/s; *g* – 13 mm, V_{max} =535.64 m/s; *h* – 15 mm, V_{max} =540.72 m/s

Fig. 2.8. The effect of throat length on outlet velocity

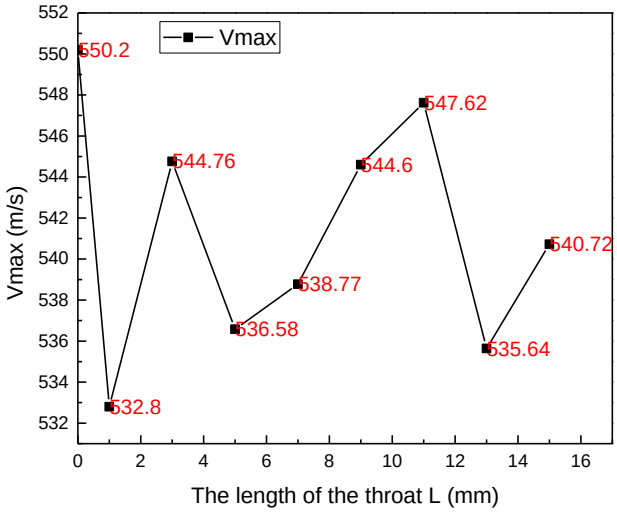

Fig. 2.9. Different nozzle throat lengths influence the outlet velocity

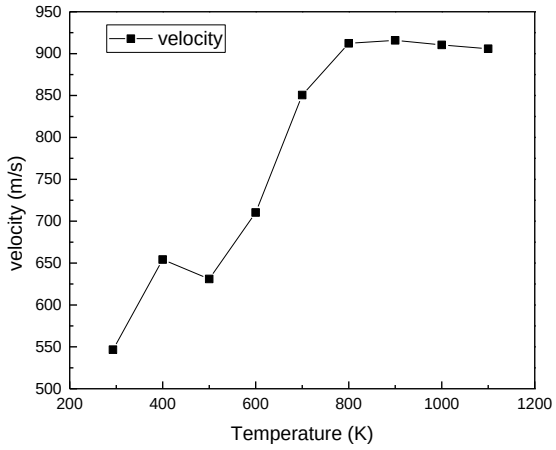

a

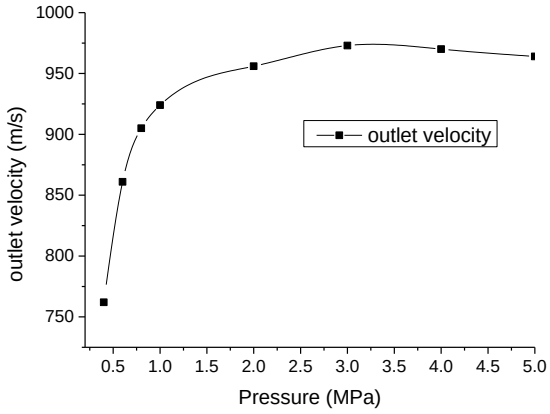

b

a – Influence of different temperatures on outlet velocity at 1 MPa;

b – Influence of different pressures on outlet velocity at 800 K.

Fig. 2.10. Different N_2 parameters influence the outlet velocity

2.2.3.2 Diameter of throat

As can be seen from the Figure 2.11, the maximum growth rate is more than 20 m/s between the size of 2…6 mm.

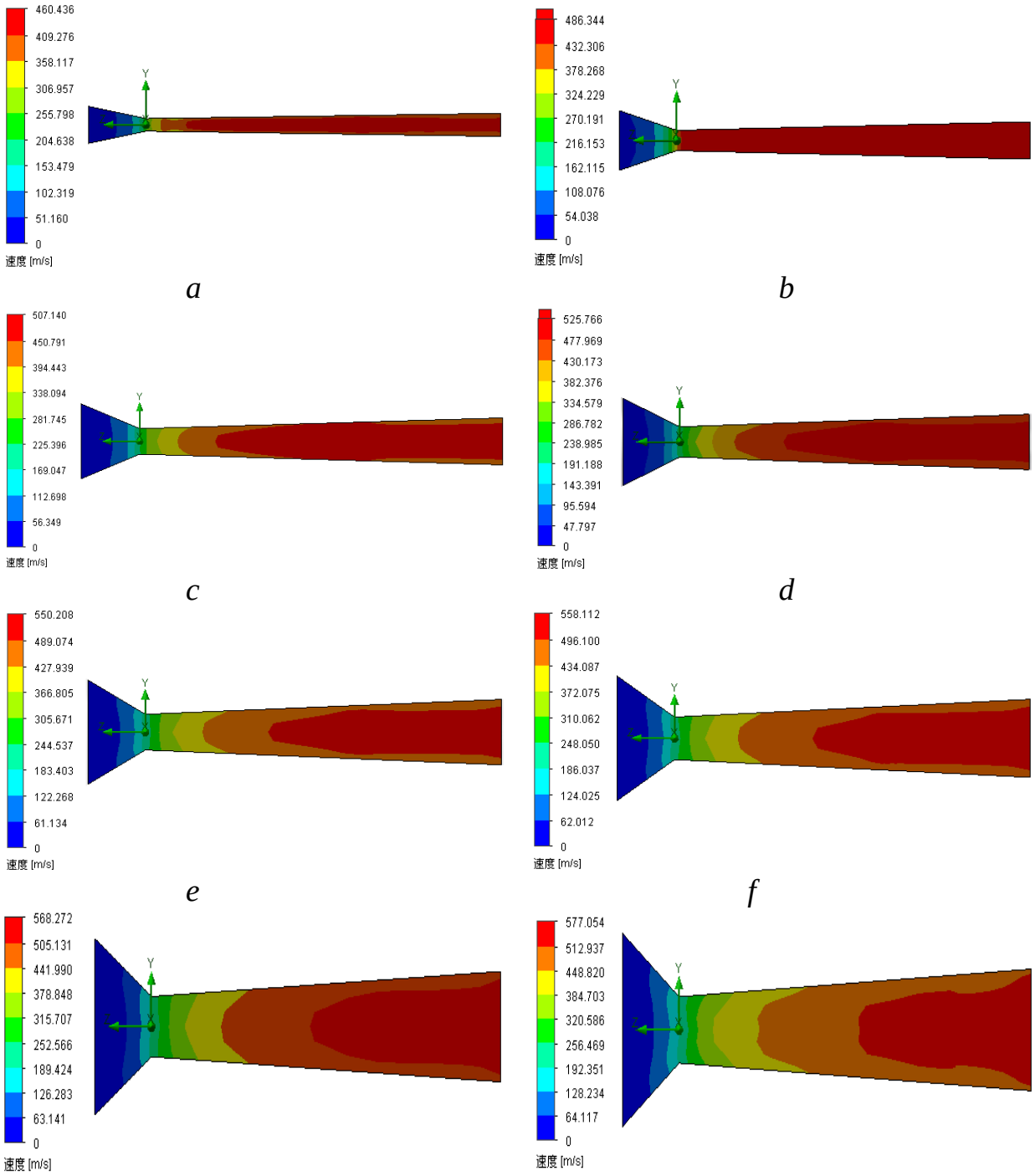

a – 2 mm, V_{max} = 460 m/s; *b* – 3 mm, V_{max} = 486 m/s; *c* – 4 mm, V_{max}= 507 m/s; *d* – 5 mm, V_{max}=526 m/s; *e* – 6 mm, V_{max}=550 m/s; *f* – 7 mm, V_{max} = 558 m/s; *g* – 8 mm, V_{max} = 568 m/s; *h* – 9 mm, V_{max} = 577 m/s

Fig. 2.11. Nozzles with different diameters of throat

When the throat exceeds 6mm, the growth rate of the outlet slows down, and the growth rate is only 8 m/s…10 m/s. The results show that the influence of throat diameter on outlet velocity increases first and then decreases. Therefore, the throat diameter was determined to be 6 mm.

2.2.3.3 The special Angle of throat

Finally, in order to facilitate the analysis of nozzle throat angle, the throat length size of 11 mm was selected. The effects of throat angles of 90°, 60° and 45° on the acceleration characteristics were studied (Figure 2.12).

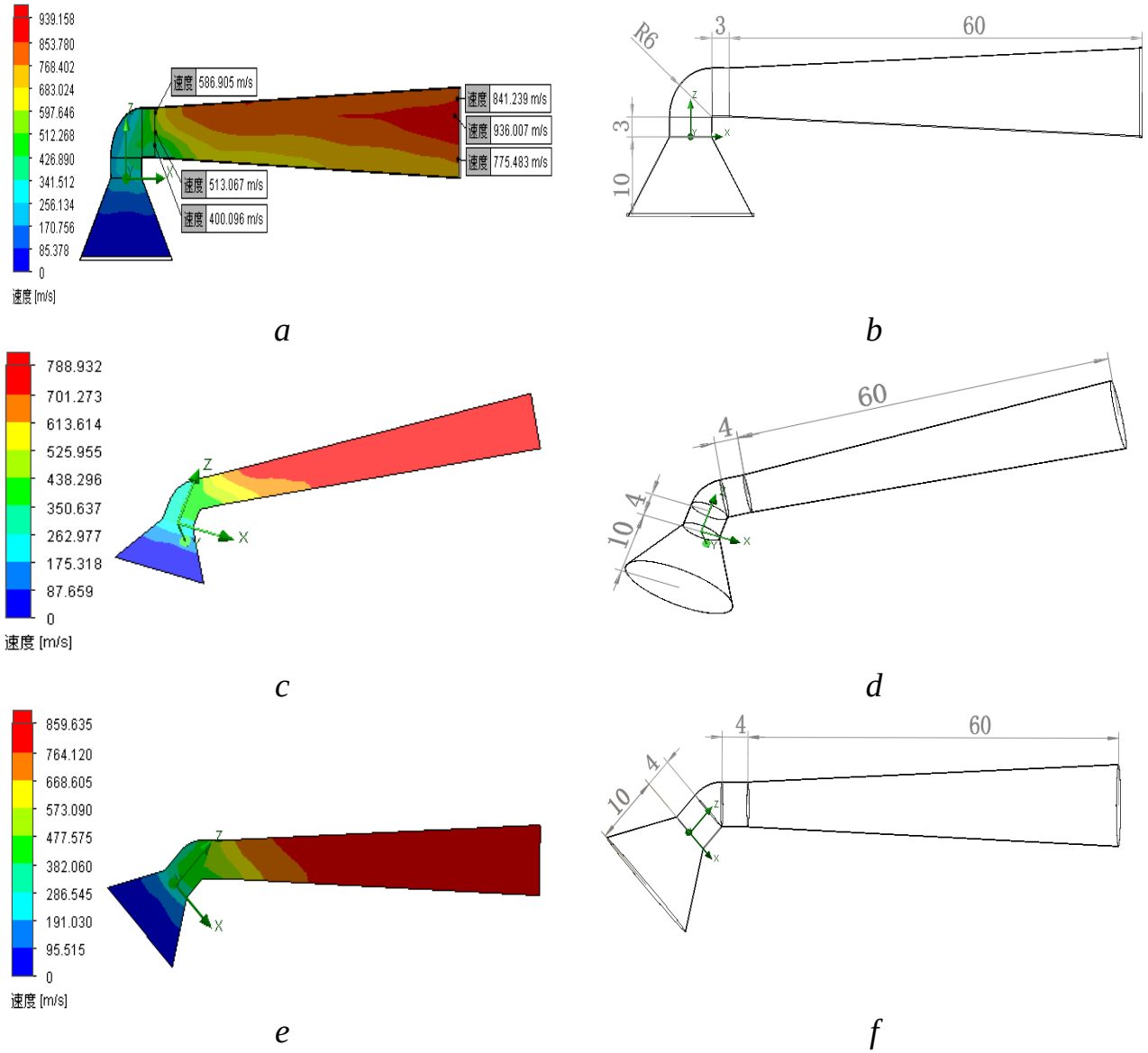

a, *b* – 90°; c, d – 60°; *e*, *f* – 45°

Fig. 2.12. Outlet velocity diagram and size at different angles at 800 K

The results show that the angle of 90° has advantage on acceleration characteristics (Figure 2.13). The simulate condition as the same Section 2.2.2.

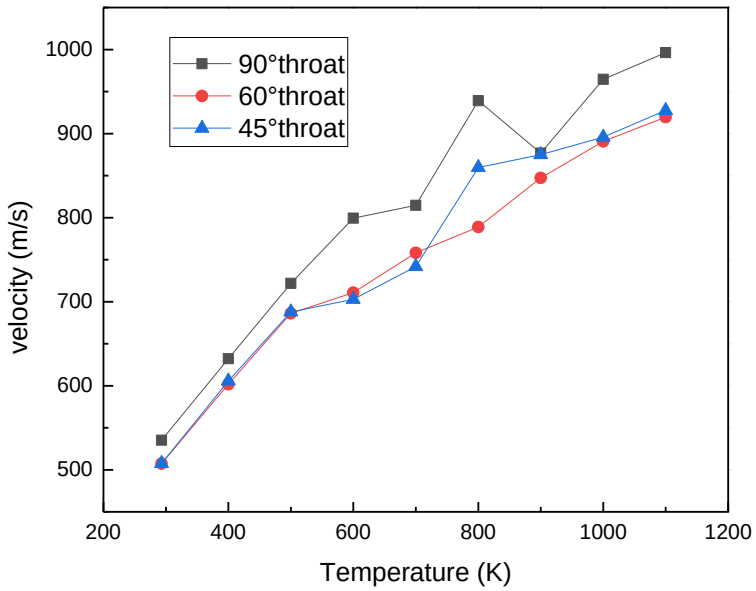

Fig. 2.13. Different angles influence the outlet velocity

In this section, the 60 mm length of L2 is selected. If it is necessary to spray in a specific small area, L2 can be shortened to the required size. Based on this, the structure can be further optimized according to the actual application situation. Although the main factors affecting the impact velocity of powder include propelling gas, particle characteristics, spraying distance and length of expansion section [117], the throat structure directly affects the acceleration characteristics of the fluid. Sequentially, it affects the deposition characteristics of powder, and the Computational Fluid Dynamics (CFD) method can give researchers a good reference.

2.2.4 Study on the particle trajectory

There are many factors influencing the acceleration characteristics of particles, including propulsion gas, temperature, pressure, and other factors, as well as the material properties of particles themselves (size, shape, etc.). Nozzle materials, such as low thermal conductivity and small heat loss of airflow and particles, which is conducive to improving the velocity of particles. However, too high a temperature

will cause throat blockage [118]. Therefore, in this study, the injector was set at the boundary between the throat and the expansion section. Studies show that [119], when the particle flow diameter is greater than 15 microns, the wall attachment effect disappears, the particle flow is mainly affected by inertia, and the influence of the airflow field on the final trajectory of the particle flow is small. However, the particle diameter is too large, and particle collisions with the nozzle's inner surface basically affect the acceleration characteristics and the simulated condition is the same Section 2.2.2.

This chapter utilize titanium particles 20 microns in diameter, aluminum particles 30 microns, and copper 15 microns, for no Angle of the nozzle, injection particles nozzle should not be too great pressure, which will lead to particle collision on the wall directly, cause energy loss, pressure is too small can't injection, hence, the injection pressure is 1.1 MPa, and the other 90° angle throat structure is 1.6 MPa. The results are shown in Figure 2.14 and Figure 2.15.

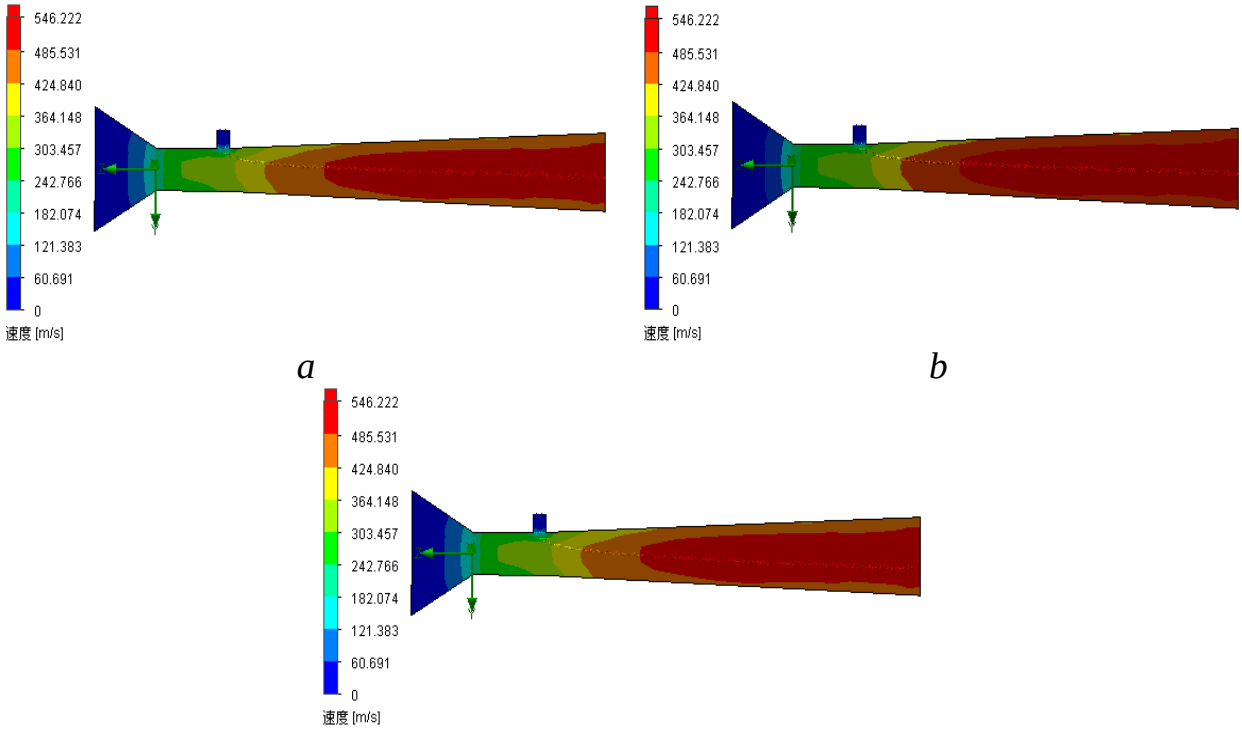

a *b*

c

a – 20 μm titanium powders; *b* – 30 μm aluminum powders;

c – 15 μm copper powders

Fig. 2.14. Optimal conditions for particle trajectories with straight-throat structures

The basic size of Figure 2.14 is consistent with that of Figure 2.8f. The center of the powder injection port is set at the boundary between the throat and the expansion segment. The basic size of Figure 2.15 is consistent with that of Figure 2.12b.

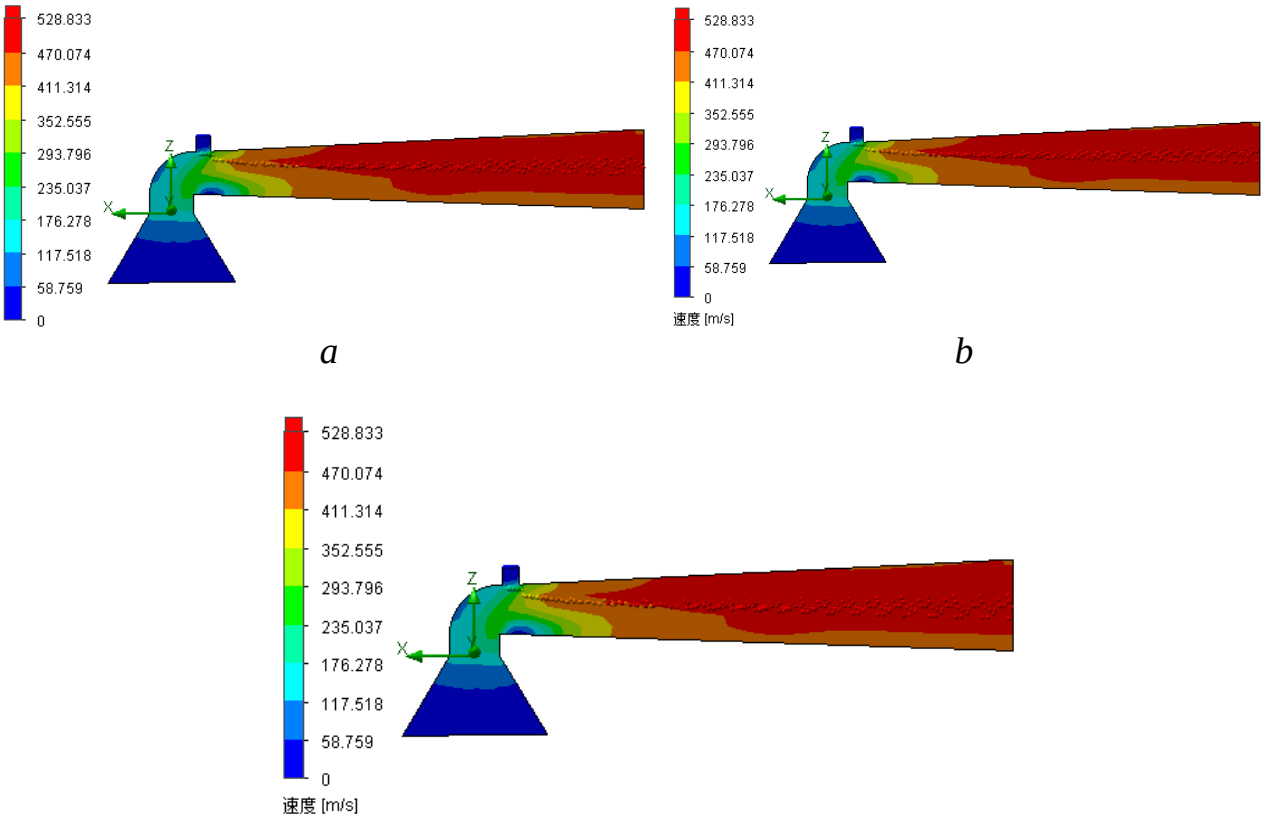

a *b*

c

a – 20 μm titanium powders; *b* – 30 μm aluminum powders;

c– 15 μm copper powders

Fig. 2.15. Optimal conditions for particle trajectories with 90° throat structures

Obviously, as a result, the trajectory of the particles is determined by the inlet pressure, powder injection pressure, and a combination of factors such as particle size, etc. In addition, the low particle velocity in Figure 2.16 is the main reason for the low initial velocity value and temperature.

As figure 2.16b shows, aluminium particles can obtain effective deposition under the collision condition of 400 ℃, but the deposition speed of copper particles cannot meet the requirements of deposition. In this case, the parameter of increasing temperature can be considered (Figure 2.10a), because the more the initial

temperature rises, the higher the speed of fluid and particle, and when the temperature of the particles increases (within the melting temperature), the critical velocity will decrease (Table 2.2), and the effective deposition will be finally achieved. The same can be done with titanium particles or Ti-6Al-4V material particles [120-122], etc.

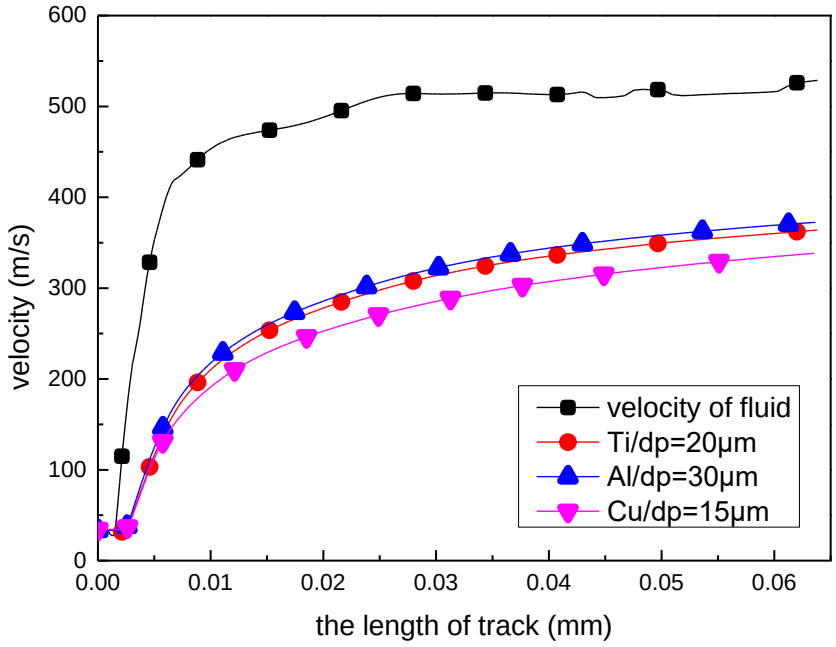

a

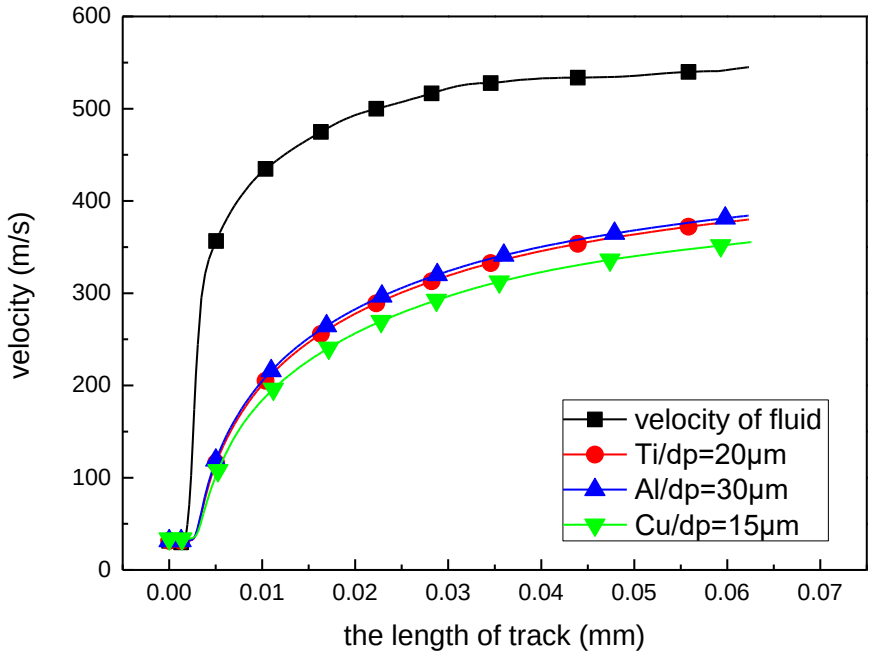

b

a – without angle; *b* – 90° nozzle

Fig. 2.16. Different powders and flow velocities

Table 2.2 – Critical velocities at different material impact temperatures（m/s）

Material	25℃	200℃	300℃	400℃	500℃	600℃	700℃	800℃	900℃
Titanium	719	662	627	590	546	507	460	408	348
Aluminum	630	488	384	239	-	-	-	-	-
Copper	532	465	421	372	316	248	151	-	-

2.2.5 Summary this section

The SolidWorks/Flow numerical simulation can well predict the acceleration characteristics of the nozzle. Some reference values were obtained by numerical analysis of the cold spray nozzle.

1) Through the analysis of the throat with 2 mm…9 mm diameter, the fluid acceleration effect is better within 6 mm. For every 1mm increase in the throat, the velocity increases by about 20 m/s. But beyond 6 mm, the acceleration becomes slow, and the speed increase is no more than 10 m/s. Throat length has little effect on acceleration characteristics; the total range fluctuated from 533 m/s to 550 m/s, and the 11 mm length of the throat is the closest to 0 mm. The temperature has a promoting effect on the acceleration of the nozzle; in a certain range, the outlet velocity has a linear relationship with the temperature. When the temperature reaches 800 K, the exit speed exceeds 900 m/s.

2) Through the numerical simulation without angle, 90°, 60° and 45°, it is found that the 90° throat has advantages over 60° and 45°. Compared to the angle nozzle, the 90° throat only reduces the speed of the outlet by 17.4 m/s, which only affects 3 %. Thus, it can be concluded that the 90° throat has little influence on acceleration characteristics. Considering the factors of different material densities, the selected 20 um titanium powder, 30 um aluminium powder, and 15 um copper powder have roughly the same path in the 90° nozzle. If considering the powder of equal diameter, there is a difference in the particle trajectory.

3) Considering that 90° throat has little influence on acceleration characteristics, it is suggested that in further research, size optimization can be carried out according to the application situations of actual components, and the length of a single direction can be optimized, which will expand the application area of cold spraying nozzle.

2.3 Study of the technological parameters on acceleration characteristics by multiple factors analysis

According to the discussion results in Section 2.2.3.3 , the throat structure of 90° is better. This section mainly discusses the process parameters affecting the particle velocity from the angle of 90°. The 90° cold spraying nozzle is mainly composed of an air intake section, contraction section, throat and expansion section. The throat adopts a 90° structure. The throat section inlet and outlet adopt a length of 6 mm, a width of 3 mm, and a circular arc chamfering of 10 mm and 5 mm respectively in the middle, as Fig. 2.17 shows, the wall thickness of the nozzle can be determined according to the actual situation, the wall thickness does not affect the numerical simulation result, hence, 1mm wall thickness is used in this dissertation.

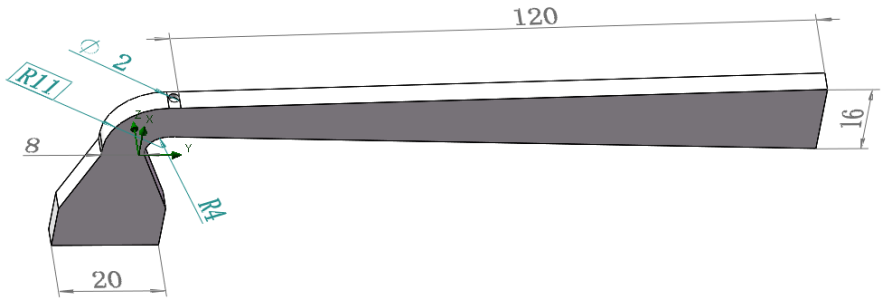

Fig. 2.17. Nozzles for numerical simulations

Before the multi-factor interaction analysis, the factorial analysis should be carried out first. In this study, three major factors were selected for univariate analysis, and their levels were determined. Due to the collision speed is mainly composed of propulsion gas characteristics of particles, particle characteristics, spraying distance and expansion length influence [123-124], this study has identified the nozzle

structure and nitrogen, assuming that the spray distance is zero, that is, the outlet velocity of the nozzle is studied. The next test design scheme mainly analyzes propulsion gas and particle characteristics, further refining the single factor is the temperature of nitrogen, the nitrogen pressure and particle diameter.

In addition, the deposition conditions are considered in this study, and the high and low levels are determined when the deposition velocity is satisfied. The key factor for the deposition is the critical velocity, and its formula can be theoretically calculated by using Equation (2.33).

$$V_{\text{crit}} = \sqrt{C_P (0.7T_{\text{m}} - T_{\text{i}})}, \tag{2.33}$$

where T_m – melting point;

T_i – collision temperature;

C_p – specific heat.

Titanium powder was selected for this study; the material parameters of the titanium particles are shown in Table 2.3.

Table 2.3 – Material properties

Material	Specific heat, j/kg ℃	Melting temp., ℃	70% of Melting temp., ℃
Titanium	452	1670	1169

2.3.1 Gas temperature

For the single factor of nitrogen temperature affecting particle velocity, the range of 800K-1100K was selected as the preheating condition of nitrogen. Since there are many injected particles, the particle exit velocity directly affects the collision deposition. In this study, the average velocity of particles was taken as the outlet velocity of particles, and the lowest temperature under deposition conditions was taken as the low level (-1), 1000 K as the middle level (0) and 1100 K as the high

level (+1). The gas pressure was 1 MPa, and the powder injection pressure was 0.71 MPa, the specific parameters of which are shown in Table 2.4.

Table 2.4 – Outlet velocity parameters of titanium particles at different temperatures

Gas temperature, K / Parameter	800	900	1000	1100
Powder velocity V_{max}, m/s	565	593	624	656
Powder velocity $V_{average,}$ m/s	530	570	601	625
Powder temperature $T_{average}$, K	666	748	836	923
Critical velocity V	592	560	523	484
Whether deposition	No	Yes	Yes	Yes
High or low-level code	-	-1	0	+1

2.3.2 Gas pressure

For the single factor of nitrogen pressure affecting particle velocity, under the conditions of deposition, 0.9 MPa was selected as the low level (-1) and 1.1 MPa as the high level (+1). The specific parameters are shown in Table 2.5.

Table 2.5 – Outlet velocity parameters of titanium particles under different inlet pressures

Gas pressure, MPa / Parameter	0.8	0.9	1.0	1.1
Powder velocity V_{max}, m/s	562	580	593	620
Powder velocity $V_{average,}$ m/s	544	561	570	577
Powder temperature $T_{average}$, K	761	750	748	747
Powder injection pressure, MPa	0.6	0.65	0.7	0.78
Critical velocity V	555	559	560	560
Whether deposition?	No	Yes	Yes	Yes
High or low-level code	-	-1	0	+1

2.3.3 Powder diameters

For the single factor of particle diameters affecting particle velocity, studies [125] show that, when the particle flow diameter is greater than 15 microns, the wall attachment effect disappears, the particle flow is mainly affected by inertia, and the influence of the airflow field on the final trajectory of the particle flow is small， therefore, at least 15-micron titanium powder was selected in this study. The 20-micron titanium powder was selected for the single-factor analysis of nitrogen temperature and nitrogen pressure. In this study, 20 microns was selected as the low level (-1), and 30 microns was selected as the high level (+1). The initial parameters were gas temperature of 1000 K, gas pressure of 1 MPa and particle inlet pressure of 0.71 MPa, the specific parameters are shown in Table 2.6.

Table 2.6 – Outlet velocity parameters of titanium particles with different particle diameters

Powder diameter, um / Parameter	15	20	25	30
Powder velocity V_{max}, m/s	665	624	596	570
Powder velocity $V_{average,}$ m/s	635	601	576	558
Powder temperature $T_{average}$, K	808	836	854	870
Critical velocity V	535	523	516	508
Whether deposition?	Yes	Yes	Yes	Yes
High or low-level code	-	-1	0	+1

As can be shown from the average velocities in Table 2.4 to Table 2.6, there is a linear relationship between the influences of each single factor within a certain range, and the order of each single influencing factor is that gas temperature is greater than particle diameter, while particle diameter is greater than gas pressure. Therefore, the variation rules of particle velocity under the condition of a single factor are different. Obviously, the prediction of particle velocity under multi-factor change is more

scientific, reasonable and of practical significance.

2.3.4 Interaction analysis of three factors

Response surface methodology (RSM) is a combination of mathematical and statistical methods, which is often applied to find the optimal process parameters in multi-parameter systems [126-127]. Response Surface Methodologies based on Box Behnken design, combining single factor numerical results, the test Design Expert software was used to set the inlet pressure P, the advance temperature T, the particle diameter D as the independent variable, and the outlet velocity as the dependent variable to construct a three-factor, three-level quadratic regression equation, and its response model was:

$$y = \beta_0 + \sum_{i=1}^{m} \beta_i x_i + \sum_{i=1}^{m} \beta_{ij} x_j + \sum_{i=1}^{m} \beta_{ii} x_i^2 + \varepsilon, \tag{2.34}$$

where y – response value of the regression equation;

X_i and X_j – independent variables;

M – the number of independent variables;

β_0 – the regression intercept;

β_i – the linear effect of X_i;

β_{ij} – the interaction effect of X_i and X_j;

β_{ii} – the secondary effect of X_i;

ε – the random error.

The high (+1) and low (-1) levels of single factors (gas temperature, gas pressure and particle diameter) were respectively input into experimental Design Expert software, and the experimental scheme and test results obtained were shown in Table 2.7.

Table 2.7 – Test analysis scheme and results

Run	High and low level code			Actual value			Powder V (m/s)
	Gas T (K)	Gas P (MPa)	Powder D(um)	Gas T (K)	Gas P (MPa)	Powder D(um)	
1	+1	0	-1	1100	1	20	625
2	-1	-1	0	900	0.9	25	541
3	-1	+1	0	900	1.1	25	547
4	0	+1	+1	1000	1.1	30	557
5	0	0	0	1000	1	25	576
6	0	0	0	1000	1	25	576
7	0	0	0	1000	1	25	576
8	0	0	0	1000	1	25	576
9	+1	+1	+1	1100	1	30	560
10	0	0	+1	1000	0.9	30	554
11	+1	+1	0	1100	1.1	25	615
12	-1	-1	+1	900	1	30	525
13	+1	+1	0	1100	0.9	25	583
14	-1	-1	-1	900	1	20	570
15	0	0	-1	1000	0.9	20	600
16	0	0	-1	1000	1.1	20	606
17	0	0	0	1000	1	25	576

As shown in Table 2.8, the p-values of A and B are all less than 0.001 (less than 0.05), and the p-values of C are 0.00141 (less than 0.05), indicating that the single factor has a significant effect on particle velocity. The p-value of AB is 0.0386 (less than 0.05), indicating that the interaction between temperature and pressure is obvious, while the p-value of AC is 0.0916 (greater than 0.05), and the p-value of BC is 0.7779 (greater than 0.05), indicating that the interaction between temperature and particle diameter, gas pressure and particle diameter is not obvious.

Table 2.8 – Results of analysis of variance

Source	Sum of squares	df	Mean square	F value	P-value
Model	11018.28	9	1224.25	46.77	＜0.0001
A-Gas T	5000	1	5000	191	＜0.0001
B-Gas P	276.13	1	276.13	10.55	0.0141
C-Powder D	5253.13	1	5253.13	200.67	＜0.0001
AB	169	1	169	6.46	0.0386
AC	100	1	100	3.82	0.0916
BC	2.25	1	2.25	0.086	0.7779
A^2	199.01	1	199.01	7.6	0.0282
B^2	23.75	1	23.75	0.91	0.3726
C^2	3.22	1	3.22	0.12	0.736
Residual	183.25	7	26.18		
Lack of fit	183.25	3	61.08		
Error	0	4	0		
Total	11201.53	16			

As can be shown from Fig. 2.18, the order of influence of the three factors is that gas temperature is greater than powder diameter and powder diameter is greater than gas pressure.

In this case, the regression equation is:

$$Y = 576 + 25A + 5.88B - 25.63C + 6.5AB - 5AC - 0.75BC - 6.88A^2 + 2.37B^2 + 0.88C^2, \quad (2.35)$$

where A – gas temperature;

B – gas pressure;

C – the particle diameter.

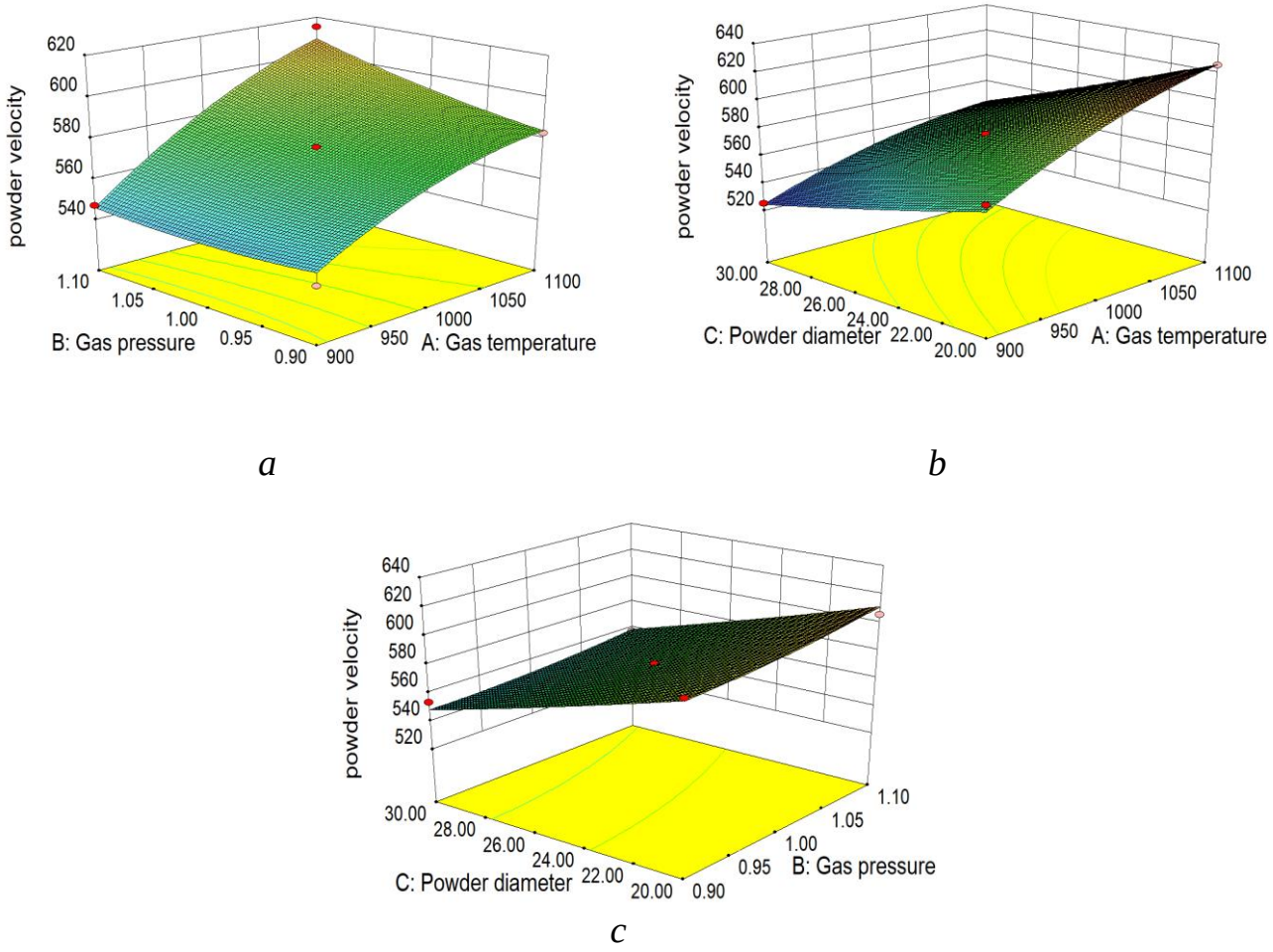

a – A and B factors interaction influence; *b* – A and C factors interaction influence; *c* – B and C factors interaction influence cure

Fig. 2.18. Response surface analysis of three factors' interaction under N_2 conditions

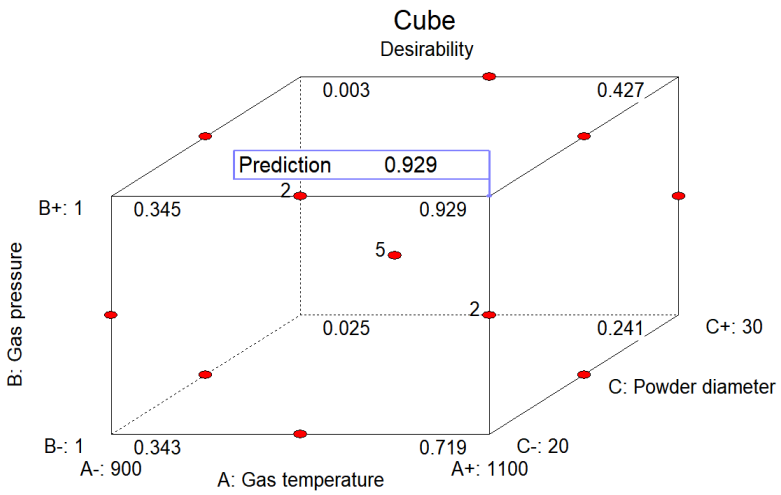

Fig. 2.19. The desirability of optimize value

The lack of fit is not significant; the determination coefficient R^2 of the regression equation is 0.9626, and the correction coefficient R^2 is 0.7383. These results indicate that the regression model can well explain the variation in powder velocity response value. The model F-value of 46.77 and P-value of 0.0001 (< 5%) imply the model is significant.

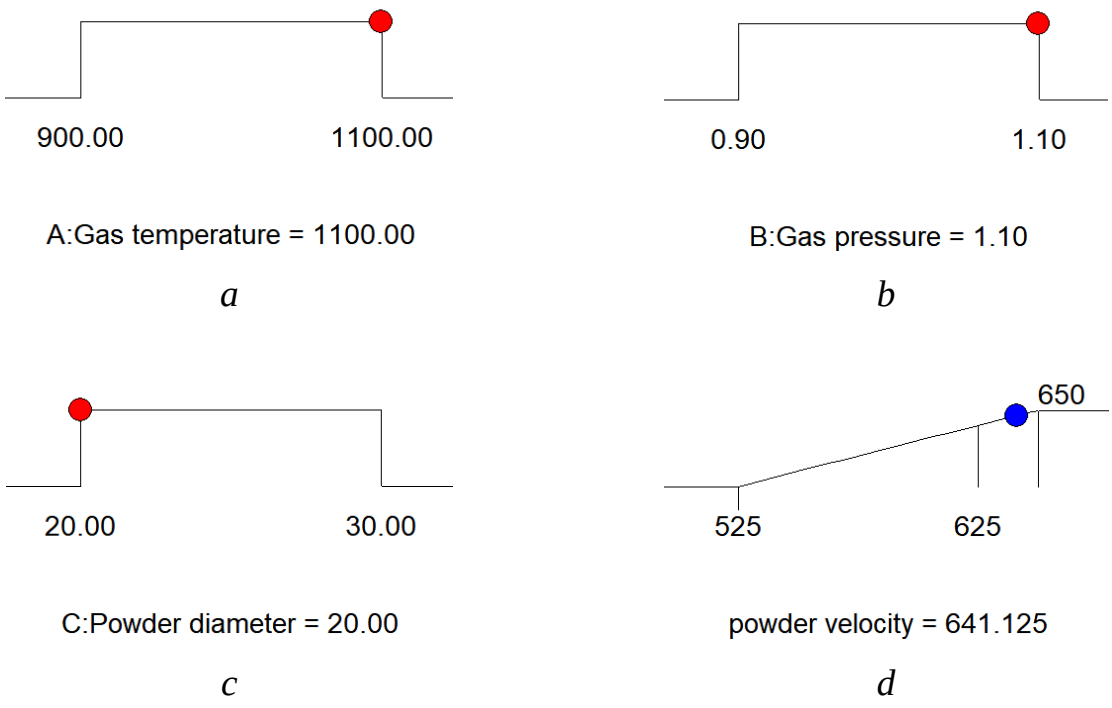

a – optimal temperature; *b* – optimal pressure; *c* – optimal particle diameter; *d* – response speed under optimal conditions

Fig. 2.20. The optimum parameters of maximum outlet velocity obtained by nitrogen as propellant gas

Taking the maximum particle velocity as the target, the optimized data is shown in Fig. 2.20, and the optimal speed is predicted to be 641.125 m/s. Moreover, Fig. 2.19 shows that the optimal value is obtained with a large probability (92.9 %). The optimized parameters are imported into the Flow Simulation module of SolidWork for numerical simulation verification. The simulation results (Fig. 2.21) showed that the average velocity of the particles was 645 m/s with an error of 0.76%. Therefore, the response surface analysis was highly accurate.

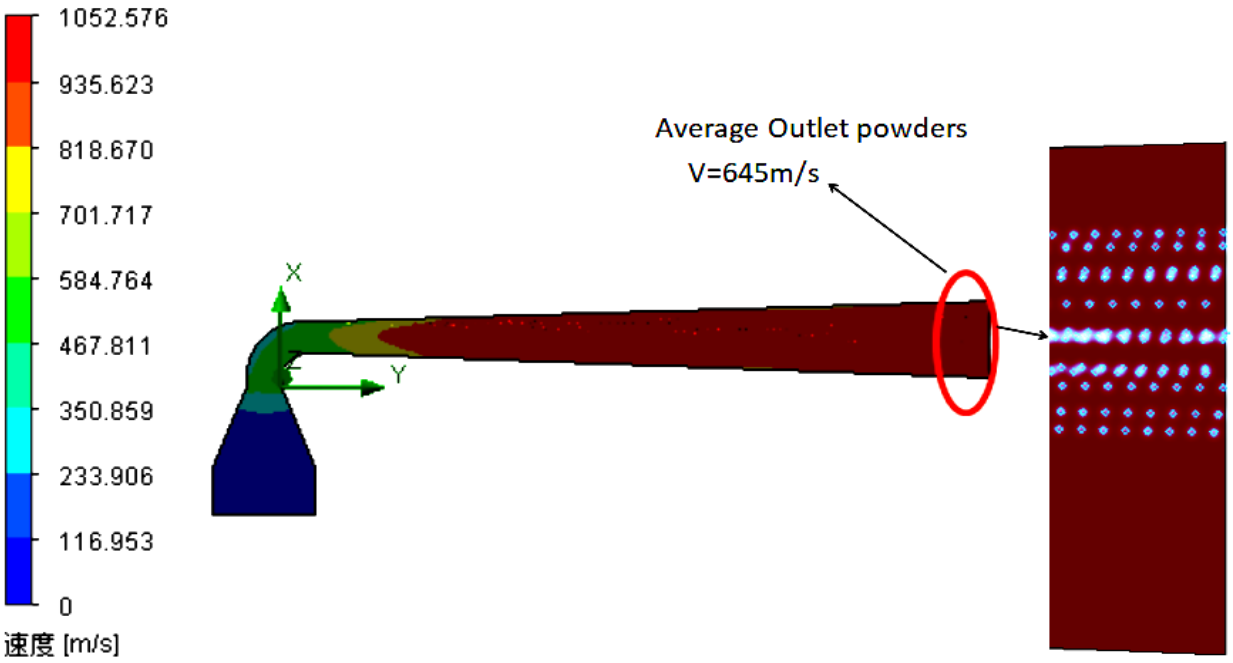

Fig. 2.21. Fluid velocity distribution program and particle trajectory

2.3.5 Summary this section

It is feasible to optimize the process parameters of cold spraying by the response surface analysis method, and the regression model has high accuracy. It can not only analyze the velocity parameters by a single factor but also analyze the influence of cold spraying parameters by multi-factor and multi-level, which has a certain theoretical reference value.

1) Under the action of a single factor, temperature, pressure and particle diameter have significant effects on particle velocity respectively, and the order of influence is that temperature is greater than powder diameter, and powder diameter is greater than gas pressure.

2) Under the interaction of multiple factors, the interaction between temperature and pressure is obvious, while the interaction between temperature and particle diameter, gas pressure and particle diameter are not obvious. The quadratic regression model established in this study can reflect the response value of the outlet velocity well by comparing the optimized parameters after RSM with the actual velocity parameters. With an error of 0.76 %, the response surface quadratic regression model has high accuracy.

2.4 Research on the special single-channel cold spraying 90° rectangular nozzle

Since the influence of spraying distance was not considered in the above study, hence, the divergence section was longer. In this section, the influences of inlet length and divergence length of cold spraying nozzle on fluid outlet velocity are studied to determine the special single-channel nozzle model. If the spraying distance is further considered, the divergent section can be shortened to the optimal value. In addition, through numerical simulation, it is found that under high pressure, the nozzle with a parallel structure can be used in the contraction section, which is more convenient for manufacturing.

2.4.1 Established the special nozzle 3D initial model

As can be seen from Sections 2.2 and Sections 2.3, the structure of 90° angle at the throat is better than 45° and 60°, and gas temperature is the biggest factor affecting particle acceleration, followed by particle size, and gas pressure is less important. Therefore, the special angle of this section is 90°, and the process parameters are discussed.

As shown in Fig. 2.22, although the flow field distribution of the circular cross-section is uniform and the turbulence can be minimized, it is not suitable for spraying fine rotating specimens and workpieces.

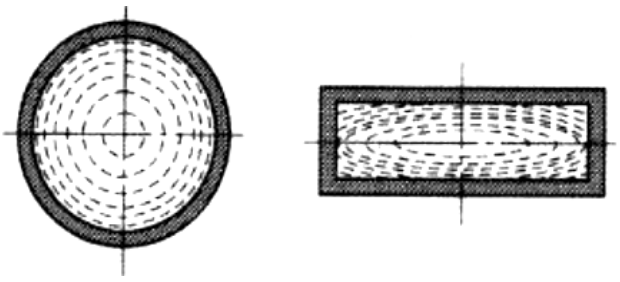

a b

a – circular; *b* – rectangular

Fig. 2.22. Three different nozzle cross-sections [128]

Therefore, from the perspective of application to smaller rotating parts, the rectangular nozzle design is considered in this study [128]. Considering the convenience of installation, the upper and lower structures are adopted, and the initial model is shown in Fig. 2.23.

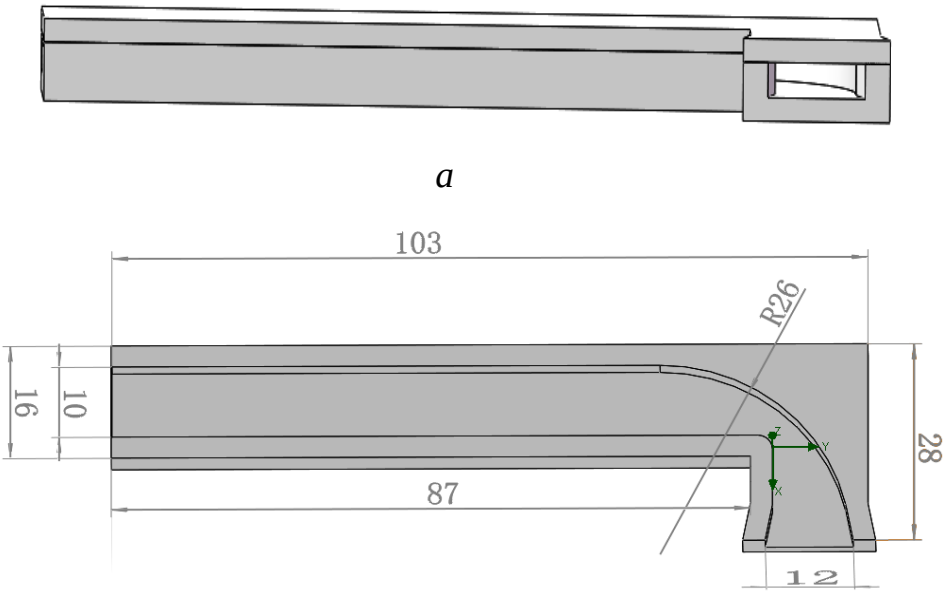

a

b

a – The combination of the upper and lower parts; *b* – Only the lower part and size

Fig. 2.23. The initial model of the 3D model

It is found [129] that when the throat diameter $D_{throat} \geq 6$ mm of the circular section nozzle, a large fluid outlet velocity can be obtained. The rectangular section width is preliminarily 3 mm, so the throat section length L ≥ 9.42 mm. This study takes the throat with the same cross-sectional area as the benchmark. To achieve the compression effect, the rectangular nozzle in this dissertation uses the fillet method to compress the cross-sectional area at the 90° corner, and the larger the fillet, the better the compression effect. Through numerical simulation, it is found that when the inlet width of propulsion gas is 10 mm, and the fillet exceeds 30 mm, the throat compression radius is close to 10 mm. The primary fillet radius R = 26 mm, and the cross-section width of the throat inlet is 10 mm; at this time, the contraction ratio is about 3, which is consistent with the compression ratio in Section 2.2.1.

2.4.2 Optimal single factor analysis of special nozzle structure

Since the particle acceleration process is mainly affected by the main drag force of the airflow, this dissertation assumes that the powder is spherical particles with smooth surfaces, and the aerodynamic drag force formula is shown in Equation (2.36):

$$F = \frac{1}{2} C_D \rho_g (v_g - v_p)^2 S, \tag{2.36}$$

where F – aerodynamic drag force on the particles;

C_D – drag coefficient;

ρ_g – density of the airflow;

V_g and V_P – gas flow velocity and particle velocity respectively;

S – upwind area of particles.

When the injection speed of powder is 0, the particles can obtain a large acceleration. If it is necessary to obtain a large acceleration, it is necessary to increase the difference between air velocity and particle velocity or reduce the powder particle size. In order to reduce the energy loss, try to avoid contact or collision between the powder and the inner wall of the nozzle. In addition, the factors affecting powder collision include powder characteristics, propulsion gas characteristics, divergent section length, spraying distance, nozzle throat size, etc. [117]. This study mainly considers the structure. Therefore, the spraying distance, throat size, and divergent section length are selected for optimization.

SolidWorks/Flow simulation module for fluid analysis is used, and the influence of turbulence is considered (turbulence intensity 2 %, and the inner wall conditions are adiabatic and smooth). Nitrogen (N_2) is selected as the propelling gas, and the internal cavity and excludes the internal non-flowing area are selected. The powder injection is selected in the low-pressure area at the junction of the throat and the divergent section.

2.4.2.1 Divergent section

To facilitate spraying in a small space, try to choose a shorter divergent section length. Although the shorter divergent section length is unfavorable to powder acceleration, optimizing the spraying distance can make up for the defect of insufficient divergent section length. Therefore, 8 mm, 12 mm, and 16 mm are selected in this paper. The spraying distance is 50 mm, nitrogen (N_2) is selected as the propulsion gas for aluminium powder, helium (He) is selected as the propulsion gas for titanium powder, and other specific fluid parameters are shown in Table 2.9.

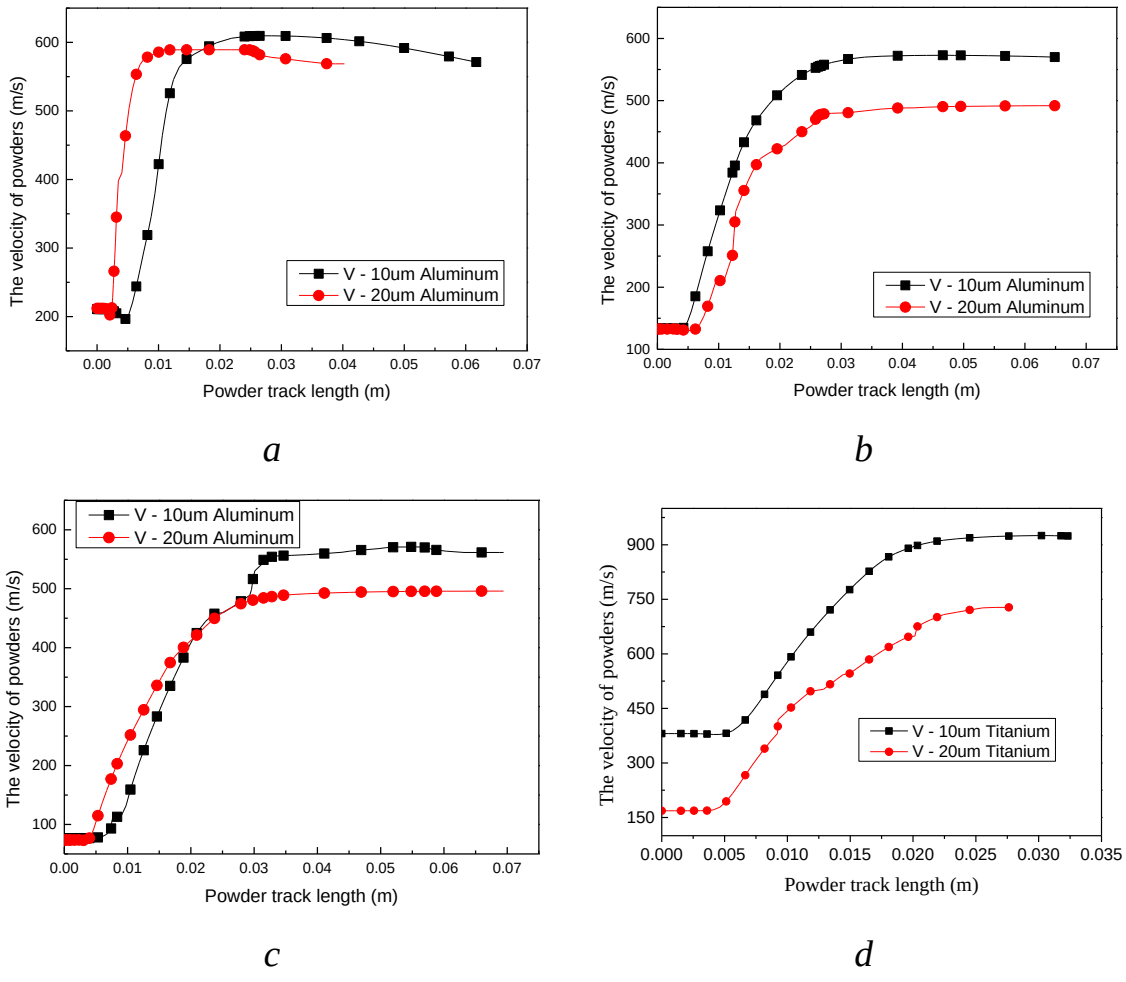

a – 8 mm, velocity curve (Al); *b* – 12 mm, velocity curve (Al); *c* – 16 mm, velocity curve (Al); *d* – 12 mm, velocity curve (Ti)

Fig. 2.24. The impact velocity and temperature changes of powder with different lengths of divergent section

Figure 2.24a-c shows that the length of the divergent section has little effect on the particle acceleration. Numerical simulation of titanium particles shows that the 10-micron titanium particles exceed 900 m/s, and the 20-micron titanium particles are about 750 m/s, as shown in Figure 2.24d.

Table 2.9 – Numerical simulation parameters for different lengths of divergent segments

Parameters / Length, mm	Propulsion gas pressure, MPa	Propulsion gas temperature, K	Powder injection pressure, MPa	Powder size, um	Materials
8	5	900 N2	0.8	10-20	Aluminum
12	5	900 N2	1.2	10-20	Aluminum
16	5	900 N2	1.0	10-20	Aluminum
12	5	900 He	0.6	10	Titanium
12	5	900 He	0.4	20	Titanium

If the spraying distance is too large, the powder speed and powder temperature will be reduced. Fig. 2.24 shows that the spraying distance is between 10 mm and 20 mm, and the powder has reached the maximum. The spraying distance is 10 mm (injection pressure 0.8 MPa), 15 mm (injection pressure 0.9 MPa) and 20 mm (injection pressure 0.95 MPa), the propulsion gas temperature is 900 K, and the powder is 10 μm aluminium. In addition, the throat size is the key factor affecting the fluid, thus affecting the particle acceleration. According to Fig. 5, the spraying distance of 15 mm is selected. Since the width of the propulsion gas inlet is 16 mm, in order to achieve the throat compression effect, the fillet is 18 mm, 22 mm and 26 mm, and the powder injection pressure is 0.9 MPa.

Hence, the powder collision velocity increases with the increase of the length of the divergent section, while the powder velocity reaches the maximum when the spraying distance is basically within 20 mm, while the collision temperature decreases

with the increase of particle trajectory, and the smaller the particle size, the more it decreases. However, 10 um aluminium powder can obtain greater collision velocity than 20 um aluminium powder under the same conditions, mainly because the obtained acceleration is greater. According to Formula 2.36, it is further deduced that the powder acceleration a = F/m, and the smaller the particle size, the greater the acceleration, which also explains the greater collision velocity of 10 um powder.

2.4.2.2 Spraying distance and throat size

Only when the spraying distance is appropriate, a better coating can be obtained. If the spraying distance is too large, the coating will be thin. This is because the size of the spraying distance affects the form of spraying airflow, which also affects the vertical velocity of spraying particles when they reach the surface of the matrix. When the distance is too small, although the airflow is all in a stable state, the powder which is not combined with the matrix will be bounced and collide with the subsequent powder after reaching the matrix, which slows down the speed of the subsequent powder and deteriorates the spraying effect. When the spraying distance is too large, although the airflow is also in a stable state near the surface of the matrix, it cannot reach the critical speed of the combination at a lower temperature. If the temperature is too high, the waste of energy and the defect of substrate and coating will be increased. If the spraying temperature and spraying pressure are increased, the deposition efficiency of powder will be improved. However, with the increase of temperature, the phenomenon of inclusion, sintering and even matrix melting will occur at the junction of substrate and coating. At the same time, due to the continuous improvement of temperature, alloy powder viscosity increases, and there will be a sticky gun problem, so the airflow in the gun is unstable, and the temperature rises suddenly, resulting in powder melting. In addition, with the constant increase of pressure, the substrate is seriously deformed and the surface appears a great depression, while the deposition efficiency is not improved but decreased.

Fig. 2.25 shows that the powder speed reaches the maximum when the spraying distance is 15 mm, indicating that the spraying distance should not be too short or too long. Too short will lead to the powder not accelerating effectively, and too long will lead to the loss of powder speed.

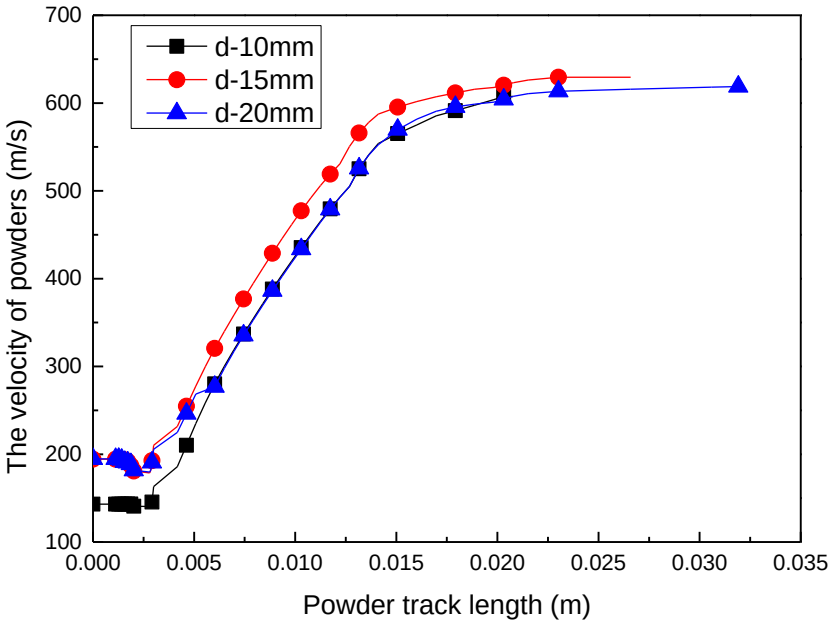

a

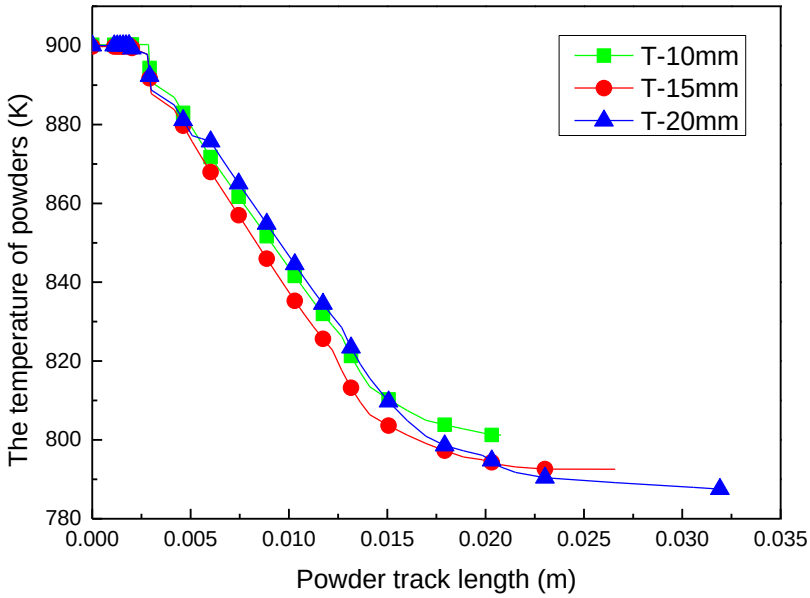

b

a – velocity curve; *b* – temperature curve

Fig. 2.25. Impact velocity and temperature variation of powder at different spraying distances

Fig. 2.26 shows that the throat is also a key factor affecting the powder collision speed. When the fillet 18 mm increases to 22 mm, the maximum powder speed increases by about 23 m/s, while when it increases from 22 mm to 26 mm, the growth rate is less, and the maximum powder speed only increases by about 8 m/s. therefore, with the increasing fillet radius (i.e., the decreasing throat size), the growth rate of the maximum powder speed will be less and less.

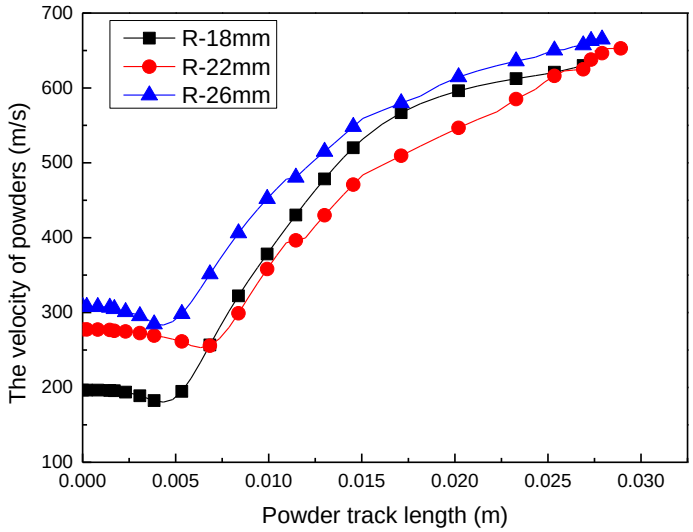

a

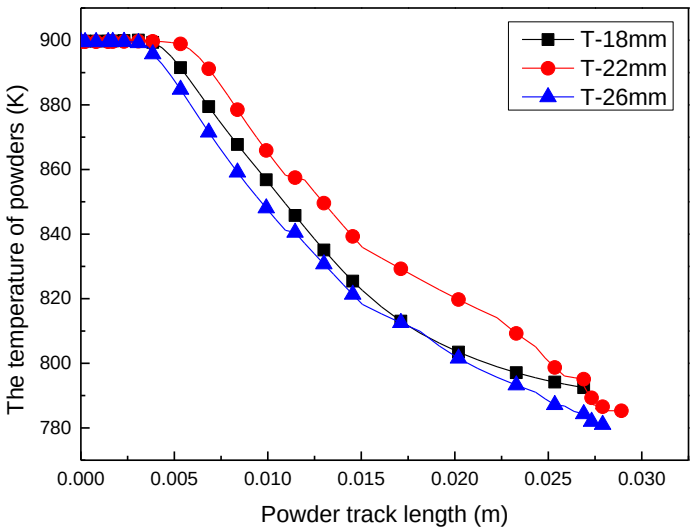

b

a – velocity curve; *b* – temperature curve

Fig. 2.26. Impact velocity and temperature variation of powder with different throat sizes

2.4.2.3 Influence of parallel inlet length

The high pressure of 5 MPa and the initial temperature of the gas is 600 K are used to discuss the influence of the inlet length on the gas outlet speed, as shown in Figure 2.27. The inlet length is too long or too short, which is not good for the growth of the gas outlet. Therefore, the 100 mm selected in this dissertation is scientific.

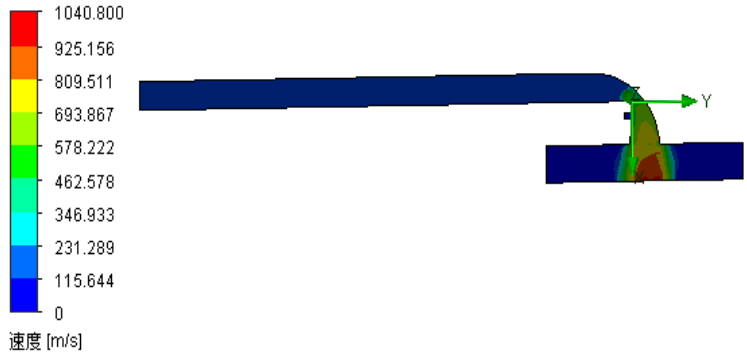

a

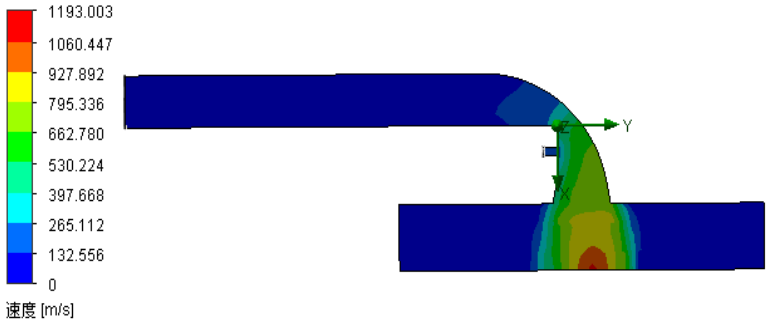

b

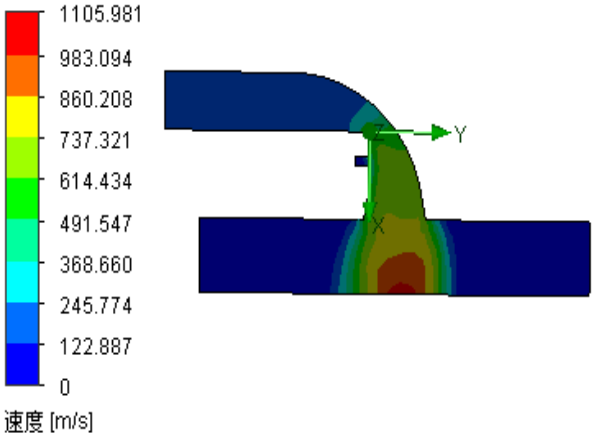

c

a – 200mm; *b* – 100mm; *c* – 50mm.

Fig. 2.27 Influence of different inlet lengths on outlet velocity

2.5 Multi-factor interaction analysis of the special single channel nozzle

According to the influence of divergence length, spraying distance and throat size on acceleration characteristics discussed by single factor [130] in Section 2.4, this is also the common analysis method used by most researchers, but the actual operation process is often multi-factor interaction. Therefore, multi-factor interaction analysis is more scientific and realistic.

2.5.1 Mathematical modeling

RSM is a product of a combination of mathematics and statistical methods. It is often used to find the optimal process parameters in a multi-parameter system [131]. This study uses the Box Behnken principle to design, and the comprehensive numerical results of the single factors, three independent variables (diffusion L, spraying D and fillet radius of throat R) are set through the Design-Expert software, and the powder speed is the dependent variable. A three-factor, three-level response surface quadratic regression equation is constructed. The model is:

$$y = \beta_0 + \sum_{i=1}^{m} \beta_i x_i + \sum_{i=1}^{m} \beta_{ij} x_j + \sum_{i=1}^{m} \beta_{ii} x_i^2 + \varepsilon, \tag{2.37}$$

Where y – response value of the regression equation;

X_i and X_j – independent variables;

M – the number of independent variables;

β_0 – the regression intercept;

β_i – the linear effect of X_i;

β_{ij} is the interaction effect of X_i and X_j;

β_{ii} – is the secondary effect of X_i;

ε – is a random error.

2.5.2 Create high and low code

Input the high (+1), medium (0), and low (-1) codes and actual parameters of the independent variable into the Expert Design software, which can reduce unnecessary testing and obtain the optimal test scheme. The test methods and results are shown in Table 2.10.

Table 2.10 – Test scheme and results

Run	High and low-level code			Actual value			Impact V, (m/s)
	Diffusion L, (mm)	Spraying D, (mm)	Fillet radius of throat, (mm)	Diffusion L, (mm)	Spraying D, (mm)	Fillet radius of throat, (mm)	
1	0	0	0	8	15	22	666
2	-1	+1	0	4	20	22	578
3	0	0	0	8	15	22	666
4	+1	0	-1	12	15	18	677
5	+1	+1	0	12	20	22	664
6	0	+1	-1	8	20	18	599
7	0	0	0	8	15	22	666
8	+1	0	+1	12	15	26	684
9	+1	-1	0	12	10	22	700
10	0	+1	+1	8	20	26	630
11	0	0	0	8	15	22	666
12	-1	0	+1	4	15	26	645
13	0	-1	+1	8	10	26	675
14	-1	0	-1	4	15	18	637
15	0	-1	-1	8	10	18	643
16	-1	-1	0	4	10	22	604
17	0	0	0	8	15	22	666

2.5.3Analysis of variance

As shown in Table 2.11, the model F-value of 7.04 and P-value of 0.0087 (less than 5%) imply the model is significant. The P-values of A and B are both less than 0.01 (less than 0.05), indicating that a single factor has a significant influence on the powder velocity. However, the P-values of C are greater than 0.05, indicating that a single factor has not a significant influence on the powder velocity. The P-values of

AB, AC, and BC are both greater than 0.05; hence, the interaction between diffusion length and spraying distance, diffusion length and Fillet radius of the throat, and spraying distance and fillet radius of the throat is not obvious. The regression equation at this time is formula 2.38:

$$Y = 666 + 32.75A - 19.25B + 9.75C - 1.75AB - 0.25AC - \\ - 0.25BC - 2.88A^2 - 26.88B^2 - 2.37C^2. \quad (2.38)$$

Table 2.11 – Analysis of variance

Source	Sum of squares	df	Mean square	F value	P-value
Model	15505.76	9	1722.86	7.04	0.0087
A-Diffusion L	8580.5	1	8580.5	35.08	0.0006
B-Spraying D	2964.5	1	2964.5	12.12	0.0102
C-Fillet radius of throat R	760.5	1	760.5	3.11	0.1212
AB	12.25	1	12.25	0.05	0.8293
AC	0.25	1	0.25	1.022e-3	0.9754
BC	0.25	1	0.25	1.022e-3	0.9754
A^2	34.8	1	34.8	0.14	0.7172
B^2	3041.12	1	3041.12	12.43	0.0096
C^2	23.75	1	23.75	0.097	0.7644
Residual	1712	7	244.57		
Lack of fit	1712	3	570.67		
Error	0	4	0		
Total	17217.76	16			

The lack of fit error is not significant. The determination coefficient of the regression equation is R^2=0.9006 and the correction coefficient R^2=0.754. These results indicate that the regression model can explain 90.06% of the change in powder velocity response.

2.5.4 Result of multi-factor interaction

It can be seen from Fig. 2.28 that the order of the influence of the three factors is that diffusion length is greater than spraying distance, spraying distance is greater than the fillet radius of the throat, and the maximum powder velocity is taken as the target, the optimal velocity is predicted to be 707.2 m/s（Fig. 2.29).

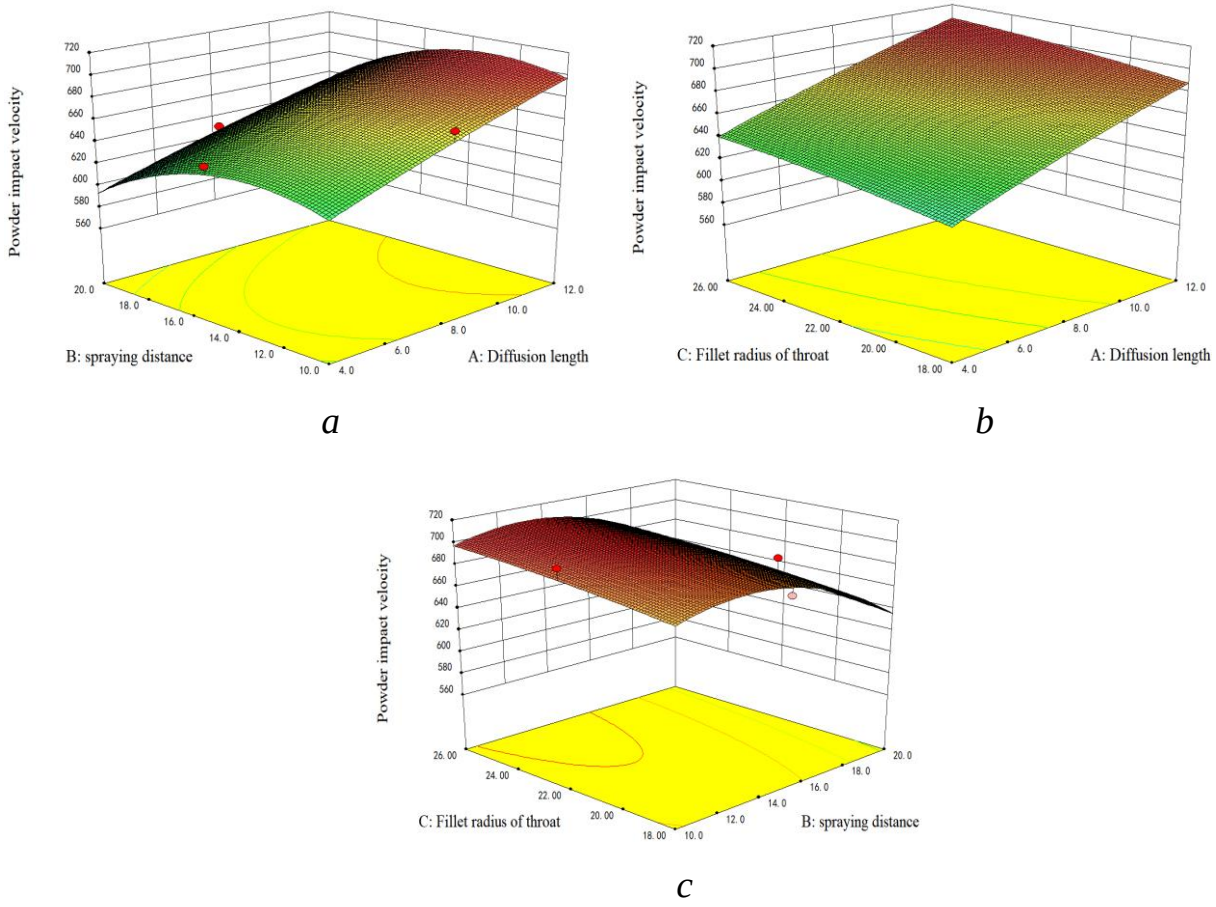

a *b*

c

a – A and B factors interaction influence; *b* – A and C factors interaction influence; *c* – B and C factors interaction influence.

Fig. 2.28. Interaction effect of three factors on response under N2 conditions

To verify the optimized parameters, import the optimized parameters into the SolidWorks flow simulation module. The simulation results (Fig. 2.30) show that the powder velocity is 705 m/s, with an error of 0.3 %. Therefore, the response surface analysis is highly accurate.

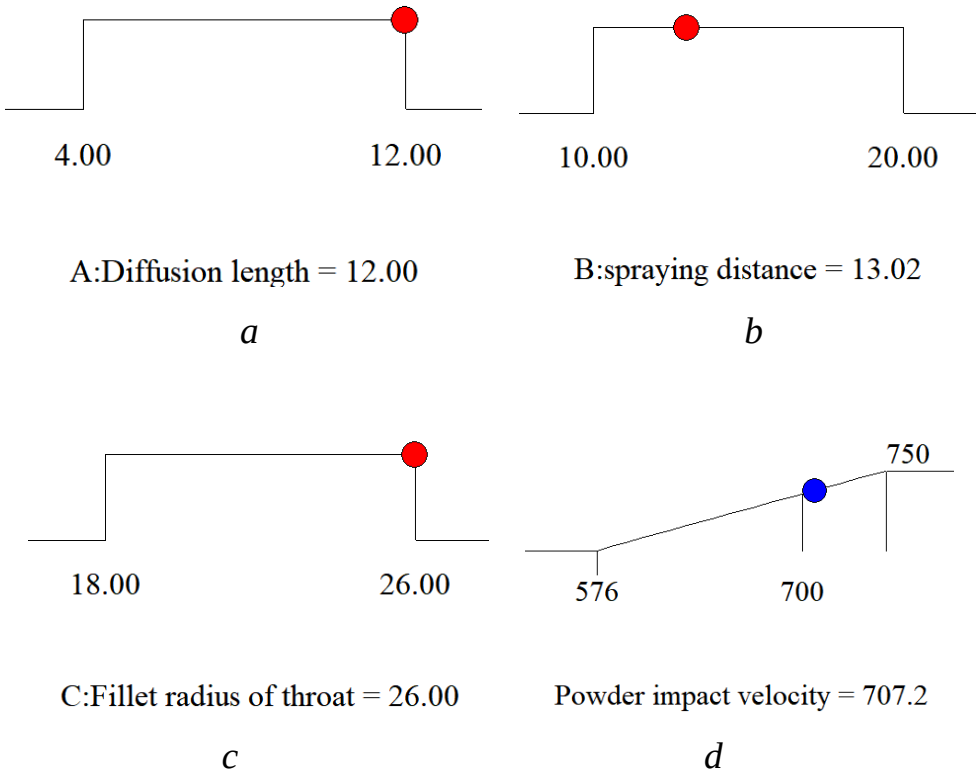

a – optimum diffusion length; *b* – optimum spraying distance; *c* – optimum fillet radius of throat; *d* – response speed.

Fig. 2.29. Numerical simulation collision velocity under optimal parameter conditions under N_2

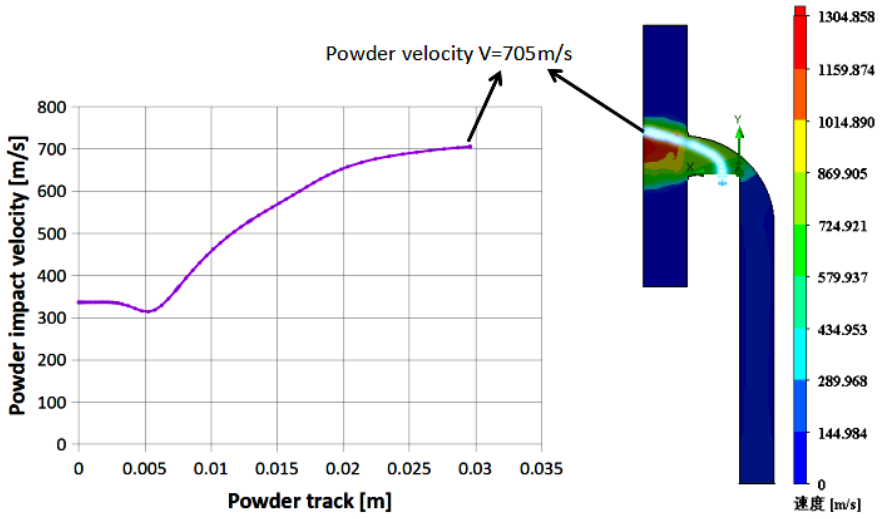

Fig. 2.30. Powder velocity trajectory and velocity nephogram after structure optimization

2.5.5 Application analysis

The application range of the optimized new nozzle structure is further discussed. Taking the critical velocity of powder as the standard, the critical velocity can be calculated theoretically. The 10-micron size powder particles are selected, the powder is injected at room temperature, and the temperature of propulsion gas ranges from 400 K to 1200 K. Through the summary of theoretical critical velocity (Eq. 2.33) and numerical simulation velocity data (Table 2.12), the new cold spraying nozzle of this study can spray Ni, Ti, Cu, Al, Zn and Mg, which has a wide application prospect.

Table 2.12 – The optimized spraying is applicable to different powder materials

Powder parameters \ Temperature, K		400	500	600	700	800	900	1000	1100	1200
Ni	Maximum speed, m/s	-	-	-	-	-	533	550	570	585
	Critical speed, m/s	-	-	-	-	-	587	574	564	552
	Recommend	-	-	-	-	-	-	-	-	[ref]
Ti	Maximum speed, m/s	-	-	-	587	615	640	658	680	698
	Critical speed, m/s	-	-	-	632	619	605	590	576	560
	Recommend	-	-	-	-	-	-	[ref]	[ref]	[ref]
Cu	Maximum speed, m/s	-	-	464	488	512	532	-	-	-
	Critical speed, m/s	-	-	480	467	452	437	-	-	-
	Recommend	-	-	-	-	[ref]	[ref]	-	-	-
Al	Maximum speed, m/s	525	568	608	-	-	-	-	-	-
	Critical speed, m/s	570	544	517	-	-	-	-	-	-
	Recommend	-	-	[ref]	-	-	-	-	-	-
Mg	Maximum speed, m/s	562	608	652	-	-	-	-	-	-
	Critical speed, m/s	630	600	570	-	-	-	-	-	-
	Recommend	-	-	[ref]	-	-	-	-	-	-
Zn	Maximum speed, m/s	432	463	-	-	-	-	-	-	-
	Critical speed, m/s	299	274	-	-	-	-	-	-	-
	Recommend	[ref]	[ref]	-	-	-	-	-	-	-

2.5.6 Summary this section

The RSM has a certain guiding significance for multi-factor parameter optimization. The response surface model obtained by this study is reliable with an error of 0.3% and high accuracy. By analyzing the structure of cold spraying 90° rectangular nozzle, some meaningful conclusions are drawn:

1) when the length of the inlet cross-sectional area of the propulsion gas is 10 mm, and the width is 3 mm, that is, the cross-sectional area of the inlet is 30 mm^2, the optimal structural parameters are as follows: the length of the divergent section is 12 mm, the spraying distance is 13 mm, and the fillet radius is 26 mm. At this time, the maximum speed of 10 um aluminum powder can reach 705m/s.

2) The optimized 90° rectangular nozzle can meet the spraying of a variety of common metal powders with a size of 10 um between 400 K…1200 K, which has a certain process reference value.

2.6 Research on the special cold spraying multi-channel nozzle

Because of the advantages of CS [132], it expands and makes up for the defects in the field of thermal spraying. Therefore, it has an optimistic prospect and market. In recent years, a lot of researchers [133–135] have been interested in CS. Moreover, more and more cold-spraying institutions in the world are being founded [136]. For the nozzle structure, the outlet of the nozzle is a mainly circular section, but there is also a square or oval nozzle because of special application occasions [137]. However, there is almost no relevant research on the multi-channel rectangular nozzle. Therefore, this study on multi-channel spraying will provide a new idea and theoretical guidance for the surface coating field.

2.6.1 Established the multi-channel model method

Due to the lack of literature on the rectangular nozzle, the CFD method is used to discuss the situation of the single-channel nozzle when the powder inlet is set

before the compression of the nozzle throat. The author uses the optimized single-channel rectangular section nozzle (the throat chamfer radius is 26 mm, the spraying distance is 13 mm, and the expansion section length is 12 mm) to discuss the multi-channel nozzle further. As shown in Fig. 2.30, the powder injection port is set in the diffusion section area, the particles meet the requirements of single-channel spraying (Table 2.12). This dissertation discussed that the powder injection port is set in front of the throat to make powder further accelerated using a multi-channel. At this time, multiple channels need to be considered to change the particle trajectory to avoid the collision between the particles (nickel, titanium, copper, aluminum, magnesium, and zinc) and the nozzle section divergence's inner wall. The technological parameters were studied as the standard with impact velocity [138] or critical velocity [139].

To facilitate the understanding of multi-channel nozzle, this paper defines some keywords based on Fig. 2.31: Internal part 1 (M), Internal part 2 (N), Internal channel 1 (U), Internal channel 2 (V), Internal channel 3 (W). It should be noted that M and N are not final optimized structures and need further discussion. U, V, and W also change with the optimization of M and N. The optimal structure can be predicted by numerical simulation methods to avoid the waste of resources caused by direct processing. The basic dimensions are shown in Figure 2.23 show.

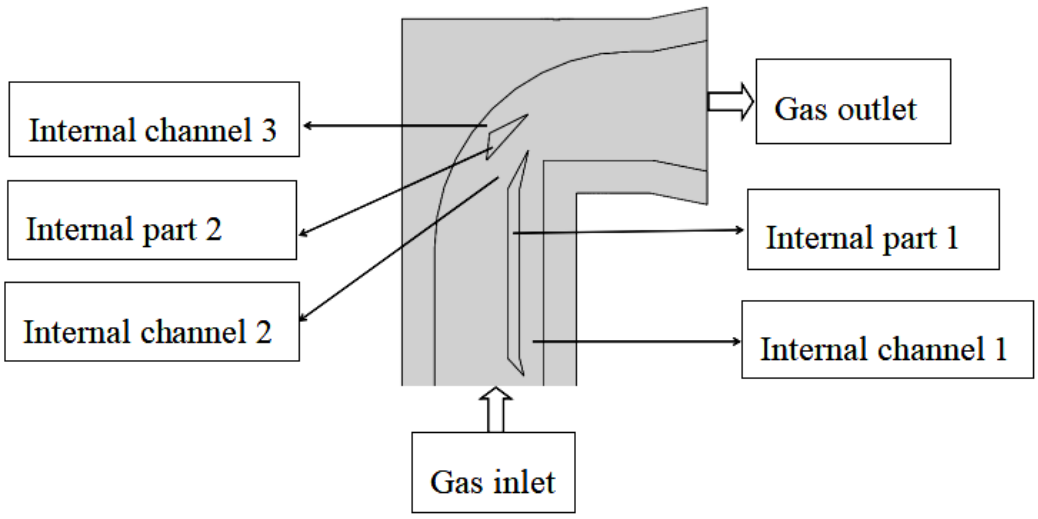

Fig. 2.31. Initial diagram model of multi-channel nozzle

2.6.2 Study on particle trajectory in multi-channel nozzle

The collision between particles and the inner wall of the nozzle divergent section is mainly affected by the position of M, recovery coefficient, particle size [140], nozzle material [118], and inject powder pressure. The influence position of M is shown in Fig. 2.32, and its parameters are: A (Fig. 10,b) of M is higher than B, the inlet pressure is 5 MPa, the temperature of N_2 is 600 K, the injection pressure is 3.1 MPa, and particle sizes are 10 μm, 20 μm, 30 μm, 40 μm, and 50 μm respectively. Maintain the inlet pressure of 5 MPa, the temperature of 600 K and the particle size of 10microns, and the particle trajectory of different injection pressures 3.1 MPa, 3.3 MPa, 3.4 MPa, 3.6 MPa, and 4 MPa) was shown in Fig. 2.33.

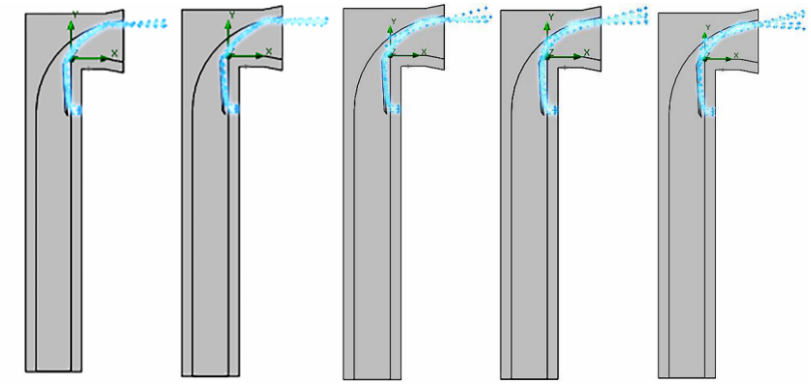

a *b* *c* *d* *e*

a – 10 μm; *b* – 20 μm; *c* – 30 μm; *d* – 40 μm; *e* – 50 μm

Fig. 2.32. Particle trajectories of different particle sizes

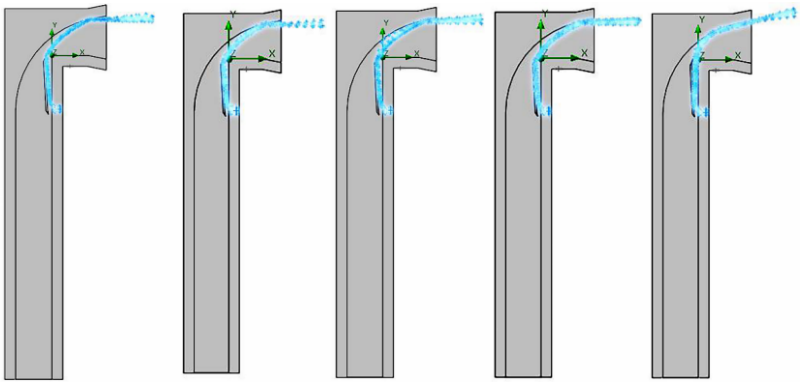

a *b* *c* *d* *e*

a – 3.1 MPa; *b* – 3.3 MPa; *c* – 3.4 MPa; *d* – 3.6 MPa; *e* – 4 MPa

Fig. 2.33. Particle tracks of powder injection ports at different injection pressures

It can be seen from Fig.2.32 and Fig. 2.33 that particle size and powder injection pressure have little influence on particle trajectory, and particles are in contact with the inner wall of the nozzle. Therefore, the structure needs to be further adjusted. The inner passage is flush with the outlet (point A and point B are of equal height), as shown in Fig. 2.33.

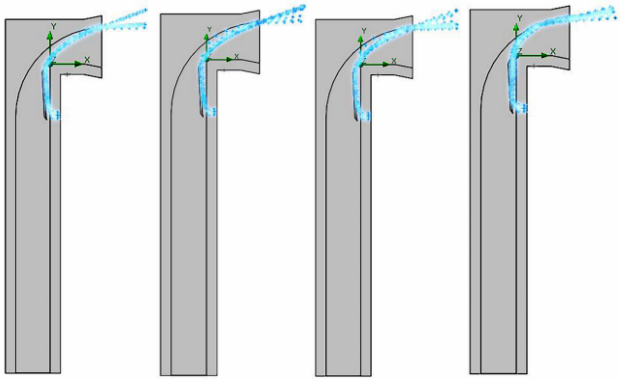

a *b* *c* *d*

a – 3.4 MPa; b – 3.6 MPa; c – 3.8 MPa; d – 4 MPa

Fig. 2.34. Particle tracks of different powder injection pressures when A and B are flush

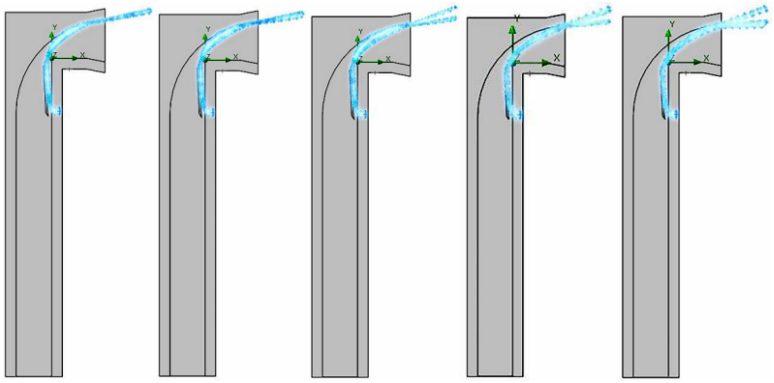

a *b* *c* *d* *e*

a – 0.2; b – 0.4; c – 0.6; d – 0.8; e – 1.0

Fig. 2.35. Particle trajectories with different recovery coefficients

Fig. 2.34 and Fig. 2.35 show that the particle trajectory can be improved by improving point A's position and recovery coefficient, but it is still not ideal.

Therefore, in the case of multiple internal channels, reducing the position and recovery coefficient of point A by changing the particle diameter and powder injection port pressure alone can not solve the problem of contact between powder and the inner wall of the nozzle.

Based on the above problems, consider adding another channel to solve. Since particles are mainly affected by drag forces in the fluid, this dissertation assumes that the powder is spherical particles with smooth surfaces (Fig. 2.36a), and the aerodynamic drag force Equation which is shown in (2.39), ignoring the particle gravity, the main force channels U and V of particles are represented by 1 and 3 respectively, and the force direction 2 is the resultant direction. The force analysis diagram is shown in Fig.2.36b, when the particle force direction of V is horizontal, the particle trajectory can be improved from force 1 direction to 2 direction.

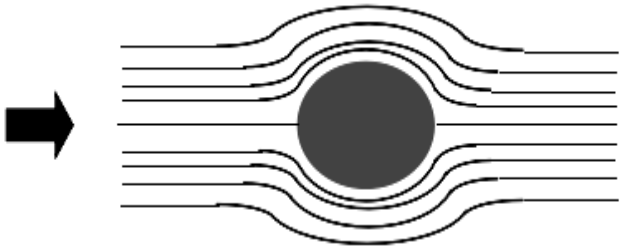

a

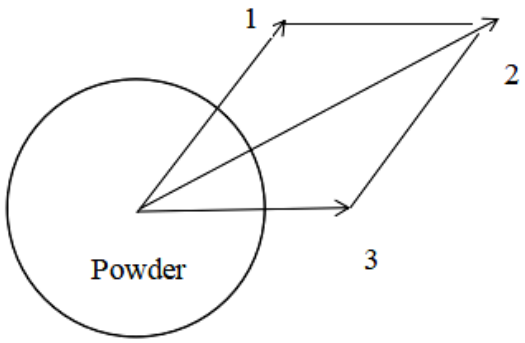

b

a – the path of a fluid through a particle; *b* – force analysis diagram of particles in fluid

Fig. 2.36. Particles are subjected to fluid action

$$F = \frac{1}{2} C_D \rho_g (v_g - v_\rho)^2 S, \tag{2.39}$$

where F – aerodynamic drag force on the particles;

C_D – drag coefficient;

ρ_g – density of the airflow;

V_g and V_P – gas flow velocity and particle velocity respectively;

S – the upwind area of particles.

Further, N was added, and the channels were changed into U, V, and W. The position of N was optimized to improve the particle trajectory. When the distance between N and M was further optimized to 1.2 mm, the result was relatively ideal, as shown in Fig. 2.37. The specific parameters are shown in Fig. 2.38.

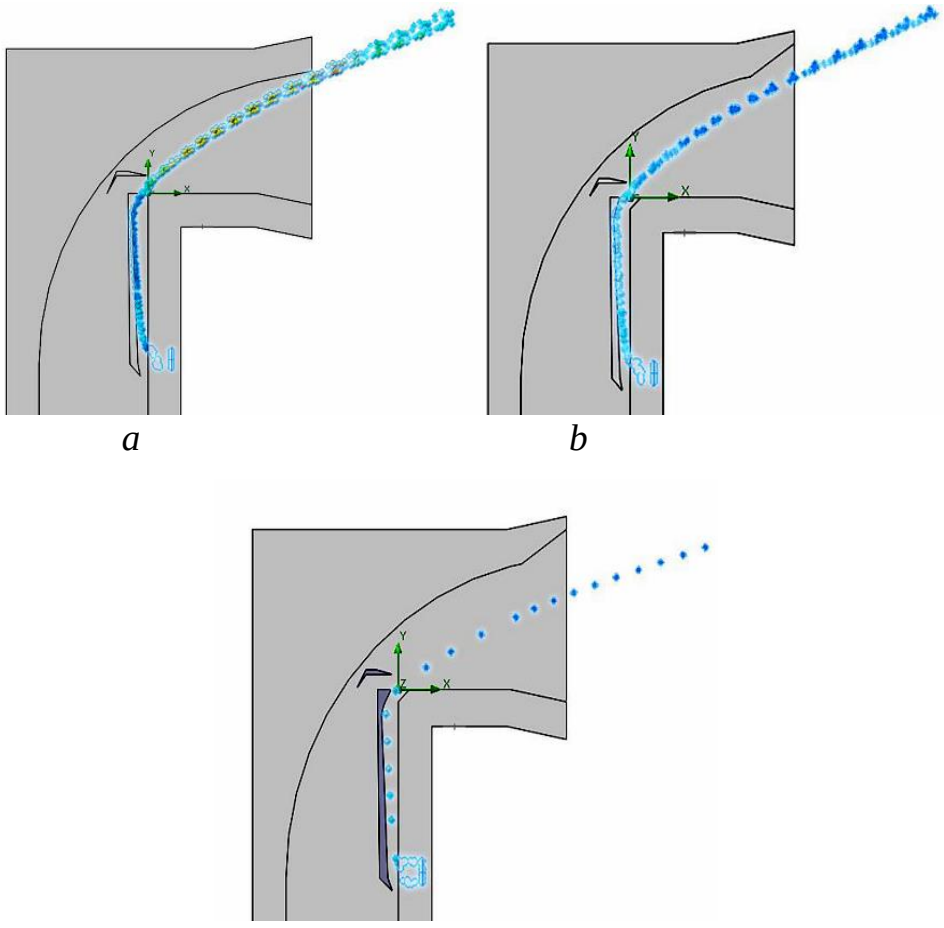

a *b* *c*

a – 1.6 mm (Al – 10 μm); *b* – 1.2 mm (Al – 10 μm); *c* – 1.2 mm (Al – 15 μm)

Fig. 2.37. Distance between M and N components

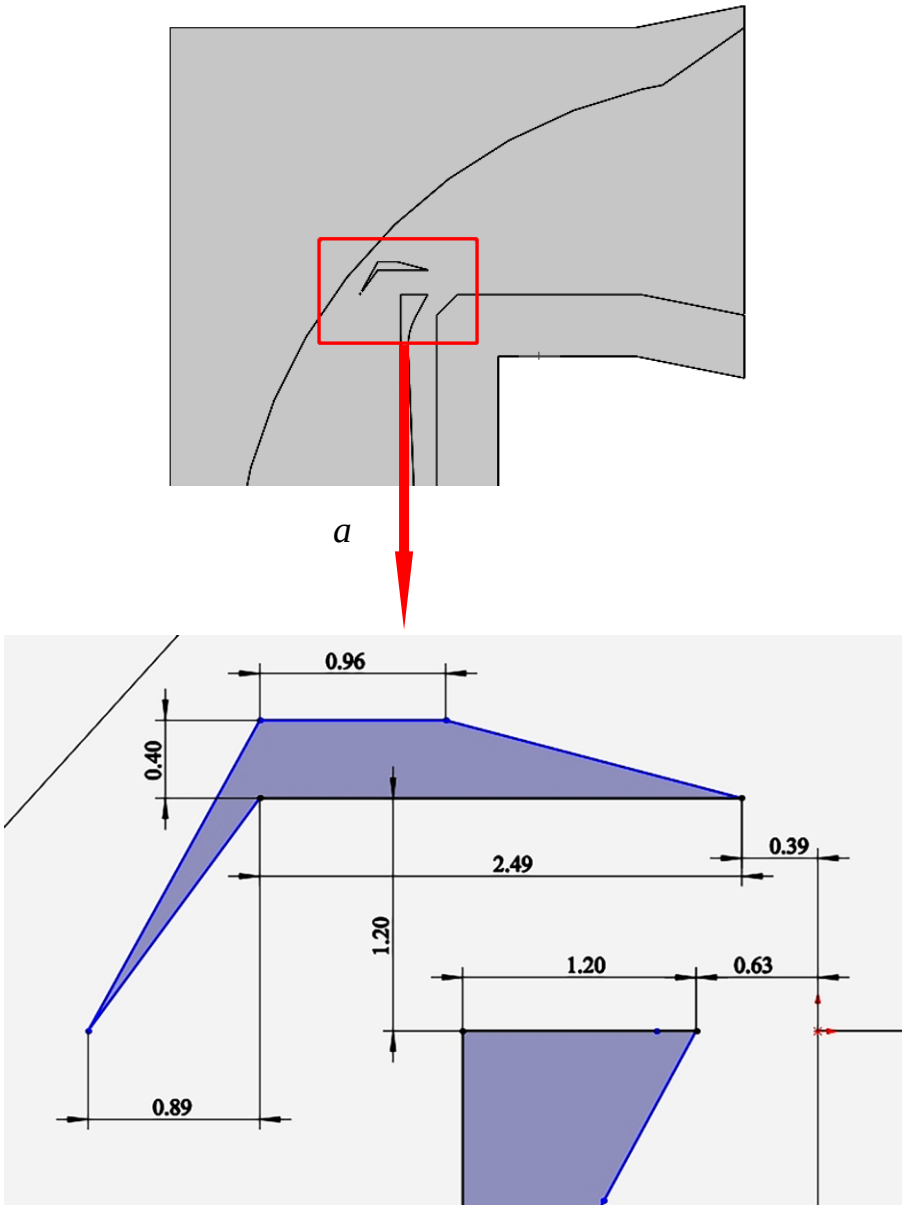

a

b

a – the dimension location of the 3D model; *b* – detailed dimensions

Fig. 2.38. The specific size after optimization

2.6.3 Analysis of technological parameters

The main factors affecting impact velocity are gas pressure, temperature, and particle diameter [117]. Although the recovery coefficient has little influence on the collision velocity (Table 2.13), it influences the particle trajectory, as shown in Fig. 2.39. Hence, selecting a smaller recovery coefficient is beneficial to the particle trajectory.

Table2.13 – Numerical simulation parameters and results of aluminum particles

The pressure of N_2, MPa	The temperature of N_2, K	Injection pressure, MPa	Particle diameter, μm	Recovery coefficient	V_{impact}, m/s
5.0	800	3.0	10	1.0	608
5.0	800	2.55	15	1.0	535
5.0	800	2.55	20	1.0	482
5.0	700	3.0	10	1.0	580
5.0	900	3.0	10	1.0	635
5.0	900	3.2	10	0.7	633
5.0	900	3.2	10	0.4	635
5.0	900	3.2	10	0.2	633
4.5	900	2.9	10	0.7	623
5.5	900	3.0	10	0.7	589

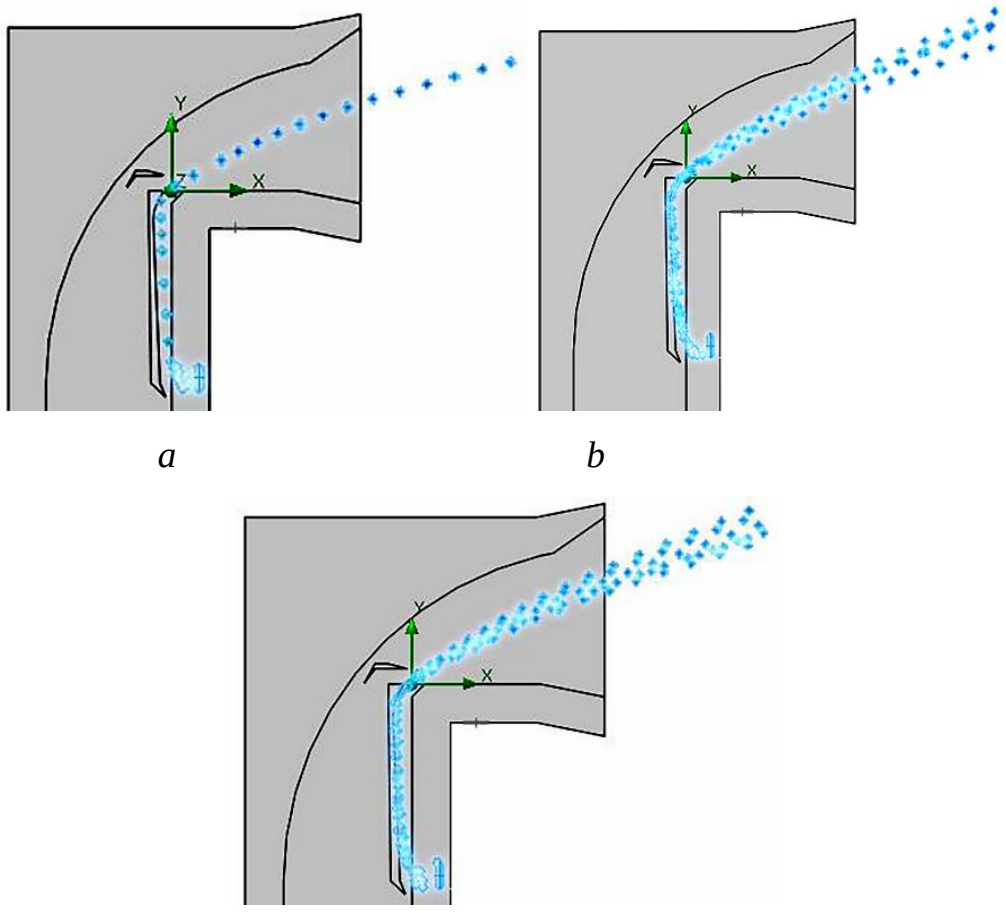

a *b*

c

a – D = 10 μm; *b* – D = 30 μm; *c* – D = 50 μm.

Fig. 2.39. Trajectory diagram of different particle sizes under recovery coefficient e = 0.1

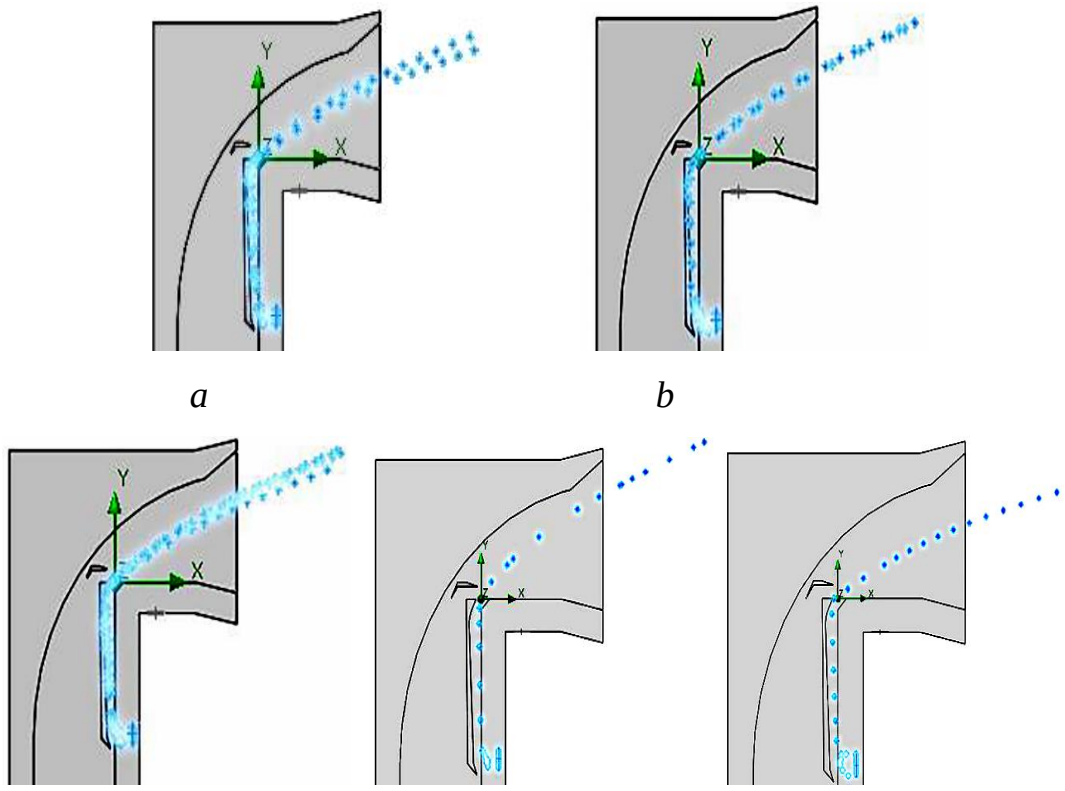

a – Ti; *b* – Cu; *c* – Ni; *d* – Mg; *e* – Zn

Fig. 2.40. Particle trajectories of different materials

Table2.14 – Technological parameters and results of other common materials

Materials	The pressure of N_2, MPa	The temperature of N_2, K	Injection pressure, MPa	Particle diameter, μm	Recovery coefficient	V_{impact}, m/s	T_{impact}, K
Ti	5	1000	2.7	10	0.1	592	808
Cu	5	900	2.7	10	0.1	485	726
Ni	5	1000	2.7	10	0.1	500	835
Mg	5	600	2.9	10	0.1	576	460
Zn	5	500	2.7	10	0.1	416	381

According to the numerical simulation results of several common materials (Table 2.14), particles of different materials have different paths (Fig. 2.40), and their collision velocities differ significantly. Magnesium powder with low density has a speed of 576 m/s at 600 K. The velocity of titanium powder can reach 592 m/s at the gas temperature of 1000 K, etc. These results show that the material with lower

density can obtain higher impact velocity, while the powder material with higher density can only obtain lower impact velocity, and the temperature has a significant influence on the impact velocity, etc.

Table2.15 – Common metal critical velocity at different temperatures

Gas T, K		300	400	500	600	700	800	900	1000	1100
Ni	Maximum speed, m/s	-	-	-	-	-	-	485	500	508
	Powder T, K	-	-	-	-	-	-	700	797	864
	Critical speed, m/s	-	-	-	-	-	-	476	428	392
	Recommend	-	-	-	-	-	-	-	Rec.	Rec.
Ti	Maximum speed, m/s	-	-	-	-	-	546	576	593	619
	Powder T, K	-	-	-	-	-	610	699	791	872
	Critical speed, m/s	-	-	-	-	-	545	507	464	423
	Recommend	-	-	-	-	-	-	Rec	Rec.	Rec.
Cu	Maximum speed, m/s	-	-	-	423	446	462	475	-	-
	Powder T, K	-	-	-	451	524	580	641	-	-
	Critical speed, m/s	-	-	-	437	404	376	344	-	-
	Recommend	-	-	-	-	Rec.	Rec	Rec.	-	-
Al	Maximum speed, m/s	-	-	503	546	-	-	-	-	-
	Powder T, K	-	-	372	451	-	-	-	-	-
	Critical speed, m/s	-	-	492	413	-	-	-	-	-
	Recommend	-	-	-	Rec	-	-	-	-	-
Mg	Maximum speed, m/s	-	-	541	582	-	-	-	-	-
	Powder T, K	-	-	379	451	-	-	-	-	-
	Critical speed, m/s	-	-	549	475	-	-	-	-	-
	Recommend	-	-	-	Rec	-	-	-	-	-
Zn	Maximum speed, m/s	350	383	419	-	-	-	-	-	-
	Powder T, K	293	309	376	-	-	-	-	-	-
	Critical speed, m/s	287	275	223	-	-	-	-	-	-
	Recommend	Rec	Rec.	Rec	-	-	-	-	-	-

Comparing the collision velocity with the critical velocity is the standard to judge whether the powder can be deposited. The critical velocities of nickel (Ni),

titanium (Ti), copper (Cu), aluminum (Al), magnesium (Mg), and zinc (Zn) can be obtained by theoretical calculation.

As the melting point of different metal materials is different, the value range of temperature data in Table2.15 is not more than $0.7T_m$. For example, the melting point of aluminum is 916 K; hence, the maximum temperature is 600 K.

2.6.4 Result and discussion

In this section, the powder track and technological parameters of powders inside the multi-channel nozzle with 90° are analyzed, it is feasible to apply the multi-channel nozzle to spray typical metal powder. The influence analysis of particle trajectory, including powder injection pressure, Inlet gas pressure, and temperature, particle size, recovery coefficient, has revealed the following:

1) due to high-pressure cold spraying, if the powder injection pressure is too small, it is difficult to inject into the internal channel of the nozzle. If the powder injection pressure is too enormous, there will be different degrees of rebound according to the recovery coefficient of M material. Therefore, it is necessary to adjust the powder injection pressure reasonably. Inlet propulsion gas pressure and temperature mainly affect fluid velocity and then affect particle acceleration, so parameters need to be adjusted according to practical engineering applications. Particle size affects particle acceleration. The larger particle trajectory is upward, mainly because the force on direction 1 is greater. Therefore, to avoid particle contact with the inner wall, the smaller particle size should be selected as far as possible for the multi-channel nozzle with 90°. Distance between M and N affects the particle trajectory. When the distance is larger, the particle trajectory is upward, mainly because the force on direction 3 is smaller, resulting in direction 2 of the resultant force being more upward;

2) as Table 2.3 shows, the process analysis of typical metal powders under the condition that the matrix and powder materials are the same, the particles that meet the critical velocity requirements include copper, magnesium, and zinc. When the

matrix and powder materials have different properties, aluminium (aluminium collides with titanium) can meet the requirements of critical velocity, which has a broad application prospect.

Compared with existing single-channel nozzles, multi-channel nozzles with 90° have advantages in limited space spraying because in practical engineering applications, only the divergence length of the nozzle is considered, and the operation is more convenient. However, this dissertation only preliminarily proposed the feasibility of multi-channel nozzle application in spraying. For the M and N structures in Fig. 2.38, if processing, cost, and other factors are taken into further consideration, their structures need to be further optimized. As shown in Fig. 2.38, many sharp points need to be filleted, etc. Alternatively, later research can consider further optimizing multiple factors by using functional relations.

Because of the technological parameters, this dissertation only discusses the several common kinds of metal powder and other materials can be discussed further in the future, because of the influence of temperature on the nozzle internal fluid velocity is larger, thus affecting powder particle velocity, it is necessary to take into account the manufacturing materials of the nozzle, such as titanium and nickel powder can raise the temperature further improve powder outlet velocity.

The 90° multi-channel nozzle presented in this dissertation is an innovative structure, and the difficulty of multi-channel nozzle research lies in the commonality of powder; after all, many factors affect the movement trajectory of powders. The future trend is to establish a perfect mathematical method for the multi-factor or experimental method to improve the multi-channel nozzle.

2.6.5. Summary of this section

1) The research of cold spraying nozzles is an interesting point for science researchers. According to different application occasions, different nozzles are designed and manufactured. Some special applications need to study special nozzles. In order to further facilitate spraying, a three-dimensional model of the multi-channel

nozzle is established in this paper, and the influencing factors of particle trajectory are discussed through the fluid module. For the multi-channel cold spraying nozzle with a divergence section of 90°, when the powder injection port is located before the throat, multiple fluid internal channels need to be set in the throat to avoid contact between particles and the inner wall of the divergent section of the nozzle. Parameters influence particle trajectory such as powder injection port pressure, particle size, recovery coefficient, etc.

2) Multi-channel cold spraying nozzles with a 90° angle will be more convenient to use, such as some corners, internal areas, etc. Proper optimization of the nozzle, which can meet a variety of powder material (aluminum, copper, magnesium, and zinc) spraying, has a good application prospect.

2.7 Conclusion of Chapter 2

The main research work in this chapter is about the structural parameters and optimization of a special cold spraying nozzle and analyzes its process parameters.

1. The theoretical parameters that need to be considered in the structural design process of a cold spraying nozzle are fluid parameter, nozzle cross-section parameter, Mechanical condition of the nozzle, and gas dynamics parameter.

2. The influencing parameters of special nozzle fluid outlet velocity are mainly gas temperature, gas pressure, nozzle throat size, nozzle special angle, spraying distance and so on.

3. The structural parameters that affect the powder impact velocity of a special single-channel nozzle include the length of the expansion section, throat structure, powder size powder material, etc.

4. Under the action of a single factor, temperature, pressure, and particle diameter have significant effects on particle velocity, respectively, and the order of influence is that temperature is greater than powder diameter and powder diameter is greater than gas pressure.

5. Under the interaction of multiple factors, the interaction between temperature

and pressure is obvious, while the interaction between temperature and particle diameter, gas pressure and particle diameter are not obvious. The quadratic regression model established in this study can reflect the response value of the outlet velocity well by comparing the optimized parameters after RSM with the actual velocity parameters. With an error of 0.76%, the response surface quadratic regression model has high accuracy.

6. For the special single-channel cold spraying nozzle, when the length of the inlet cross-sectional area of the propulsion gas is 10 mm, and the width is 3 mm, that is, the cross-sectional area of the inlet is 30 mm^2, the optimal structural parameters are as follows: the length of the divergent section is 12 mm, the spraying distance is 13 mm, and the fillet radius is 26 mm. At this time, the maximum speed of 10 um aluminum powder can reach 705 m/s.

7. For the special multi-channel cold spraying nozzle with a divergence section of 90°, when the powder injection port is located before the throat, multiple fluid internal channels need to be set in the throat to avoid contact between particles and the inner wall of the divergent section of the nozzle. Parameters influence particle trajectories, such as powder injection pressure, Inlet gas pressure, temperature, particle size, Recovery coefficient, etc.

8. Multi-channel cold spraying nozzles with a 90° angle will be more convenient to use, such as some corners, internal areas, etc.

CHAPTER 3
SIMULATION RESEARCH ON COLD SPRY DEPOSITION ONTO TITANIUM ALLOY SUBSTRATE

3.1 Cold spray deposition characteristics

Cold spraying is a new surface technology completely different from thermal spraying. Compared with traditional thermal spraying technology [141], cold spraying has the following characteristics [142-143]:

1) low deposition temperature and has little thermal influence on coating and matrix. Cold spraying is realized by strong plastic deformation at low temperatures. The deposited particles will not be affected by obvious thermal effects and can well retain the organizational structure and physical properties of the original powder, basically avoiding oxidation, component burn loss, grain growth, and other problems [144]. It is of great significance to prepare thermal-sensitive coatings (such as Cu, Ti and their alloys), phase change-sensitive coatings (such as carbon matrix composites) and nanocrystalline coatings, which are difficult to obtain by conventional thermal spraying. The thermal effect of cold spraying on the matrix is also very small, and the most direct advantage is to expand the choice space of the base material. Currently, the available base material has been expanded from the traditional metal alloy to ceramics, plastics, etc.

2) A wide selection of materials can be used to prepare composite coating. There are many kinds of materials that can be deposited by cold spraying. According to current studies, metal materials include Al, Ni, Ti, etc.; refractory metals include Mo, Ta, etc.; alloy materials include Ni-Al, Cu-W, MCrAlY, etc.; and ceramic materials include Al2O3, Cr3C2-NICR, WC-Co, etc. [145]. Cold spraying of powder does not have a high standard; as long as the particle size can meet the requirements, spraying can generally be implemented. Therefore, the mechanical mixing method is usually used to freely combine, and compound powder is prepared, and then cold spraying is used to obtain a heterogeneous composite coating with uniform composition.

3) The porosity of the sedimentary layer is low, and the bonding strength with the matrix is high. The coating is formed by the high-speed impact of powder and substrate and the severe plastic deformation. In the process of deposition, the high-speed impact of subsequent particles will tamp the coating deposited earlier. At the same time, the coating does not undergo the shrinkage process of cooling from the molten state, so the porosity of the coating obtained is low, and the density can be as high as 98% or more [137], which can be used to prepare some coatings with high thermal conductivity, high electrical conductivity and anti-corrosion. In addition, the bonding strength between the coating and the substrate is enhanced by the tamping effect of spray particles, which can reach more than 100 MPa.

4) The deposition layer bears compressive stress and can be used to prepare the large-thickness coating. Different from thermal spraying, cold spraying realizes coating deposition at low temperatures, and the residual stress in the coating is low, and both are compressive stress, which is conducive to the preparation of coating with a larger thickness [146].

5) High powder utilization rate, safety and environmental protection. Cold spraying is to realize deposition at low temperatures. The undeposited powder will not change its physical and chemical properties at low temperatures and can be recycled and used continuously to achieve 100% [147]. At the same time, cold spraying is easy to operate, safe, has no radiation, and no pollution to the environment. Is a green, environmental protection, energy-saving spraying technology.

6) High cost and investment. Helium gas is usually used in the cold spraying process to improve spraying quality, especially when spraying steel base, nickel base or superalloy, which greatly increases the cost compared to thermal spraying.

In this dissertation, the Abaqus/Explicit method was used to spray aluminum, copper, Ti-6Al-4V, titanium and tungsten alloy onto Ti-6Al-4V substrate to study the effects of different metal particle properties. The research map of this chapter is shown in Fig. 3.1.

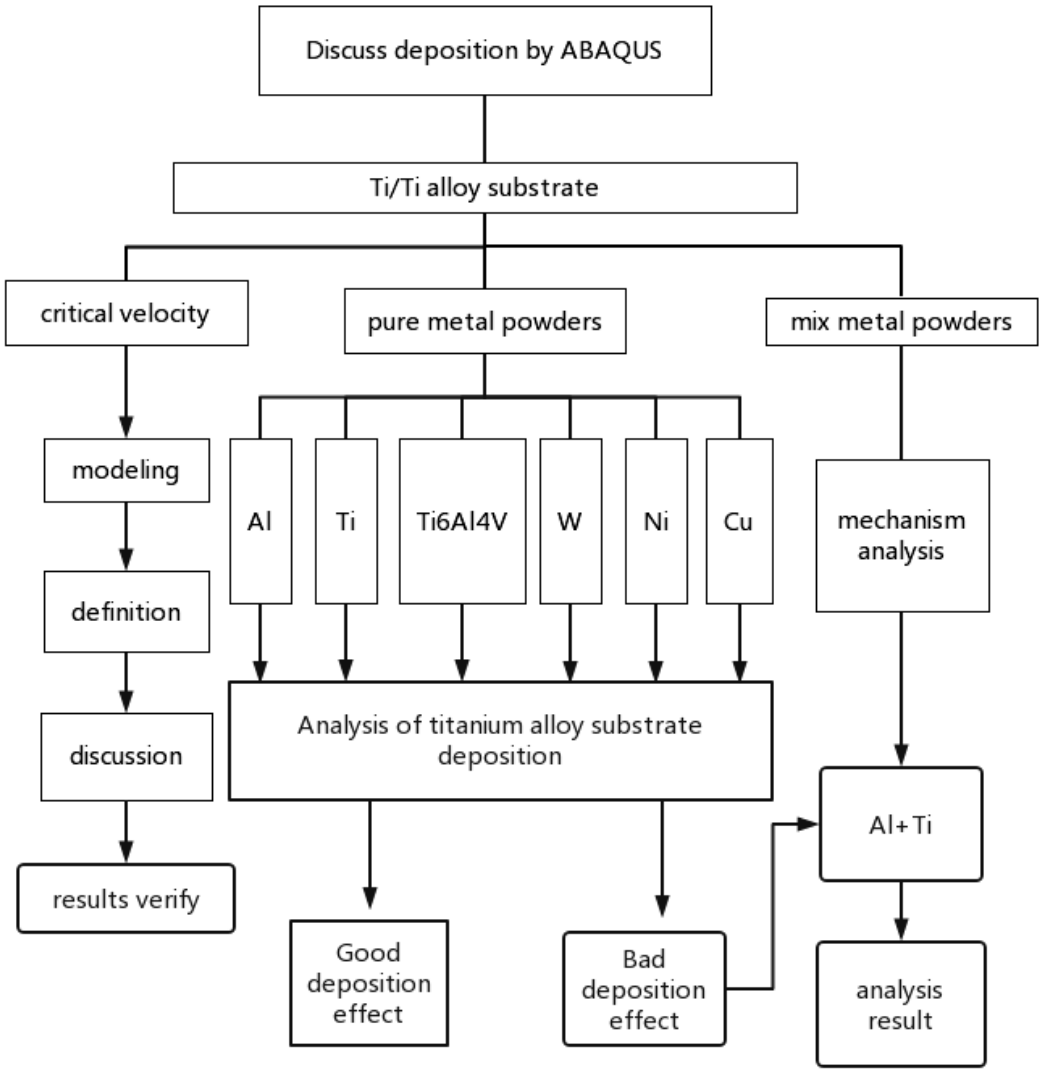

Fig. 3.1. The research map of this chapter

3.2 Deposited process based on ABAQUS

3.2.1 The J-Cook plastic model

The common cold spraying metal powder is a plastic material, and the numerical simulation process generally adopts the J-Cook Plastic Model [148-150] defined in Eq. (3.1).

$$\sigma = \left[A + B\varepsilon_{\mathrm{p}}^{\mathrm{n}}\right]\left[1 + C\ln\left(\frac{\dot{\varepsilon}_p}{\dot{\varepsilon}_0}\right)\right]\left[1 - \left(T^*\right)^{\mathrm{m}}\right], \tag{3.1}$$

where σ – the equivalent flow stress;

$\dot{\varepsilon}_p$ – the equivalent plastic strain rate;

$\dot{\varepsilon}_0$ – the reference strain rate;

ε_{p} – the equivalent plastic strain;

A, B, C, n, and m – the material constants;

T^* – the normalized temperature.

As Eq. (3.2) shows:

$$T^* = \begin{cases} 0; & T < T_{\mathrm{trans}} \\ (T - T_{\mathrm{trans}})/(T_{\mathrm{melt}} - T_{\mathrm{trans}}); & T_{\mathrm{trans}} \le T \le T_{\mathrm{melt}} \\ 1 & T_{\mathrm{melt}} \le T \end{cases}, \tag{3.2}$$

where T_{melt} – the melting temperature;

T_{trans} – a reference transition temperature at or below which there is no temperature dependence of the response [151].

The main parameters of the simulation process are shown in Table 3.1. The material failure model used in this dissertation is the Johnson-Cook dynamic fracture model. Considering the influence of static pressure, strain rate and temperature, it can be expressed in Eq. (3.3) [152].

$$\varepsilon_{\mathrm{f}} = \left[\mathrm{d}_1 + \mathrm{d}_2 \exp\left(\mathrm{d}_3 \frac{\mathrm{p}}{\mathrm{q}} \right) \right] \left[1 + \mathrm{d}_4 \ln\left(\frac{\dot{\varepsilon}_{\mathrm{p}}}{\dot{\varepsilon}_0} \right) \right] (1 + \mathrm{d}_5 T^*), \tag{3.3}$$

where ε_{f} – fracture strain;

d1-d5 – material fracture constant;

p – static pressure;

q – mises yield stress.

Table 3.1 – Material parameters of aluminum, copper, Ti-6Al-4V, titanium and tungsten alloy

Material	Aluminum	Copper	Ti-6Al-4V	Titanium	Tungsten alloy
Density, $\rho/(g.m^{-3})$	2.7	8.9	4.5	4.54	17
Poisson's ratio ν	0.33	0.35	0.3	0.3	0.3
Yield strength, A/MPa	148.4	90	862	175	790
Hardening index, B/MPa	345.5	292	331	380	510
Strain index, N	0.183	0.31	0.34	0.32	0.27
Softening index, M	0.895	1.09	0.8	0.55	1.05
Strainrate, C	0.001	0.025	0.014	0.06	0.016
D1	0.071	0.54	-0.09	-0.09	3
D2	1.248	4.89	0.25	0.27	0
D3	1.142	3.03	-0.5	0.48	0.78
D4	0.147	0.014	0.014	0.014	0
D5	1	1.12	3.87	3.87	0
Shear modulus/MPa	27	44.7	59.6	44	77
Specific heat, $Cp/(J.Kg^{-1}.K^{-1})$	898.2	383	612	452	134
Thermal conductivity coefficient λ $(W.m^{-1}.K^{-1})$	237.2	386.5	7.955	16.3	170
Melting temperature, T_m/°C	916	1356	1878	1811	1800
Transformation temperature, T_{tran}/°C	298	298	298	298	298

In the Johnson-Cook model, fracture occurs when the damage factor D reaches 1.0. The evolution of D can be obtained by summation of equivalent plastic strain increment divided by current failure strain (Eq. 3.4):

$$D = \frac{\Delta \varepsilon^{P}}{\varepsilon_{\text{failure}}}. \tag{3.4}$$

3.2.2 The material state equation

The linear EOS_GRUNEISEN state equation as the material state equation defines Eq. (3.5), the parameters as Table 3.2 shows.

$$U\text{s} = C_0 + \text{s}U\text{p}, \tag{3.5}$$

where C_O and s – define the linear relationship;

U_S – the linear shock velocity;

U_P – the particle velocity.

Table 3.2 – U_S-U_P state equation parameters of SPH simulation process

Materials	C_O	S	Gamma
Aluminum	5386000	1.339	2.18
Copper	3940000	1.489	1.97
Ti-6Al-4V	5130000	1.028	1.23
Titanium	4700000	1.489	1.97
Tungsten alloy	3990000	1.24	1.54

3.2.3 Numerical method

The Abaqus/Explicit method includes three algorithms: ALE (Arbitrary Lagrangian-Eulerian), CEL (Couple Lagrangian-Eulerian), and SPH (Smoothed

Particle Hydrodynamics); this dissertation uses the SPH method, which is a meshless method that has been gradually developed in the past 20 years. Its advantage lies in avoiding mesh distortion during large deformations. In addition, the SPH method belongs to the Lagrange algorithm. Compared with the Euler method, it does not need to discretize the empty area, saving a lot of internal storage and calculation time. Hence, the SPH method is very suitable for dealing with various large deformation and fluid-structure coupling problems. Unit type of the model is a hexahedral element (C3D8R). The deposition time of supersonic cold aerodynamic spraying is short, and the strain rate is large. Therefore, the material model needs to consider parameters such as plasticity, friction, damage, etc.

3.3 New method determination of critical velocity

The critical velocity is the key to the cold spraying deposition process. If the impact velocity is smaller than the critical velocity, effective deposition cannot form. However, too large an impact velocity will cause substrate erosion. Therefore, the research on critical velocity has a positive significance.

There are many research methods on the critical velocity of cold spraying, which are summarized into three categories: the first is the numerical simulation method [153-156], the second is the theoretical formula calculation method [52, 157-158], and the third is the experimental results [139, 159-160]. Different researchers have different research results on the critical velocity, but they are generally in a specific range. As we all know, after the powders collide with the substrate at supersonic speed, the substrate will produce a foundation pit, and the powders will deform, so this study discusses the law between the two and provides a simple method to judge the critical velocity. A large number of numerical simulation results found that the ratio of the depth of the foundation pit to the height and size of the deformed powders can judge the critical velocity, and the judgment result is simple and effective.

3.3.1 The introduction of the principle

The deposition of powders into the substrate mainly involves mechanical bonding, and a small part has metallurgical bonding. The depth of powders embedded into the substrate will change with the change in powder collision velocity. The ratio of the depth of the foundation pit (H1) to the height after the deformation of the powder collision substrate (H2) is defined as the deformation ratio Y to discuss the rules between the critical velocity and the variable parameters after deposition. As the formula 3.6 show.

$$Y = \frac{H_1}{H_2}. \tag{3.6}$$

3.3.2 Determination of critical velocity

The larger the Y value, the deeper the foundation pit is, and the smaller the height of powders after deformation, which reflects the more extensive the deformation of powders. On the contrary, when the Y value is small, the foundation pit is shallow, and the powder deformation is small. Of course, the depth of the foundation pit is relative. For example, the depth of the foundation pit in which hard powders collide with the soft substrate is more significant than that in which soft powders collide with hard powders and vice versa. In addition, when the powders fully deposit into the substrate, i.e., Y = 1, it is not conducive to the formation of the coating. Therefore, the Y = 0.8 (i.e., the powders embedded in 80 % of the substrate) take the upper limit.

3.3.2.1 Powder and substrate are the same material

Figure 3.2 shows that when soft powders collide with the soft substrate (aluminium/aluminium) at 650 m/s, Y = 0.5. At this time, 650 m/s can be used as the critical reference velocity, which is consistent with the reference [162, 165]. If it

collides with the maximum critical velocity of the reference [162], Y reaches 0.8. Figure 3.3 shows that when hard powders collide with the hard substrate (titanium/titanium) at 700 m/s, Y is close to 0.5, which is used as the initial value of reference critical velocity, which is consistent with references [162, 165] Consistent. Further, expand the range. The maximum critical velocity in reference [162] reaches 1000 m/s, and Y is 0.8. 80 % of the powders embedded in the substrate is the upper limit of the critical maximum velocity set in this dissertation. Therefore, in the deposition process of the same material (titanium and aluminum) with the substrate, the critical velocity is defined as Y in the range of 0.5 - 0.8.

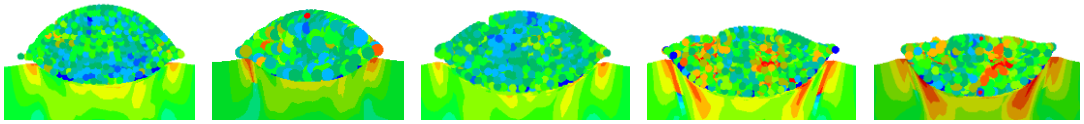

a *b* *c* *d* *e*

a – 600 m/s； *b* – 650 m/s； *c* – 700 m/s； *d* – 800 m/s； *e* – 870 m/s

Fig. 3.2. Aluminum/Aluminum

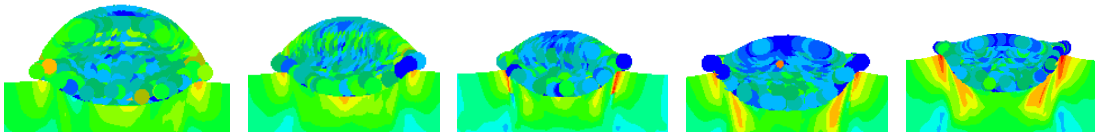

a *b* *c* *d* *e*

a – 600 m/s； *b* – 700 m/s； *c* – 800 m/s； *d* – 900 m/s； e – 1000 m/s

Fig. 3.3. Titanium/Titanium

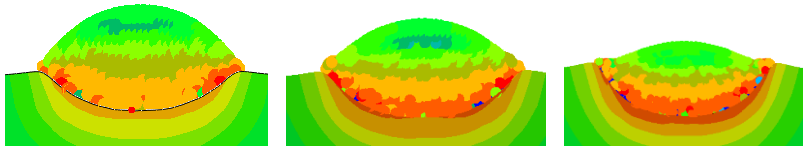

a *b* *c*

a – 350 m/s； *b* – 400 m/s； *c* – 500 m/s

Fig. 3.4. Copper/Copper

Figure 3.4 shows that a more bottomless foundation pit can be obtained at a

lower speed when copper powders collide with the copper substrate. When the collision speed reaches 500 m/s, it is consistent with the data in reference [26], at this time, Y = 0.8. While nickel powders are similar to copper powders, a more bottomless foundation pit can be obtained at a lower speed (Fig. 3.7). When the powder speed reaches 600 m/s, it is close to reference [26]; at this time, Y = 0.8

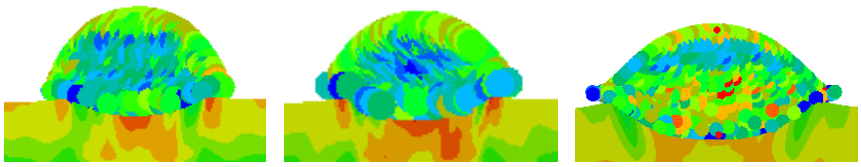

a *b* *c*

a – 650 m/s; *b* – 750 m/s; *c* – 850 m/s

Fig. 3.5. Ti-6Al-4V/Ti-6Al-4V

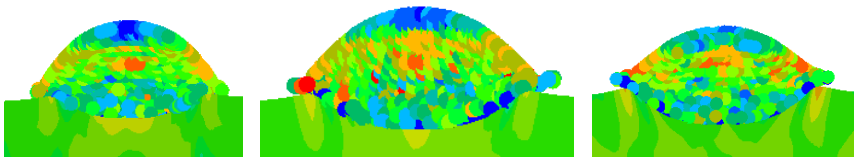

a *b* *c*

a – 400 m/s; *b* – 450 m/s; *c* – 500 m/s

Fig. 3.6. Tungsten alloy/Tungsten alloy

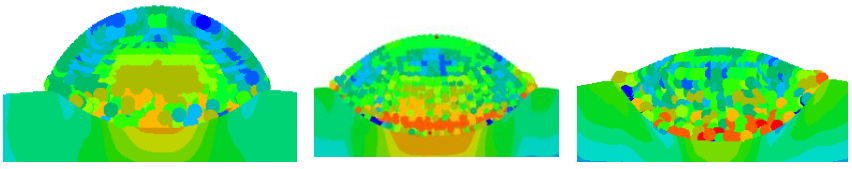

a *b* *c*

a – 400 m/s; *b* – 500 m/s; *c* – 600 m/s

Fig. 3.7. Nickel/Nickel

Figure 3.5 shows that Ti-6Al-4V powders collide with the Ti-6Al-4V substrate when the collision velocity reaches 850 m/s, Y = 0.5, which is close to the critical

velocity in reference [23].

Figure 3.6 shows that tungsten alloy powders collide with the tungsten alloy substrate when the collision velocity is 400 m/s, Y = 0.4, consistent with reference [23]. When the collision velocity reaches 450 m/s, the deposition effect is also good, and there is no shear slip erosion phenomenon. At this time, Y = 0.5, which is recommended as the reference critical velocity.

3.3.2.2 Powder and substrate are different materials

This section studies two types of collision deposition of heterogeneous materials: hard powders colliding with the soft substrate and soft powders colliding with the hard substrate (Table 3.5). For example, titanium powders colliding with aluminum powders (Fig. 3.8) belong to hard collision with soft, generally obtaining a more bottomless foundation pit. When the collision speed reaches 650 m/s…850 m/s, a better deposition can obtain. At this time, Y = 0.5…0.8. It suggested taking 650 m/s…850 m/s as the critical speed, which is close to the references [162, 151].

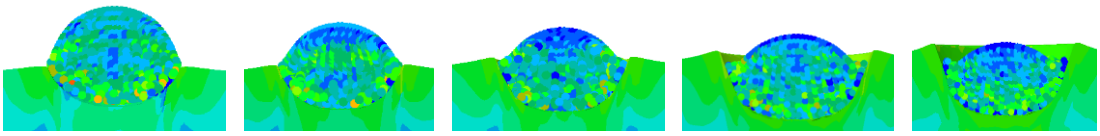

a *b* *c* *d* *e*

a – 550 m/s; *b* – 650 m/s; *c* – 750 m/s; *d* – 850 m/s; *e* – 950 m/s

Fig. 3.8. Titanium/Aluminum

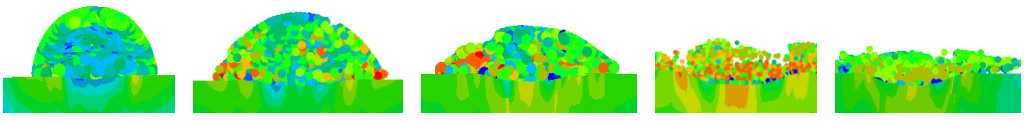

a *b* *c* *d* *e*

a - 400m; *b* - 500m/s; *c* - 600m/s; *d* - 700m/s; *e* - 800m/s

Fig. 3.9. Aluminum/Titanium

The collision of aluminum powders with titanium powders belongs to the

collision of soft powders with the hard substrate, and the depth of the foundation pit generally obtained is relatively shallow. As shown in Fig. 3.9, when the collision speed reaches 700 m/s, the powder damage occurs in the SPH Simulation process, mainly because the impact speed is too large, and the powders appear a certain "splitting" phenomenon. It suggested that the critical velocity of aluminum powders colliding with titanium powders is less than 700 m/s. considering 500 m/s…700 m/s as the critical velocity, the Y value is between 0.3…0.5. At this time, there is a certain foundation pit depth, which is well combined. This range is within the scope of reference [162]. Aluminum powder is not recommended to be used alone but can consider mixed with other powders because the powders appear "splitting" phenomenon when the collision speed exceeds 600 m/s, and the Y value is too small.

3.4 Theoretical calculation of critical velocity

3.4.1 The detail of the theoretical principle

Common theoretical calculation formulas include Alhualaifi's simple formula [117], as Equations (2.33) shows.

Its principle is to define the critical velocity when the matrix temperature reaches 70 % of melting temperature (T_m) at the collision interface. On the basis of Assadi [158] and other semi-empirical formulas, Schmidt Equation [52] considers the influence of particle size on matrix and thermal effect, which can calculate the critical velocity and erosion velocity (Eq. 3.7):

$$v_{crit} = \sqrt{\frac{F_1 \cdot 4 \cdot \sigma_{TS} \cdot \left\{1 - \frac{T_i - T_R}{T_m - T_R}\right\}}{\rho} + F_2 \cdot C_P \cdot (T_m - T_i)}, \tag{3.7}$$

where σ_{TS} – tensile strength;

ρ – the density;

C_p – specific heat;

T_m - melting point;

T_i – the impact temperature;

T_R – the reference temperature.

Take room temperature (293 K) and thermal calibration factor (F1 = 1.2, F2 = 0.3). Under the condition of not considering erosion, particle velocity greater than the theoretical, critical velocity value is taken as a standard to discuss deposition on the substrate surface. Therefore, Alhualaifi's simple formula was used to calculate the critical velocity. It can be seen from Eq. (3.7) that temperature is one of the main factors affecting critical velocity.

3.4.2 Comparison between theory and numerical simulation

The critical velocities of various materials are summarized in Table 3.3 by referring to a large amount of literature.

Table 3.3 – Summary of critical velocity studies at room temperature

Powder/substrate	Critical velocity (m/s）
Al/Al	800 [161], 650 (SPH) [162], 680…870 (experiment) [162], 780 [151], 620…660 [165]
Ti/Ti	700 (FEM) [162], 750…1000 (SPH) [162], 820 [151], 700…890 [165]
Ti-6Al-4V/Ti-6Al-4V	657[157], 730[162][164], 830[151]
Ti/Al(1100-H2)	650 (FEM) [162], 630…800 (SPH) [162], 650 [151]
Al/Ti	400…1050 (SPH) [162], 450…1000 (experiment) [162]
Walloy/W alloy	400 [151]
Cu/Cu	531.5 [158], 550 [161], 520 (Imaging experiments) [162], 538 (Dykhuizen calculate [163]) [162], 550 [151], 460…500 [165]
Ni/Ni	700 [161], 720 [151], 610…680 [165]

It can be seen from Table 3.4 that the critical velocities of different materials are

different, the maximum and minimum values of critical velocities from a large number of references are collated and compared with the critical velocities studied in this dissertation [166].

Table 3.4 – Numerical parameters of materials with the same properties after CS

Materials	V_{impact}	H_1, μm	H_2, μm	Y	Critical velocity V_{ref}, m/s	Critical velocity V_{rec}, m/s
Titanium/ Titanium	600	7.3	22.8	0.3	700…1000	700…1000
	700	11.9	22.7	0.5		
	800	12.2	22.8	0.5		
	900	12.9	22.8	0.6		
	1000	19.3	22.8	0.8		
Aluminum/ Aluminum	600	8.9	23.8	0.4	650…870	650…870
	650	11.2	23.8	0.5		
	700	13.1	23.8	0.6		
	800	16.2	23.8	0.7		
	870	19	22.8	0.8		
Copper/ Copper	350	11	23.7	0.5	520…550	500
	400	13.7	23.9	0.6		
	500	18.9	22.9	0.8		
Ti-6Al-4V / Ti-6Al-4V	650	6.9	22.6	0.3	657…830	850
	750	7.3	23.8	0.3		
	850	11.8	23.8	0.5		
Tungsten alloy/ Tungsten alloy	400	10	23.7	0.4	400	450
	450	11	23.7	0.5		
	500	13	22.7	0.6		
Nickel/ Nickel	400	10	23.8	0.4	610…720	600
	500	14	23.9	0.6		
	600	18.6	22.7	0.8		

Table 3.5 compares the critical velocity of Titanium/Aluminum and

Aluminum/Titanium, and obtains the recommended critical speed value in this dissertation.

Table 3.5 – Numerical parameters of materials with different properties after CS deposition

Materials	Titanium/Aluminum					Aluminum/Titanium				
V_{impact}	550	650	750	850	950	400	500	600	700	800
H_1, μm	10.9	13	16.2	20.4	24.2	3.1	5.8	7.7	11.6	12.6
H_2, μm	24.8	24.5	24.4	24.7	24.5	23.9	23.8	23.7	23.5	21.7
Y	0.4	0.5	0.7	0.8	1	0.1	0.2	0.3	0.5	0.6
Critical velocity V_{ref}, m/s	630…800					400…1050				
Critical velocity V_{rec}, m/s	650…850					600…700				

In summary, the critical velocity of cold spraying is related to the Y value; that is, the depth of the foundation pit after powders collide with the substrate at high speed is related to the powder size after deformation. It is feasible to predict the critical velocity by calculating the ratio Y by the SPH method. Although the collision velocity range discussed in this dissertation is extensive, the velocity parameters or Y values can optimize further with more decimal points in the later study. Different Y values will predict the critical velocity according to the classification of powders' soft and hard properties. Some meaningful conclusions were obtained in this dissertation.

1) The Y value of hard powders colliding with the hard substrate and hard powders colliding with the soft substrate is in the range of 0.5…0.8. For instance, the Y value of titanium colliding with titanium and aluminum is 0.5…0.8 to meet the critical velocity requirements. Some materials need the Y value to reach the lower limit of 0.5 to meet the critical velocity requirements. For example, when Ti-6Al-4V powders and tungsten alloy powders impact the homogeneous materials, respectively, the Y value is 0.5.

2) The Y value of the soft substrate colliding with the soft substrate is also in the range of 0.5…0.8. For example, the critical speed of aluminium colliding with

aluminium is 650 m/s…870 m/s and the Y value is 0.5…0.8. For a few materials, the Y value needs to reach the upper limit of 0.8 to meet the critical speed requirements, such as copper colliding with copper and nickel colliding with nickel, and the critical speeds are 500 m/s and 600 m/s, respectively.

3) When soft powders collide with hard substrate, the collision speed is too large, which makes it easy to cause powder "splitting" and is not conducive to the formation of the coating. For example, when aluminium collides with titanium, the recommended Y value range is 0.5, and its critical speed is 700 m/s. For Ti-6Al-4V substrate with large hardness, not recommended aluminium powders because the collision speed exceeds 600m/s, the powders "split" and the Y value is too small.

3.5 Research on the deposition of traditional pure metal powder on Ti-6Al-4V substrate

3.5.1 Material properties

Assuming that the material particles are spherical particles with a diameter of 10 μm and a Ti-6Al-4V matrix radius of 130 μm. Studies have shown that [120- 121, 164] the critical velocities of Ti-6Al-4V is 502…780 m/s. This dissertation utilizes 400 m/s, 600 m/s, 800 m/s, and 1000 m/s to collide with the Ti-6Al-4V substrate vertically. In order to further study the energy conversion process, 650m/s is used to analyze energy for different particles [167].

3.5.2 Numerical simulation results

Ti-6Al-4V particle collide Ti-6Al-4V alloy is a hard material collision hard material. As Fig. 3.10 shows, it can be seen that the 600 m/s…800 m/s deposition effect is the best. When the particles exceed 1000 m/s, adiabatic shear instability begins to occur during the deposition process.

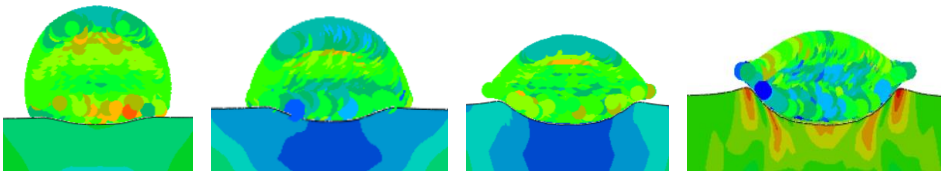

a *b* *c* *d*

a – 400 m/s; *b* – 600 m/s; *c* – 800 m/s; *d* – 1000 m/s

Fig. 3.10. Ti-6Al-4V/Ti-6Al-4V, 50 ns

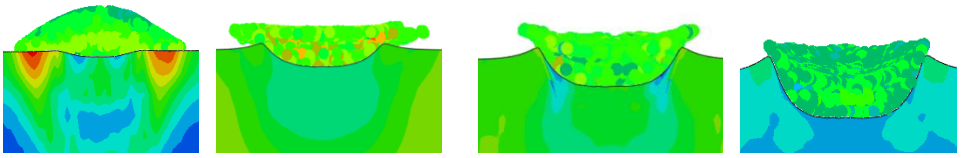

a *b* *c* *d*

a – 400 m/s; *b* – 600 m/s; *c* – 800 m/s; *d* – 1000 m/s

Fig. 3.11. Copper/Ti-6Al-4V, 50 ns

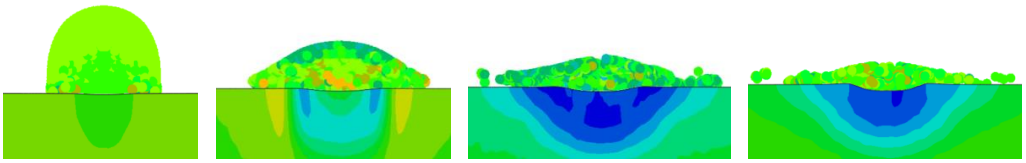

a *b* *c* *d*

a – 400 m/s; *b* – 600 m/s; *c* – 800 m/s; *d* – 1000 m/s

Fig. 3.12. Aluminum/Ti-6Al-4V, 50ns

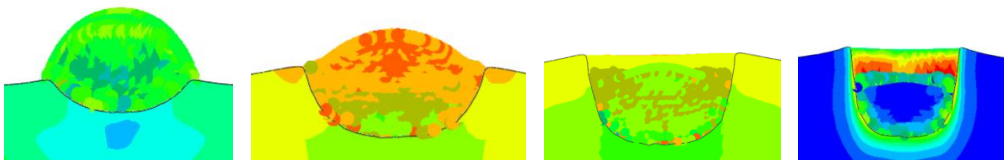

a *b* *c* *d*

a – 400 m/s; *b* – 600 m/s; *c* – 800 m/s; *d* – 1000 m/s

Fig. 3.13. W alloy/Ti-6Al-4V, 50 ns

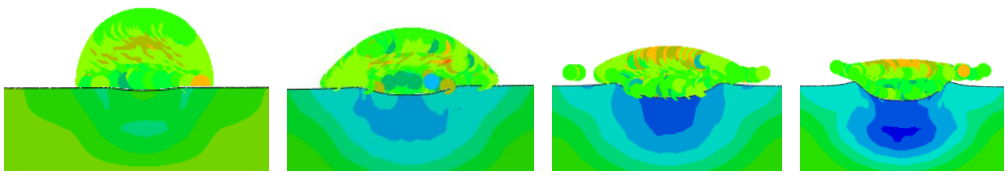

a *b* *c* *d*

a – 400 m/s; *b* – 600 m/s; *c* – 800 m/s; *d* – 1000 m/s

Fig. 3.14. Titanium/Ti-6Al-4V, 50 ns

Copper particles collide with Ti-6Al-4V titanium alloy, which is a hard material that collides with hard material. As Fig. 3.11 shows, it can be seen that the deposition effect of over 600 m/s is good.

Aluminum particles collide with Ti-6Al-4V alloy, which is a soft material colliding with a hard material. It can be seen from Fig. 3.12 that the deposition effect is the best. The best deposition effect is around 600 m/s, but the foundation pit is very shallow. When the particle velocity reaches above 800 m/s, the particle fails and cannot be deposited effectively.

Figure 3.13 shows the tungsten alloy collides with the Ti-6Al-4V alloy substrate; it can be seen that the 400 m/s…600 m/s deposition effect is the best. When the particles exceed 800 m/s, the foundation pit depth is deeper than other materials, and all erode into the Ti-6Al-4V matrix.

Titanium particle collide Ti-6Al-4V titanium alloy is a hard material collision hard material. As Fig. 3.14 shows, it can be seen that the 600 m/s…800 m/s deposition effect is the best. When the particles exceed 800 m/s, adiabatic shear instability begins to occur during the deposition process, in addition, foundation pit depth is shallower than Ti-6Al-4V particles from 600 m/s to 800 m/s.

3.5.3 Energy analysis

From the energy view, as the energy evolution process is shown in Fig. 3.15 - Fig. 3.19, where ALLAE is artificial strain energy, ALLFD is frictional dissipation, ALLIE is internal energy, ALLKE is kinetic energy, ALLPD is plastic dissipation, ALLSE is strain energy, and ALLVD is viscous dissipation. Take Ti-6Al-4V/Ti-6Al-4V (650 m/s, powder temperature is room temperature) as the example, artificial strain energy value (Fig. 3.15) is very small, it is ignored， as Fig. 3.16 shows, total strain energy ALLIE=ALLPD+ALLSE， however, there are also frictional dissipation and material viscous dissipation in the collision process (Fig. 3.17). Hence， the final energy change process is shown in Figure 3.19 (the

same as below), in which the formula is expressed as ALLKE=ALLIE+ALLFD +ALLVD.

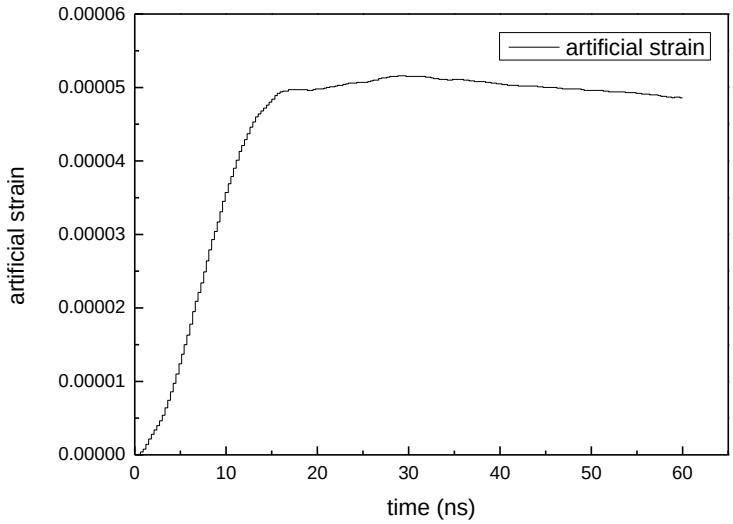

Fig. 3.15. Artificial strain energy

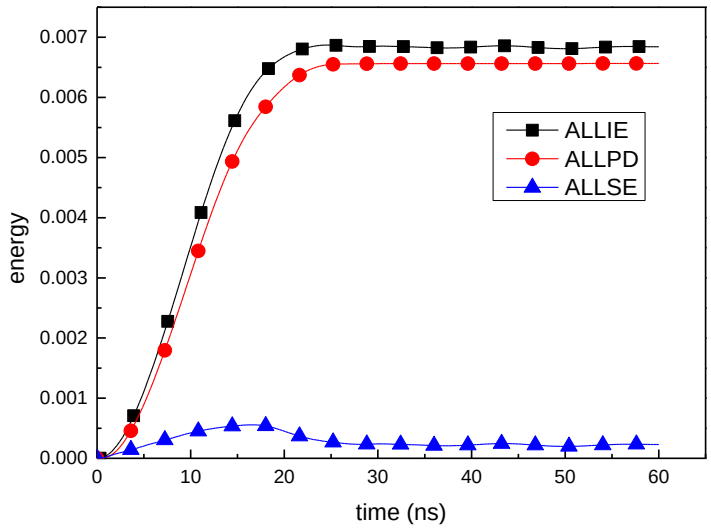

Fig. 3.16. Internal energy change process

Due to the difference in the initial kinetic energy and energy conversion rate of the particles, the internal energy obtained by each substrate is also different. Fig. 3.20 shows the energy transition process during particle collision process. The results show that the initial particle when velocity is the same, and the particles have the greater initial kinetic energy.

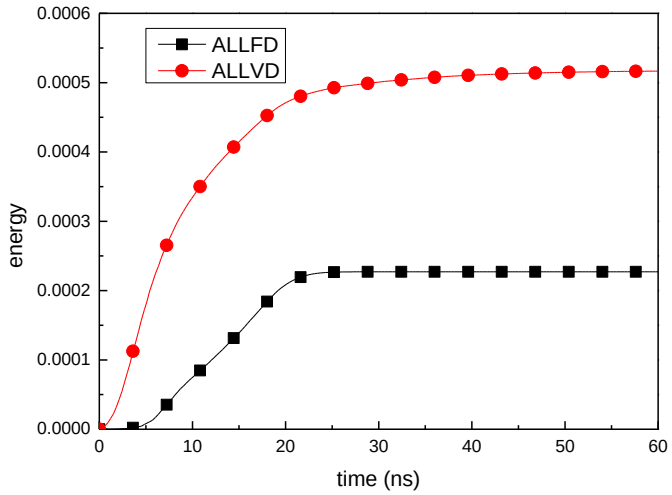

Fig. 3.17. Frictional and viscous dissipation energy

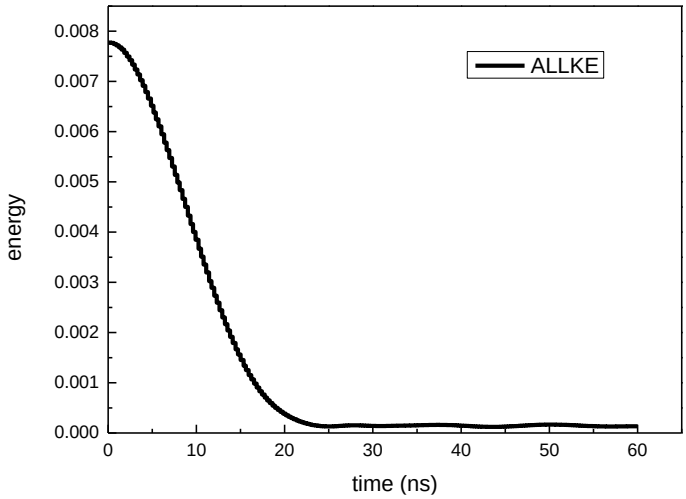

Fig. 3.18. Kinetic energy change process

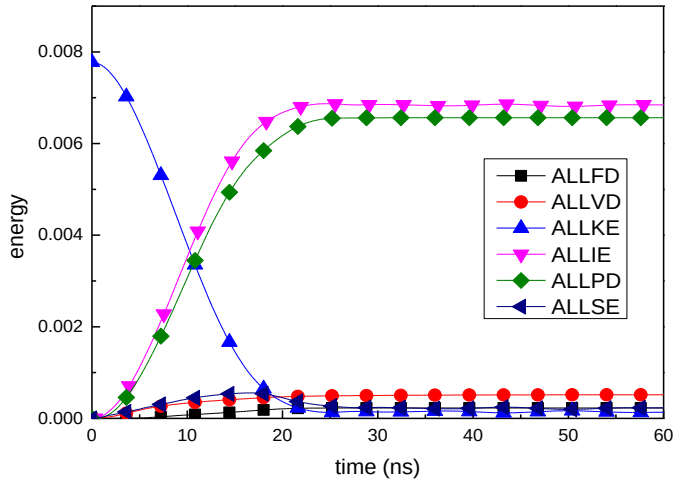

Fig. 3.19. Energy change process of whole model

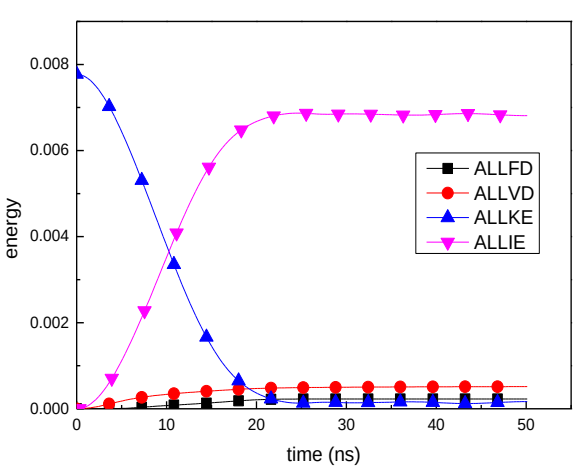

a

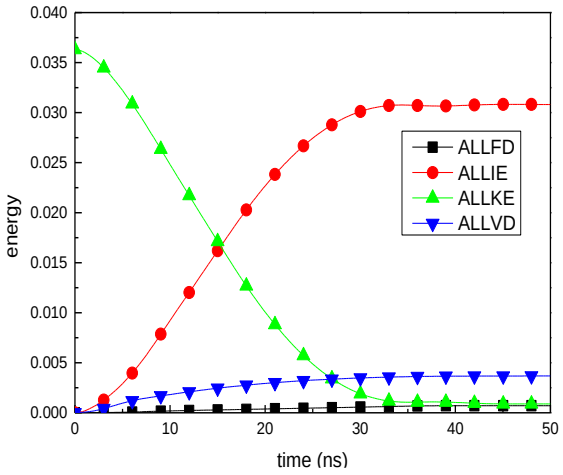

b

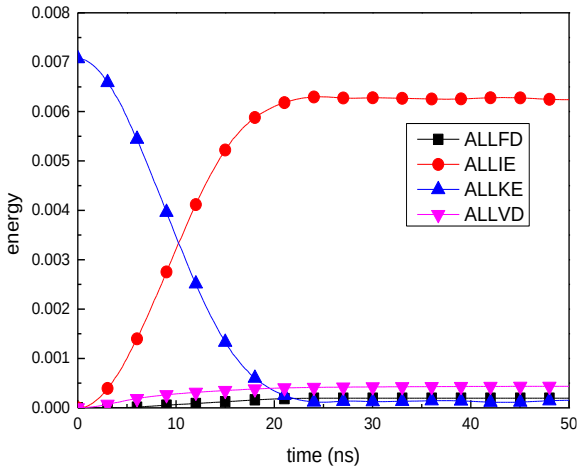

c

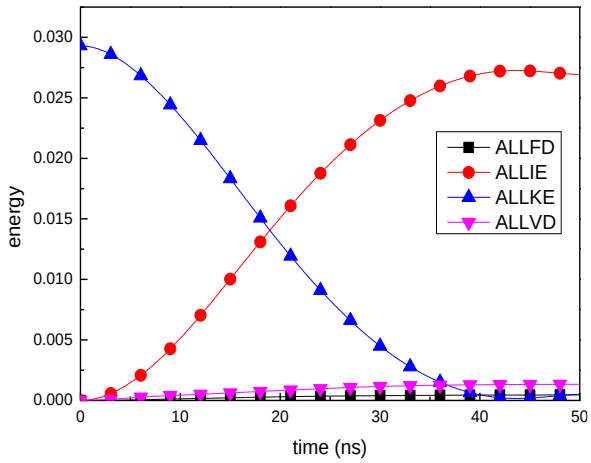

d

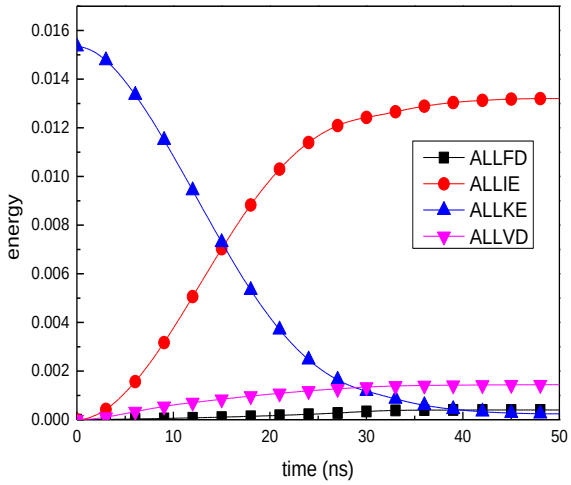

e

a – Ti-6Al-4V/Ti-6Al-4V; *b* – Copper/Ti-6Al-4V; *c* – Aluminum/Ti-6Al-4V; *d* – W alloy/Ti-6Al-4V; *e* – Nickel/Ti-6Al-4V

Fig. 3.20. Deposition velocity at 650m/s with energy curve within 50 nanoseconds

The Ti-6Al-4V matrix particles deposited on the surface of the Ti-6Al-4V substrate belong to the same material properties (Fig. 3.20a). Due to the larger specific heat capacity and low thermal conductivity, it is easier to absorb more energy and the deposition effect is better, so it can finally get more energy.

It can be seen from Fig. 3.20 because the density of copper, Ti-6Al-4V, titanium and tungsten alloy are larger than aluminium, and the initial kinetic energy is larger at the beginning of the collision. The internal energy of the substrate rises rapidly, causing the particles to be in contact， and the temperature rises sharply. Hence, it is easier to get a deeper foundation pit. As we know, aluminium/Ti-6Al-4V belongs to soft material collision hard material, which has a small shear modulus. Hence, its foundation pit is shallow, and the bonding performance needs to be further studied. In addition, the internal energy (ALLIE) does not drop rapidly in the later stage, and it is still at a large value. This is mainly due to the release energy of accumulated plastic deformation process.

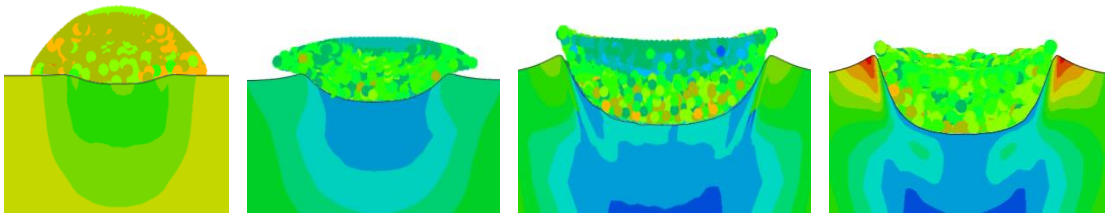

a *b* *c* *d*

a – 400 m/s; *b* – 600 m/s; *c* – 800 m/s; *d* – 1000 m/s

Fig. 3.21. Nickel/Ti-6Al-4V, 50 ns

In order to verify that the initial kinetic energy is large, the energy is large, and the deeper the foundation pit is, nickel particles are used for verification. Since the initial kinetic energy is related to the mass and initial speed, this article uses the same volume and the same speed to collide. The simulation result of the nickel foundation pit should be larger than aluminium, and it is close to copper particles. As shown in Fig. 3.21, it meets expectations.

3.5.4 Study on multi-particle aluminum collision with Ti-6Al-4V matrix

Section 3.5.2 shows that a single copper, W alloy, nickel, titanium and Ti-6Al-4V particles deposited on the surface of Ti-6Al-4V has a deep foundation pit, while the effect of depositing Ti-6Al-4V on a single pure aluminum particle is not ideal. The Section 3.5.3 energy map shows that the initial energy of aluminium is small. In order to explore whether the depth of the foundation pit is related to energy, a number of aluminum particles are studied. The model is shown in Fig. 3.22.

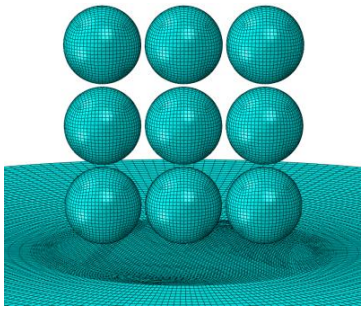

Fig. 3.22 – Calculation model

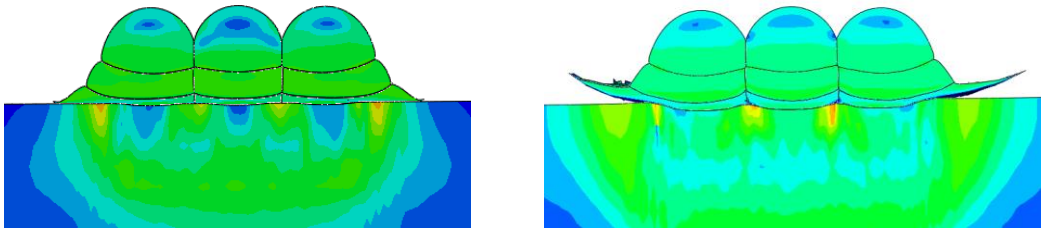

a *b*

a – 650m/s; *b* – The particle velocity of the third layer exceeds 650 m/s.

Fig. 3.23. Multiple aluminum particles deposited onto titanium within 70 nanoseconds

As Fig.3.20c and Fig. 3.24 show multiple particles increase the initial kinetic energy. Although the subsequent particles have a compacting effect on the previous particles, the deposition effect is still not good (Fig.3.23). Hence, pure aluminium particles are not recommended for Ti-6Al-4V surface deposition; further studies are needed for aluminium mixed with other particles for deposited onto Ti-6Al-4V.

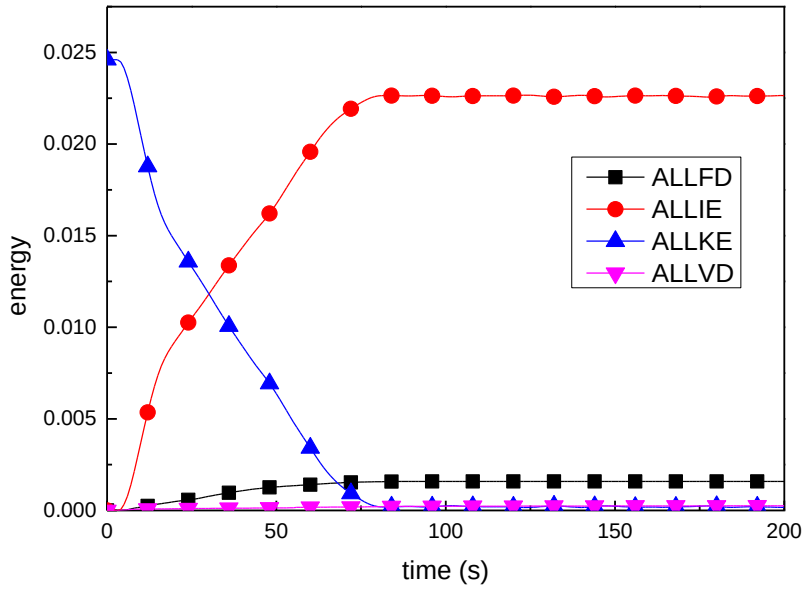

Fig. 3.24. An energy diagram of multiple aluminium particles colliding with the titanium surface within 200 nanoseconds.

5.4.5 Summary this section

The surface of the Ti-6Al-4V alloy substrate can be cold sprayed with aluminium, copper, W alloy, nickel, titanium and Ti-6Al-4V particles. The impact deposition effect is mainly affected by factors such as material hardness, density, specific heat capacity, thermal conductivity, etc. According to different particle deposition characteristics, for Ti-6Al-4V substrate, it is recommended to use of Ti-6Al-4V, nickel, copper, W alloy and titanium particles as surface restorative, protective and functional coating materials and pure aluminium particles are not recommended.

Compared with the hardness of Ti-6Al-4V matrix, the particles with larger hardness in the collision process lead to deeper foundation pits, for example, at a speed of 600bm/s, nickel particles deposit deeper pits than aluminum particles; particles with higher density have larger initial kinetic energy, the better the deposition effect, for an instant, the density of nickel particles (density is 8.9 g/cm^3) is higher than that of aluminum particles (density is 2.7 g/cm^3), the foundation pit is

deeper during the deposition process, hence, the bonding performance is better. Similarly, the foundation pit deposited by tungsten alloy is deeper than nickel, etc.

The energy conversion process of collision is mainly kinetic energy (ALLKE) conversion to internal energy (ALLIE), and a small part into frictional dissipation (ALLFD) and viscous dissipation (ALLVD). As the single-particle and multi-particle energy processes of aluminium particles show, the increase of the initial energy does not necessarily lead to better deposition, depending on the physical properties of the substrate and particles.

3.6 Research on the deposition of mixed metal powders on Ti-6Al-4V substrate

There are many research methods on the critical velocity of cold spraying, which are summarised into three categories: The numerical simulation method [160], the theoretical formula calculation method [117], and the experimental method [139, 161]. There is no unified standard for the theoretical calculation of the critical velocity of mixed powder; experimental methods usually obtain it. To reduce the number of experiments and avoid unnecessary waste, scientific researchers use numerical simulation in advance.

However, there are few reports on the numerical simulation of the deposition process of mixed particles. In practical engineering applications, it’s often a mixture of different materials to obtain optimal performance. Hence, the numerical simulation of cold spraying of a mixed powder of different materials multi-particle is an urgent focus of discussion. This study represents the Al+Ti mixed powder deposited onto Ti-6Al-4V, the research results have specific guiding significance [168].

3.6.1 Material and methods

As Figure 3.25 shows, the time of the analysis step is 50 ns, and the output parameter selects energy. Particle surfaces need to select external areas and internal areas, which is the key factor for the success of the numerical simulation.

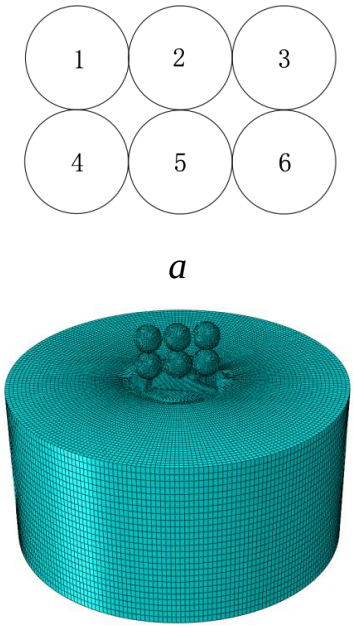

a

b

a – particles to be deposited (1 – Al, 2 – Al, 3 – Al, 4 – Ti, 5 – Ti, 6 – Ti);

b – three-dimensional model

Fig. 3.25. Model of the deposition process

The load parameter needs to fix the lower surface of the matrix. Considering the gravity of all particles, the value is 9810 mm/s^2. Unit type of the model is a hexahedral element (c3d8r), and the hexahedral reduction integral is selected.

The Abaqus/Explicit includes three algorithms, arbitrary Lagrangian-Eulerian, Couple Lagrangian-Eulerian, and Smoothed Particle Hydrodynamics (SPH). Recommend the SPH method for single-particle. However, for multi-particle mix powder simulation, it is not recommended to use the SPH method because of mutual infiltration in the process of large deformation between powders. It is challenging for the meshless method to achieve internal surface contact.

3.6.2 Result and discussion

Figure 3.26 represents the deposition of Al + Ti mixed powder impacting the Ti-6Al-4V matrix at the speed of 300 m/s…1100 m/s. When particles collide with the Ti-6Al-4V matrix, particles 4, 5, and 6 collide with the substrate first, and the

effective plasticity strain of particles mainly concentrates at the edge of the contact interface between particles and matrix, and the particles closely bond to the substrate and the particles change from spherical to flat. At 500 m/s, particles 1, 2, and 3 collide with particles 4, 5, and 6, respectively, and embed into their interstices. 4, 5, and 6 collide with the matrix, there is a particular foundation pit, and the recovery coefficient is small. Hence, as the lower boundary of the critical velocity. With the increase of velocity, the strong impact force of particles causes the matrix material to flow to the periphery, which makes the matrix material contact closely with the surface of particles 4, 5, and 6. Under the action of subsequent tamping of Al particles, the sedimentary layer deepens, the effective plastic strain increases as the velocity increases and the pits on the surface of the matrix deepen. In the whole process of particle deposition, the effective plastic strain of particles is much smaller than that of the substrate. When the velocity exceeds 900 m/s, the metal-plastic rheology appears on the surface of the matrix, and its plastic rheology inertia is greater than the viscosity resistance of the material, and the surface becomes unstable, suggested being the upper boundary of the critical velocity. Al and Ti particles are embedded in the softened Ti-6Al-4V matrix, resulting in mechanical bite-type bonding.

The kinetic energy (ALLKE) is transformed into plastic dissipation energy (ALLPD), friction dissipation energy (ALLFD), elastic strain energy (ALLSE), and material Dissipation energy (ALLVD). Ignore the smaller energy in the energy transformation process, as shown in Fig.3.27a, which can be expressed as total energy ALLKE=ALLPD+ALLSE+ALLFD +ALLVD. Plastic dissipation and frictional dissipation can also be known as bonding energy and strain energy storage called rebound energy [151].

Powder for deposition condition is that the bounce energy is less than the bonding energy, and the ratio of rebound energy and bonding energy is defined as the recovery coefficient. When the recovery coefficient decreases with the increase of the speed in a certain range, the deposited effect is better; when exceeding a certain speed, the recovery coefficient increases, and the speed between the minimum values of the

recovery coefficient is determined as the maximum critical speed. As shown in Fig. 3.27b, rebound energy increases gradually with speed, especially when the speed is 900 m/s…1000 m/s. Although the speed interval is 100 m/s, the rebound energy increases the most, exceeding the increased range of rebound energy between 500 m/s…700 m/s and 700 m/s…900 m/s. Fig. 3.27(c) shows that the increased range of plastic dissipation energy is small in the range of 900 m/s…1000 m/s. Thus, the recovery coefficient is large. As shown in Fig. 3.27d, the recovery coefficient in the range of 500 m/s…900 m/s is small; hence, recommend the critical speed, which is very consistent with Figure 3.27. When the speed is less than 500 m/s or more than 900 m/s, the recovery coefficient increases, indicating that the rebound strength increases and the bond performance is poor.

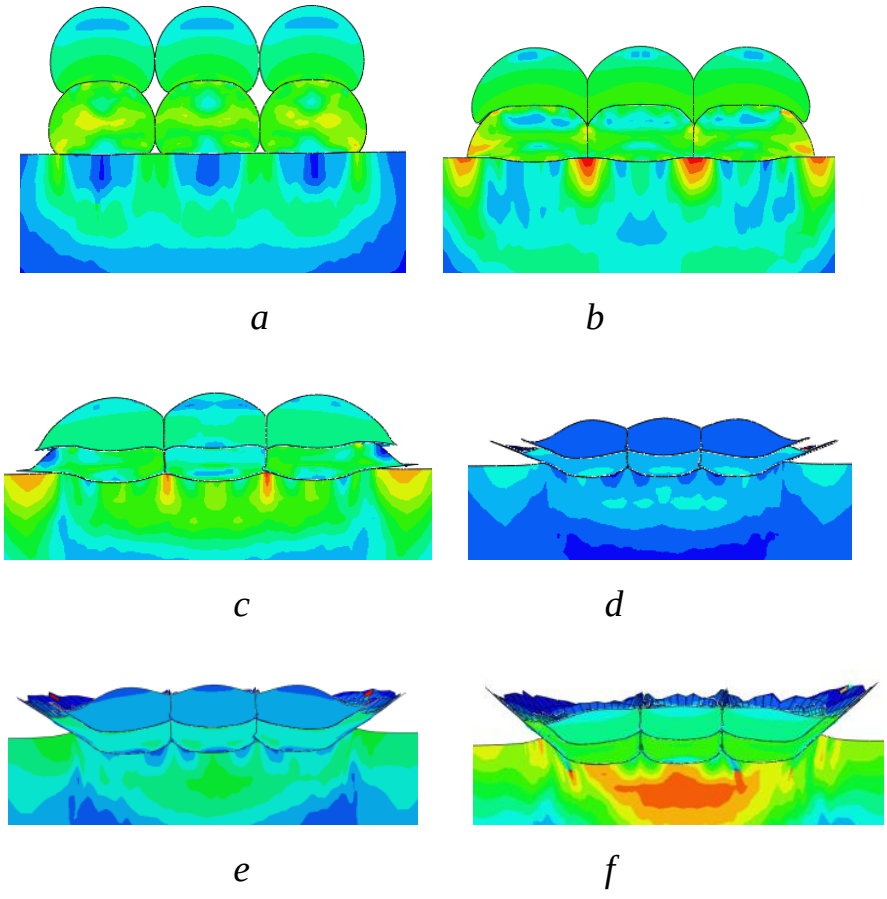

a *b*

c *d*

e *f*

a – 300 m/s; *b* -500 m/s; c – 700 m/s; *d* – 900 m/s; *e* – 1000 m/s; *f* – 1100 m/s

Fig. 3.26. Al+Ti/Ti-6Al-4V

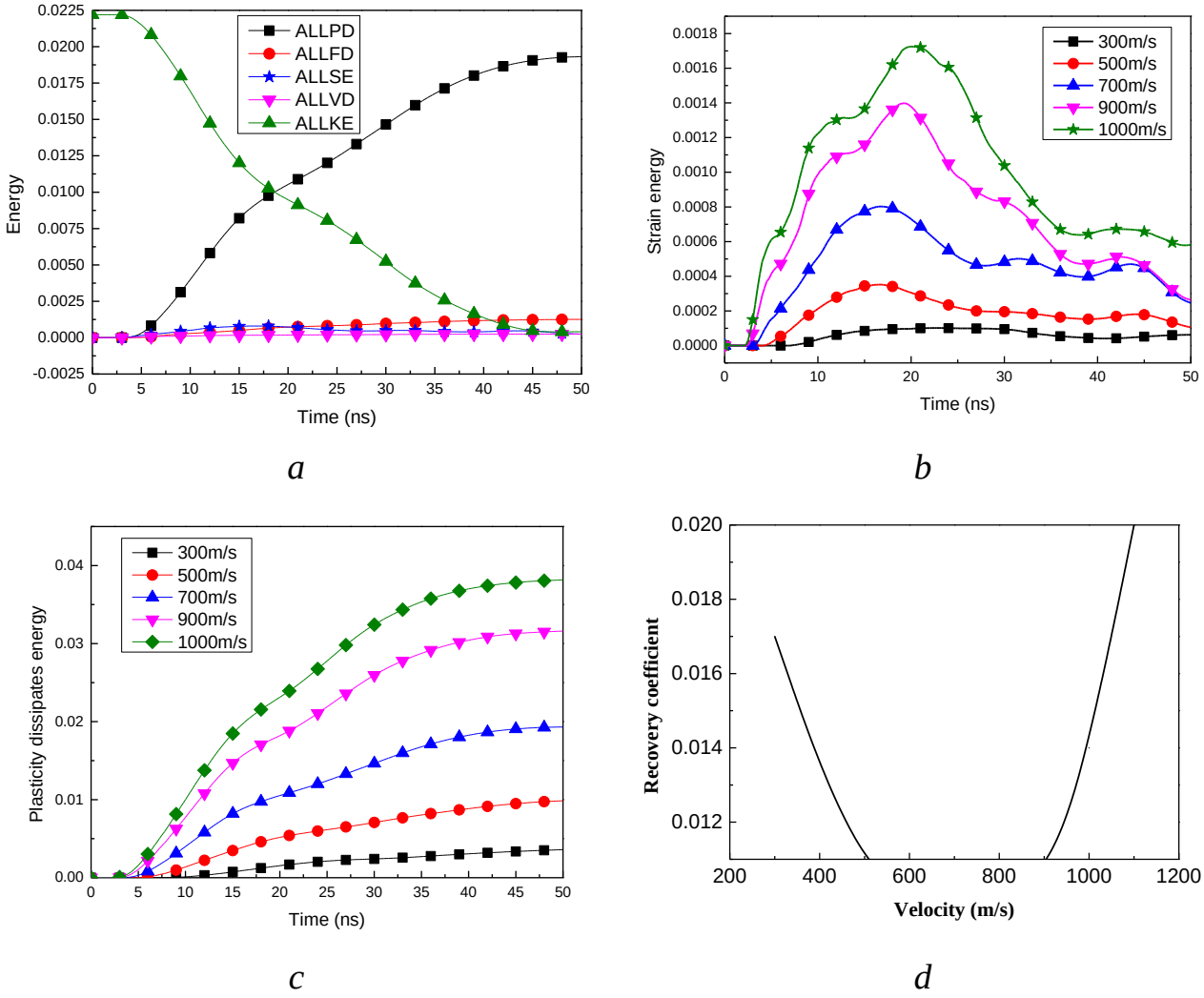

a – ALLPD, ALLKE, ALLFD, ALLSE and ALLVD at 700m/s; *b* – Strain energy; *c* – plasticity dissipates energy; *d* – coefficient of recovery at different speeds

Fig. 3.27. Energy trace

3.7 Conclusion of Chapter 3

1. The critical velocity of cold spraying is related to the Y value; that is, the depth of the foundation pit after powders collide with the substrate at high speed is related to the powder size after deformation. It is feasible to predict the critical velocity by calculating the ratio Y by the SPH method.

2. The impact deposition effect is mainly affected by factors such as material hardness, density, specific heat capacity, thermal conductivity, etc. According to different particle deposition characteristics, for Ti-6Al-4V substrate, it is recommended to use of Ti-6Al-4V, nickel, copper, W alloy and titanium particles as

surface restorative, protective and functional coating materials and pure aluminium particles are not recommended.

3. Compared with the hardness of Ti-6Al-4V matrix, the particles with larger hardness in the collision process lead to deeper foundation pits, for example, at a speed of 600m/s, nickel particles deposit deeper pits than aluminum particles; particles with higher density have larger the initial kinetic energy, the better the deposition effect, for an instant, the density of nickel particles (density is 8.9 g/cm^3) is higher than that of aluminium particles (density is 2.7 g/cm^3), the foundation pit is deeper during the deposition process, hence, the bonding performance is better. Similarly, the foundation pit deposited by tungsten alloy is deeper than nickel, etc.

4. The energy conversion process of collision is mainly kinetic energy (ALLKE) conversion to internal energy (ALLIE), and a small part into frictional dissipation (ALLFD) and viscous dissipation (ALLVD). As the single-particle and multi-particle energy processes of aluminium particles show, the increase of the initial energy does not necessarily lead to better deposition, depending on the physical properties of the substrate and particles.

5. Abaqus/Explicit used to simulate the bonding process of Al+Ti mixed powder deposited onto Ti-6Al-4V is worth recommending. Using the recovery coefficient to evaluate the critical velocity of mixed powder is feasible. This section recommends that 500 m/s…900 m/s as the critical speed.

CHAPTER 4
IMPLEMENTATION RECOMMENDATIONS OF COLD SPRAYING REPAIR TI ALLOY TECHNOLOGICAL, SPECIAL NOZZLE AND OPTIMIZATION METHOD

4.1 The recommendations of the technological process using cold spraying to repair aircraft titanium parts

Titanium alloy is widely used in the field of aerospace, which is a heat-sensitive material. Cold spraying technology has obvious advantages in depositing protective and restorative coatings on its surface [169]. For titanium alloy substrate spraying, this dissertation gives two suggestions:

1. Titanium alloy substrate hardness is high; try to choose high hardness or high-density powder, For example, Ti-6Al-4V, nickel, copper, and tungsten alloy. Titanium alloys are not recommended to be sprayed directly with soft powder with low density, such as pure aluminium powder, because the pure aluminium is directly sprayed on the surface of the titanium alloy, and the coating bonding effect is not good.

2. For soft powder with low density, the intermediate transition coating method can be recommended, such as Ti-6Al-4V substrate, which is sprayed with Ti powder first and then sprayed with aluminum powder to obtain better bonding properties of the coating. This method can also be extended to other high-hardness substrate surface deposition.

4.2 Suggestion about implementation of the theoretical results for the special nozzle

The use conditions of the special cold spray nozzle studied in this work are high-pressure, and the implementation suggestions are divided into the following three points.

4.2.1 Summary factors about the special nozzles design under high pressure

Due to the final goal is to discuss the multi-channel nozzle, this dissertation studied various factors affecting the nozzle outlet velocity under high pressure, including nozzle structure parameters and fluid process parameters (temperature and pressure), indicating that nozzle structure, gas temperature and pressure are the main factors to outlet velocity.

The factors that influence powder impact velocity need to be analyzed, including fluid characteristics, particle material, nozzle structure, spraying distance, etc., indicating that those parameters are vital factors in collision velocity. The response surface method was used to analyze the interaction of various factors, indicating the order of influence is that temperature is greater than powder diameter and powder diameter is greater than gas pressure. Special nozzles were designed, and multi-channel nozzles were further discussed for the different powder injection positions; in addition, it needs to be emphasized that the powder passage inlet in the multi-channel nozzle can be designed to a certain radian to reduce the powder passage pressure. Its advantage lies in convenient operation and can reflect its advantage more in limited space. For application of the special nozzle, Ni, Ti, Cu, Al, Mg and Zn powders can be sprayed at a certain initial gas temperature.

4.2.2 Recommendations about the technological parameters under high pressure

This dissertation discusses the spraying effects of special single-channel nozzles and multi-channel nozzles using Ni, Ti, Cu, Al, Mg and Zn powders, and selects targets with collision velocity much higher than the critical velocity. The results show that the powder process is recommended for using single-channel nozzles. Ti powder is 950 K and above, Cu is 800 K and above, Mg and Al suggested 600 K, Zn powder suggested about 400 K; For the use of multi-channel nozzle powder technological recommendations: Ti powder is 1000 K and above, Cu is 800 K and above, Mg and

Al recommended 600 K, Zn powder recommended about 400 K.

4.2.3 Implementation recommendation of high-pressure cold spraying nozzle for powder injection

At present, the high-pressure powder channel used in engineering applications is higher than the main gas channel pressure to transport particles, resulting in a sharp increase in pressure between the main channel and the powder channel, leading to an unstable pressure state. Therefore, designing a nozzle with a buffer pressure device to smoothly inject particles and stabilize the gas pressure at the nozzle throat and expansion section of the cold spraying device is of great significance.

To achieve the above objectives, it is recommended to adopt the following structure (Fig. 4.1): a piston-type cold spraying device, characterized in that it mainly includes a front chamber, a nozzle expansion section, a main gas path channel, and a secondary gas path channel. The small open end of the front chamber and the small open end of the nozzle expansion section are connected by a throat pipeline. The upper part of the throat pipeline is connected to the auxiliary gas channel, and the lower part of the throat pipeline is connected to the bypass of the main gas channel through a stabilizing pipeline. The main air passage is connected to the front chamber through a structure with holes, and the main particle passage passes through the structure with holes and extends to the front chamber. One end of the pressure stabilizing pipeline near the throat is equipped with a piston, and the other end is fixed with a one-way valve. One end of the piston rod is connected to the piston, and the other end is connected to the ball valve, which is placed below the opening of the one-way valve. Set a pressure-regulating spring between the piston and the one-way valve. Install overflow ports on the side walls of the pressure-stabilizing pipeline near the throat pipeline and the one-way valve.

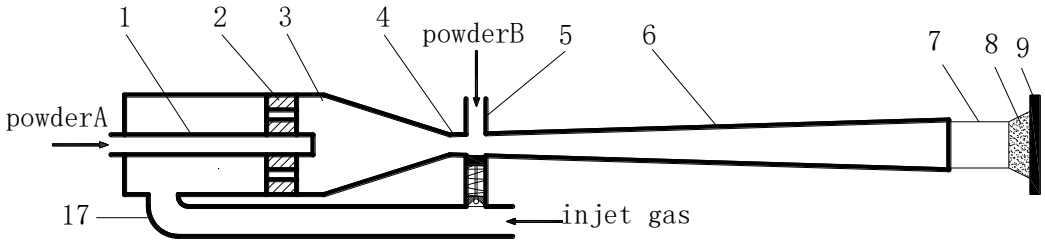

a

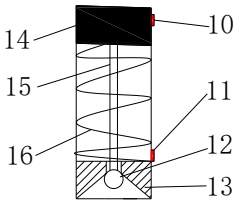

b

a – nozzle structure; *b* – partial enlarged drawing. Here: 1 – main powder channel; 2 – gasket with holes; 3 – front room; 4 – throat channel; 5 – auxiliary gas channel; 6 – Lafar expansion segment; 7 – jet port; 8 – coating; 9 – substrate; 10 – steady pressure; 11 – overflow port; 12 – ball valve; 13 – pneumatic check valve; 14 – piston; 15 – piston rod; 16 – pressure regulating spring; 17 – main gas channel.

Fig.4.1. Structural schematic diagram

The working process is as follows: the main gas channel 17 first takes in gas, and at the same time, particle A enters the front chamber 3 from the main particle channel 1. When gas is injected into the secondary gas path channel 5 with particle B, nozzle expansion, section 6 shows a pressure increase in gas path pressure. At this time, the piston 14 and piston rod 15 move downwards. During the process of piston rod 15 moving downwards, it acts on the ball valve 12 of the one-way valve 13, and some gas in the main gas path passes through the one-way valve 13 and overflows from the overflow port 11 below, relieving the pressure brought by the gas in the secondary gas path channel 5 and having a certain stabilizing effect. When the injection pressure into the secondary air channel 5 is too high and exceeds a certain value, overflow port 10 at piston 14 can also alleviate some of the pressure, playing a stabilizing effect. In this way, the spray port 7 can spray paint particles relatively

smoothly, forming a relatively uniform coating 8 on the substrate 9. When there is no gas injection in the secondary gas channel 5, piston 14 returns to its original position through the pressure regulating spring 16, thereby achieving smooth injection and the cold spraying process.

4.3 Recommended method for CS technical parameter optimization

4.3.1 Response surface method

Response surface analysis method for multiple factor interaction analysis has obvious advantages, because it is based on the principle of the BOX (Figure 2.19), and some single factor comprehensively presented on the basis of the linear rule, to obtain the optimal value, hence, RSM is feasible, this method has been verified in the second chapter of this dissertation, and has high accuracy, therefore, It is not covered in this section.

4.3.2 BP neural network and GA optimization

4.3.2.1 Latin Hypercube Sampling

Latin Hypercube Sampling (LHS) was first proposed by McKay and mathematically formulated by Stein. LHS has been widely used in optimization calculation. Latin hypercube sampling was used to obtain 30 groups of samples in this section. For each group of samples, the corresponding powder impact velocity V was obtained by testing, and the data were recorded in Table 4.5. Twenty-four groups were used for training BP neural network, and the remaining six groups were used for prediction. Temperature (X1), pressure (X2), and particle size (X3) range from 400-600 K, 1-5 MPa, and 10-20μm, respectively. Program with the following formulas (4.1)-(4.3). As the formula 4.1 show, when X_1 is zero, the y_1 takes a minimum value, that is 400, and when X_1 is 1, the y_1 takes a maximum value, that is 600. The y_2 and y_3 work the same way.

Table 4.5 – Latin Hypercube Sampling data about Al powder

	Gas T	Gas P	Powder size	-	Powder V_{impact}
Training Sample (input)	400.5600584	4.780317649	18.1517613	Train-ing Sample (output)	402
	519.9923263	4.642797766	14.11756284		464
	583.5836723	4.381895105	10.81870469		509
	557.1710064	1.940643452	12.42631779		421
	430.2605576	3.37214201	11.15916823		436
	474.8656018	1.03876244	12.66876513		316
	504.5168546	2.835169256	14.59377446		400
	588.101738	2.1840805	15.63140058		399
	423.5242856	1.719026141	14.96343418		349
	579.7615818	1.873314974	19.31213621		369
	552.1608372	2.672169934	15.19847333		424
	481.8549464	1.445074033	19.51720903		285
	436.8434267	3.430628598	16.21139461		395
	498.9818587	2.953304265	19.74549845		373
	511.0591693	3.97839872	11.79070121		479
	415.9507386	4.144512188	17.40933987		373
	538.7216983	3.68774278	13.02238214		460
	441.7438211	1.155611091	16.67575305		290
	491.714336	1.365807868	17.93599055		285
	520.5505044	2.251538568	10.62037527		421
	451.5395894	3.055700111	12.10124455		436
	461.5633332	3.861234755	11.63539332		459
	545.4089202	2.484007862	16.49153187		391
	458.0833455	4.56469613	18.82321859		419
Predict-ing samples (input)	572.7259102	4.290923457	13.37962006	Predict-ing samples (output)	454
	596.1586041	4.984104728	18.50504889		465
	562.1109117	3.141356071	17.20218121		391
	469.6893792	2.380593083	10.10952295		399
	530.4951411	1.602738237	15.75291402		391
	409.0370481	3.581424405	13.82664918		410

$$y_1 = 200 \times X_1 + 400; \quad (4.1)$$

$$y_2 = 4 \times X_2 + 1; \quad (4.2)$$

$$y_3 = 10 \times X_3 + 10. \quad (4.3)$$

4.3.2.2 Back propagation neural network

BP neural network (Back Propagation) was proposed by D. E. Rumellhart and J. L. McClelland in 1986. It is a neural network training algorithm by error Back Propagation. It includes an input layer, hidden layer and output layer. Information spreads forward and backwards between layers through connection weights. The basic principle of the algorithm is the gradient steepest descent method, whose central idea is to adjust the weights and thresholds of the network to minimize the mean square error between the actual output value and the expected output value

Because the three layers of the neural network are of high precision [170], this section defines the gas temperature, gas pressure and particle size for the input, particle collision speed for the output and hidden layer neural network of three layers of the middle, the number of hidden layers was analyzed and tested from 7 to 12 [171], and the results were shown in Figure 4.2. When the number of neurons was 9, the mean square error (MSE) was the smallest。Hence, the three-layer neural network model is shown in Figure 4.3.

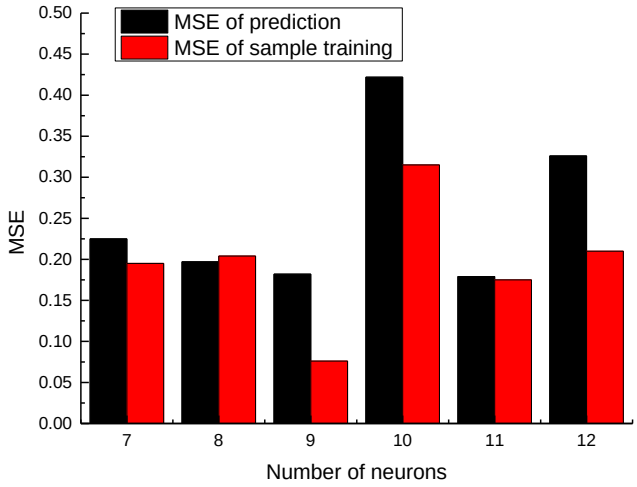

Fig 4.2. Mean square error of different number of neurons

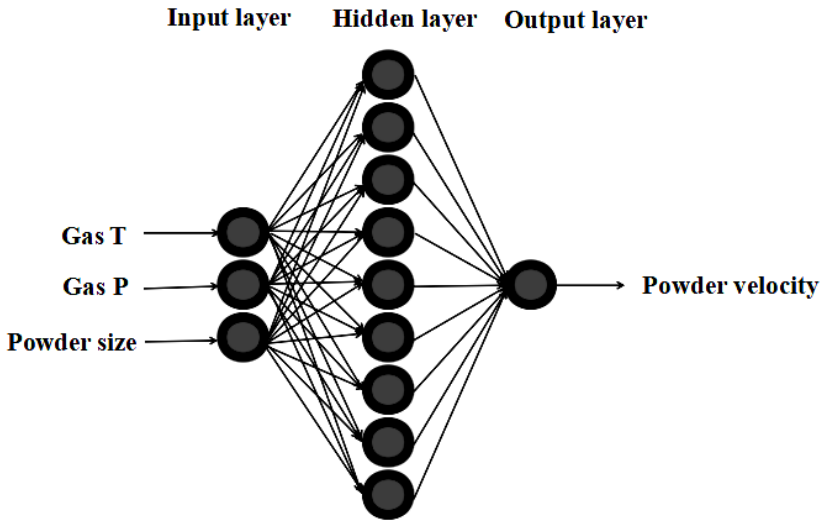

Fig 4.3. Three-layer neural network model

The transfer function of the hyperbolic tangent function, respectively (tensing) and linear function (purely), is the training algorithm of the gradient descent method. Normalized processing is adopted for different units, the data is limited within the range of [-1, 1], and the normalized expression is:

$$y_i = 2 \times \frac{x_i - x_{\min}}{x_{\max} - x_{\min}} - 1, \quad (4.4)$$

where x_i (i = 1, 2, ..., 30) – the training sample;

x_{max} – the maximum value of the training sample;

X_{min} – the minimum values of the training sample;

Y_i – the normalized training sample.

4.3.2.3 Genetic algorithm optimization

A genetic algorithm is, in essence, a kind of evolutionary algorithm that can solve nonlinear function optimization problems better. Therefore, a genetic algorithm is used to optimize the initial weight value and thresholds of the BP neural network to improve the training and prediction accuracy. In addition, it is necessary to determine

individual fitness, which is defined as follows

$$\text{fitness} = \frac{1}{M}\sum_{j=1}^{M}\sum_{i=1}^{q}(Y_i - T_i)^2, \tag{4.5}$$

where M – the number of samples;

Q – the number of nerve in the output layer;

Y_i – the output;

T_i – expected output.

The smaller the fitness value of the individual, the greater the probability of being selected. The crossover mode is actual recombination, and the mutation mode is real value mutation. In this section, the crossover probability is 0.9, the mutation probability is 0.01, the group number is 30, and the maximum iteration number is 200.

The parameters optimized by the Genetic Algorithm were as follows: temperature 600 K, air pressure 4.2 MPa, particle size 10 μm, exit collision velocity 538m/s. The parameters were verified by numerical method, and V = 520 m/s with an error of 3.3 %; in a similar way, by optimizing the value three times, the average error is 4.4 % (Table 4.6).

Table 4.6 – The optimal value using BP+GA method and RSM

Method	T, °C	P, MPa	Powder size	$V_{optimal}$	V_{actual}	Error	Average error
BP+GA	600	4.2	10	538	520	3.3%	4.4%
BP+GA	600	4.4	10	562	531	5.5%	
BP+GA	600	4.3	10	550	525	4.5%	
RSM	600	5	10	543	545	0.4%	-

In summary, a Back propagation neural network and genetic algorithm (BP+GA) are applied in the parameters of cold spraying technology and also have good prediction and optimization ability. It can also be used for other cold spraying nozzles' practical engineering applications by proper adjustment, thus providing an effective optimization method for the optimization and prediction of process parameters.

CONCLUSIONS AND SUGGESTIONS FOR FUTURE WORK

In this dissertation, the main research work and conclusions are as follows:

1. Titanium alloy is a heat-sensitive material, which has poor resistance to abrasive wear for rotating or rubbing aerospace components. Cold spraying technology is suitable for the surface of titanium alloy wear-resistant coating.

2. The theoretical parameters that need to be considered in the structural design process of a cold spraying nozzle are the fluid parameter, nozzle cross-section parameter, mechanical condition of the nozzle, and gas dynamics parameter.

3. The influencing parameters of special nozzle fluid outlet velocity are mainly gas temperature, gas pressure, nozzle throat size, nozzle special Angle, spraying distance, etc.

4. The structural parameters that affect the powder impact velocity of a special single-channel nozzle include the length of the expansion section, throat structure, powder size and powder material, etc.

5. Under the condition of a single factor, temperature, pressure, and particle diameter have significant effects on particle velocity, respectively, and the order of influence is that temperature is greater than powder diameter and powder diameter is greater than gas pressure.

6. Under the interaction of multiple factors, the interaction between temperature and pressure is obvious, while the interaction between temperature and particle diameter, gas pressure and particle diameter are not obvious. The quadratic regression model established in this study can reflect the response value of the outlet velocity well by comparing the optimized parameters after RSM with the actual velocity parameters. With an error of 0.76 %, the response surface quadratic regression model has high accuracy.

7. For the special single-channel cold spraying nozzle. When the length of the inlet cross-sectional area of the propulsion gas is 10 mm, and the width is 3 mm, that is, the cross-sectional area of the inlet is 30 mm^2, the optimal structural parameters are as follows: the length of the divergent section is 12 mm, the spraying distance is 13 mm,

and the fillet radius is 26 mm. At this time, the maximum speed of 10 um aluminum powder can reach 705 m/s.

8. For the special multi-channel cold spraying nozzle with a divergence section of 90°, when the powder injection port is located before the throat, multiple fluid internal channels need to be set in the throat to avoid contact between particles and the inner wall of the divergent section of the nozzle. Parameters influence particle trajectories, such as powder injection pressure, Inlet gas pressure, temperature, particle size, recovery coefficient, etc.

9. Multi-channel cold spraying nozzle with a 90° angle will be more convenient to use, such as some corners, internal areas, etc.

10. The critical velocity of cold spraying is related to the Y value; that is, the depth of the foundation pit after powders collide with the substrate at high speed is related to the powder size after deformation. It is feasible to predict the critical velocity by calculating the ratio Y by the SPH method.

11. The impact deposition effect is mainly affected by factors such as material hardness, density, specific heat capacity, thermal conductivity, etc. According to different particle deposition characteristics, for Ti-6Al-4V substrate, it is recommended to use of Ti-6Al-4V, nickel, copper, W alloy and titanium particles as surface restorative, protective and functional coating materials and pure aluminium particles are not recommended.

12. Compared with the hardness of Ti-6Al-4V matrix, the particles with larger hardness in the collision process lead to deeper foundation pits, for example, at a speed of 600m/s, nickel particles deposit deeper pits than aluminum particles; particles with higher density have larger the initial kinetic energy, the better the deposition effect, for an instant, the density of nickel particles (density is 8.9 g/cm^3) is higher than that of aluminum particles (density is 2.7 g/cm^3), the foundation pit is deeper during the deposition process, hence, the bonding performance is better. Similarly, the foundation pit deposited by tungsten alloy is deeper than nickel, etc.

13. The energy conversion process of collision is mainly kinetic energy (ALLKE) conversion to internal energy (ALLIE), and a small part into frictional dissipation

(ALLFD) and viscous dissipation (ALLVD). As the single-particle and multi-particle energy processes of aluminium particles show, the increase of the initial energy does not necessarily lead to better deposition, depending on the physical properties of the substrate and particles.

14. Abaqus/Explicit used to simulate the bonding process of Al+Ti mixed powder deposited onto Ti-6Al-4V is worth recommending. Using the recovery coefficient to evaluate the critical velocity of mixed powder is feasible. This study recommends 500 m/s…900 m/s as the critical speed.

15. Back propagation neural networks and genetic algorithms (BP+GA) are applied to the parameters of cold spraying technology and have good prediction and optimization ability. It can also be used for other cold spraying nozzles' practical engineering applications by proper adjustment, thus providing an effective optimization method for the optimization and prediction of process parameters

Suggestions for future work

This conducted research work shows that the special nozzle suitable for spraying titanium alloy materials is designed, and some suggestions for surface repair of titanium alloy are put forward. However, the inevitable shortcoming in the research process exists due to the limitation of academic level and time. The following aspects can be further studied in the future:

1. Computer simulation is a good way to solve engineering problems, which saves unnecessary waste of raw materials for practical application. In this dissertation, CFD is used to obtain the optimal geometric parameters of a cold spraying nozzle, which can be processed and manufactured in the future, and the nozzle can be further optimized in combination with practical application factors.

2. Titanium alloy materials are widely used in the aviation field. This dissertation only provides several common metal materials spraying, including soft materials and hard materials, but all of them are metal powder spraying. In the future, non-metal spraying can be further tried to master its combination mechanism, and

suitable plastic models and failure models can be selected to carry out numerical simulation and experimental research. In addition, molecular dynamics simulation can be further used to find out the binding mechanism in the microscopic state. Lastly, there are few studies on the wear resistance characteristics of titanium alloy substrates using cold spray technology. At present, most researchers only focus on Ti-6Al-4V alloy, and further research is needed for other titanium alloys.

3. For multi-variable parameter optimization methods, this thesis introduces the RSM method in detail and BP+GA briefly, both of which are feasible. In the future, relevant workers can further try other multi-parameter optimization methods to compare error values, such as the least square method, etc. In addition, this dissertation provides RSM and genetic algorithms to study cold spray parameters, but only three parameters are selected. Hence, it will be interesting to establish mathematical models for four or more parameters for comprehensive optimization analysis in the future.

REFERENCES

1. Hu, Wenjie, S. Markovych, Kun Tan, O. Shorinov, Tingting Cao. Surface repair of aircraft titanium alloys by cold spray technology. Aerospace technic and technology. 2020, 3:30-42.

2. B. Liu, Y. B. Liu, X. Yang. TITANIUM 2008: the international titanium industry, preparation technology and application development. Powder Metallurgy Materials Science and Engineering. 2009, 2(14): 67–73.

3. Jin, H. X. Research development of titanium alloy in aerospace industry. The Chinese Journal of Nonferrous Metals. 2015, 2(35): 280–292.

4. Wenjie Hu, S. Markovych, Kun Tan, O. Shorinov, Tingting Cao. Research on Wear Resistance Coating of Aircraft Titanium Alloy Parts by Cold Spraying Technology. Aerospace technic and technology. 2020, 6:61-71. DOI: https://doi.org/10.32620/aktt.2020.6.07.

5. Wang, J. S. The corrosion behavior and its effect on fatigue life of TC17 Titanium alloy. Xiamen university. 2017.

6. Zhao, Z. Discussion on preparation technology of titanium coating by thermal spraying. Welding. 2011(6): 16–21.

7. W. Sun, A. W. Y. Tan, I. Marinescu et al. Adhesion, tribological and corrosion properties of cold-sprayed CoCrMo and Ti6Al4V coatings on 6061-T651 Al alloy. Surface and Coatings Technology. 2017(326): 291–298.

8. X. Liu, et al. Influence of α/β interface phase on the tensile properties of laser cladding deposited Ti–6Al–4V titanium alloy. Journal of Materials Science & Technology. 2017(33): 675–681.

9. X. Liu, et al. In-situ synthesized TiN coating by laser nitriding on TC_4 surface. Aviation manufacturing technology. 2018, 61(23): 52–57.

10. Y. M. Li, et al. Investigation on preparation and wear resistance of micro-arc oxidation composite ceramic coating on TC4 titanium alloy. Function Materials. 2015, 9(46): 09128–09132.

11. Wu, Y. Research of composite coating on TC4 titanium alloy surface.

Shenyang Ligong University. 2016.

12. Song, Y. Z. Microstructure analysis of laser melt injection WC/TC_4 composite coating on titanium alloy surface for aircraft flaps. Weld. 2018(11): 44–49.

13. Han, X. J. Research on preparation of Zn-Al alloy coating on the surface of TC4 Alloy and its resistance to titanium/aluminum contact corrosion. Nanjing University of Aeronautics and Astronautics, 2016.

14. B. Li, L. J. Wu, et al. Micro-structure and corrosion-resistant property of Ti6Al4V coating prepared by supersonic laser deposition. China Surface Engineering. 2018, 5(31): 159–166.

15. Liu, M. Property Investigation of Ti Coating Deposited by Supersonic Plasma Spray. Thermal Spray Technology. 2016, 1(8): 5–10.

16. T. Goyal, T. S. Sidhu, R. S. Walia. An overview on cold spray process over competitive technologies for electro-technical applications. Presentation made at The National Conference on Advancements and Futuristic Trends in Mechanical and Materials Engineering, YCoE, Talwandi Sabo. 2013.

17. Hu, F. Y. The wear and corrosion behavior of Ti-matrix functional gradient layer. Function Materials. 2012, 1(43): 36–38.

18. Zhou, H. Effect of Preparation of NiCrAl+YSZ+NiCrAl / Bentonite Flame-retardant Sealing Composite on Titanium Alloy. Thermal spray Technology. 2018, 3(10): 12–16.

19. Y. F. Zhang, et al. Numerical simulation on the erosion behaviour of aero-engine blade substrate with TiN/Ti coating. Surface Technology. 2015, 7(44): 81–85.

20. Cai, J. Q. Study on the micro-cracks in fretting wear of Ti-6Al-4V titanium alloy. Lanzhou university of technology, 2017.

21. Papyrin, A. N. Cold spray technology 2007. – Elsevier, 2017.

22. G. F. Zhao, Y. Y. Wang et al. Zhao. G. F. Application of cold spraying equipment and cold spraying technology. Surface technology. 2017, 11(46): 198-205.

23. E. Irisson, J. G. Legoux, A. N. Ryabinin, B. Jodoin, C. Moreau. Review on cold spraying processes and technology: Part 1 – Intellectual property. Therm. Spray Technol. 2008(17): 495–516.

24. R. N. Raoelison, Y. Xie et al. Cold gas dynamic spray technology: a comprehensive review of processing conditions for various technological developments till to date. Addit. Manuf. 2018(19): 134-159.

25. Singh, H. Cold spraying technology: future of coating deposition processes. Frat. Ed. Integrita Strutt. 2012(22): 69-84.

26. Moridi, A. Cold spraying coating: review of material systems and future perspectives. Surf. Eng. 2014(30): 369–395.

27. Wenya Li, Kang Yang, Shuo Yin, Xiawei Yang, Yaxin Xu, Rocco Lupoi. Solid-state additive manufacturing and repairing by cold spraying: A review, Journal of Materials Science & Technology. 2018, 3(34): 440–457.

28. D. Boruah, B. Robinson, T. London, et al., Experimental evaluation of interfacial adhesion strength of cold sprayed Ti-6Al-4V thick coatings using an adhesive-free test method, Surface & Coatings Technology. 2019, 381, 125-130: 1 – 15. doi: https://doi.org/ 10.1016/j.surfcoat.2019.125130

29. W. Sun, et al., Surf. Coat. Technol. Effect of substrate surface condition on fatigue behavior of cold sprayed Ti6Al4V coatings. 2016, 320:452-457.

30. S. I. Imbriglio, M. Hassani-Gangaraj, D. Veysset, M. Aghasibeig, R. Gauvin, K. A. Nelson, C. A. Schuh, R. R. Chromik. Adhesion strength of titanium particles to alumina substrates: A combined cold spray and LIPIT study, Surface & Coatings Technology. 2019, 361: 403–412.

31. Alessio Silvello, Pasquale Daniele Cavaliere, Vicente Albaladejo, Ana Martos, Sergi Dosta and Irene G. Cano. Powder Properties and Processing Conditions Affecting Cold Spray Deposition, Coatings. 2020, 10(91): 1–9. doi: 10.3390/coatings10020091

32. Libin Lalu Koithara, Rija Nirina Raoelison, Sophie Costil. Flow phenomenon of micron-sized particles during cold spray additive manufacturing:

High-speed optic observation and characterization, Advanced Powder Technology. 2020, 31(3): 1060–1079. doi: https://doi.org/10.1016/j.apt.2019.12.037

33. B. Lu, D. H. Wang, L. Xiao. Microstructure Analysis of Laser Remelting for Thermal Barrier Coatings on the Surface of Titanium Alloy – International symposium on materials applications and engineering. FRANCE: EDP Sciences. 2016.

34. Venkata Naga Vamsi Munagala, Tyler B. Torgerson, Thomas. W. Scharf, and Richard. R. Chromik. High Temperature Friction and Wear Behavior of Cold-Sprayed Ti6Al4V and Ti6Al4V-TiC Composite Coatings. Wear. 2019, 426–427:357–369. doi:10.1016/j.wear.2018.11.032

35. W. Wong, E. Irissou. Influence of helium and nitrogen gases on the properties of cold gas dynamic sprayed pure titanium coatings, in Thermal spray: Global Solutions for Future Applicaton. ASM International: Singapore. 2010.

36. Shvortsova A. N, Tolochko, O. V. The influence of technological parameters of cold gas dynamic spray on wear resistance of aluminum-carbon nanofibers coatings. Inorganic materials: Applied research. 2019, 10(6): 1365–1371. Available at: https://doi.org/10.1134/S2075113319060248.

37. J. Chen, H. Song, et al. Wear and corrosion properties of cold sprayed 420 stainless steel/WC-17Co coating on magnesium alloy. Journal of aeronautical materials. 2018, 38(4): 82–86.

38. S. Kumar, M. Ramakrishna, N. Chavan, S. V. Joshi. Correlation of Splat State with Deposition Characteristics of Cold Sprayed Niobium Coatings. Acta Materialia. 2017, 130: 177–195. DOI: 10.1016/j.actamat.2017.03.023.

39. J. R. Tang, Z. P. Zhao, X. Cui. Microstructure and bioactivity of a cold sprayed rough/porous Ta coating on Ti6Al4V substrate. Sci China Tech. 2020, 63: 1–9.

40. Chen. W. Y, Yu. Y, Cheng. J. Microstructure, Mechanical Properties and Dry Sliding Wear Behavior of Cu-Al2O3-Graphite Solid-Lubricating Coatings Deposited by Low-Pressure Cold Spraying. Journal of thermal spray technology. 2018, 27: 1652–1663. DOI:10.1007/s11666-018-0773-4.

41. Ruben Fernandez-Urrutia. Consolidation of Cermet Coatings by Cold Gas Dynamic Spraying, Ottawa, Canada, 2017.

42. Li, T. F. Development on Cold Spray Apparatus. Thermal Spray Technology. 2011, 3(2): 15–34.

43. Zhang H. B, Shan A. D, Wei L, et al. Research progress on bonding mechanism and process of cooling power spray coating. Material review. 2007, 21(4): 80–83.

44. Klinkov S. V., Kosarev V. F., Rein M. Cold spray deposition: significance of particle impact phenomena. Aerospace Science and Technology, 2005, 9: 582–591.

45. Liu, C. G. The analysis on the particles acceleration performance and deposition mechanism in the cold-gas dynamic spraying processes. University Of South China. 2015.

46. Zhao, M. Effects of particle and substrate property on impact and adhesion process in clod spray by numerical simulation. Chongqing university. 2015.

47. Wu, X. K. Numerical investigation on acceleration of gaseous mixture of nitrogen and helium on particles during cold spraying. Materials engineering. 2010, 8: 12–15.

48. Meng, X. M. Numerical simulation of the effects of the impact velocity on the particle deposition characteristics in cold gas dynamic spraying. Baosteel technology. 2011, 5: 17–22.

49. Han, L. Critical deposition velocity calculations and properties investigations of TC4 cold spray coatings. Surface Technology. 2017, 8(46): 96–101.

50. Bu hengyong, Lu Chen. Critical velocity of cold spraying and its influencing factors, Materials Protection. 2011: 46–49.

51. Marrocco, T. Production of titanium deposits by cold-gas dynamic spray: numerical modeling and experimental characterization. Thermal Spray Technology. 2006, 2(15): 263–272.

52. Schmidt, T. Development of a generalized parameter window for cold

spray deposition. Acta Materialia. 2006, 3(54): 729–742.

53. Wong, W. Effects of Gas Temperature, Gas Pressure and the Particle Characteristics on Cold Sprayed Pure Titanium Coatings, in Thermal Spray 2009: Expanding Thermal Spray Perormance to New Markets and Applications. A. Rezaeian. ASM International : Las Vegas, NV. 2009: 231–236.

54. Wang, H. R. Corrosion behavior of cold sprayed titanium protective coating on 1Cr13 substrate in seawater. Surf. Coatings Technol. 2007(201): 5203–5206.

55. Zahiri, S. H. Elimination of porosity in directly fabricated titanium via cold gas dynamic spraying. J. Mater. Process. Technol. 2009(209): 922–929.

56. Cizek, J. Infuence of plasma and cold spraying deposited Ti Layers on high-cycle fatigue properties of Ti6Al4V substrates. Surf. Coatings Technol. 2013, (217): 23–33.

57. Fukumoto M, Wada H, Tanabe K. et al. Effect of Substrate Temperature on Deposition Behavior of Copper Particles on Substrate Surfaces in the Cold Spray Process. Journal of Thermal Spray Technology. 2007, 16 (5–6): 643–647.

58. Huo S. B, Wang J. J. Analysis of properties and deposition behavior of Cold sprayed Al coatings. Albuquerque, NM, USA，Proceedings of surfacing technology in manufacturing and remanufacturing. 2002.

59. Zhang D, Shipway P H, McCartney D G. The effect of processing variables on deposition characteristics of aluminium by cold gas dynamic spraying. China Surface Engineering, 2008, 21(4):1–7.

60. Pattison J, Celotto S, Khan A, et al. Standoff distance and bow shock phenomena in the cold spray process. Surface ＆ Coatings Technology. 2008, 202: 1443–1454.

61. Ning Xian-Jin, Jang Jae-Hoon, Kim Hyung-Jun. The effects of powder properties on in-flight particle velocity and deposition process during low-pressure cold spray process. Applied Surface Science, 2007. 253: 7449–7455.

62. Jodoin B, Ajdelsztajn L, Sansoucy E, et al. Effect of particle size, morphology, and hardness on cold gas dynamic sprayed aluminum alloy coatings. Surface & Coatings Technology. 2006, 201: 3422–3429.

63. Wang J. J，Wei Z. J，Huo S. B，et al．Bonding mechanism of supersonic cooling power spray coating．Weld. 2005, 9:36–39.

64. Wang J. J，Wang Z. P，Huo S. B，et al．Characteristics analysis of copper coating by supersonic cold spraying. Journal of welding. 2007, 28(4): 77–80.

65. Liu Y. X，Yuan X. G，Huang H. J，et al．Study on cold spraying Quick setting Zn-Al alloy powder on magnesium alloy surface．Special casting and nonferrous alloys. 2006, 26(4): 204–207．

66. Fu W，Chen Q. Y, Ji G. C．Microstructure and properties of cold spraying Copper coating on stainless steel．Material heat treatment technology. 2009, 38(22): 111–112．

67. Lee H., Shin H., Lee S. et al. Effect of gas pressure on Al coatings by cold gas dynamic spray. Materials Letters. 2008, 62: 1579–1581．

68. Ajdelsztajn L, Zu niga A, Jodoin B et al. Cold gas dynamic spraying of a high-temperature Al alloy. Surface & Coatings Technology. 2006, 201: 2109–2116.

69. Li W. Y，Chen L，Yu M，et al．Effect of heat treatment on microstructure and properties of Cold sprayed Fe coatings. China Surface Engineering. 2010 23(2): 90–97.

70. Mei X. Z，Wang L，Ma J. H，et al. Application status and prospect of cold spraying technology．Nonferrous metals. 2006: 77–79．

71. Liu Y. X，Yuan X. G，Lv N et al. Wear behavior of cold sprayed Zn-al alloy coating on magnesium alloy surface [J]. Journal of Shenyang University of Technology.2005，27 (4): 385–388．

72. Li, Q. Structure design and optimization of cold spray gun, Shenyang University of Technology. 2008.

73. Arndt, A., U. Pyritz, H. Schiewe, and R. Ullrich. Method and device for the cold-gas spraying of particles having different solidities and/or ductilities. US Patent 8197895 B2, 12 June. 2012.

74. Hu, W., Tan, K., Markovych, S., Cao, T. Research on structure and technological parameters of multi-channel cold spraying nozzle. Eastern-EuropeanJournal of Enterprise Technologies. 2021, 5 (1 (113)), 6–14.

75. Wu Z. L. Numerical simulation research of the internal flow field cold of the spray gun nozzle and structural optimization, Henan Polytechnic University. 2011.

76. Eric I, Legoux J-G, Anatoly N. R, Bertrand J, and Christian M. Review on Cold Spray Process and Technology: Part I – Intellectual Property. Journal of thermal spraying technology. 2008, 17(4):495–516.

77. Li W. Y., Li C. J. Optimal design of a novel cold spray gun nozzle at a limit space. Journal of thermal spray technology. 2005, 14: 391–396. doi: https://doi.org/10.1361/105996305X59404

78. Canales H., Litvinov A., Sergii. M, Dolmatov A.. Calculation of the critical velocity of low pressure cold sprayed materials," Aircraft design and manufacturing issues. 2014, 3:86–91. doi: http://nbuv.gov.ua/UJRN/Pptvk_2014_3_11

79. Cao Tingting, Wenjie Hu. A piston type cold spray device, 2020. (Chinese patent: CN211756622U).

80. Dolmatov A. I. and Polyviany S. A. Interaction of Solid Particles from a Gas Stream with the Surface of a Flat Nozzle，Metallophysics and Advanced Technologies, 2021, 43(3): 319–328. doi: https://doi.org/10.15407/mfint.43.03.0319

81. Hu W. J, Tan K., Sergii. M., Liu X. L. Study of a Cold Spray Nozzle Throat on Acceleration Characteristics via CFD. Journal of Engineering Sciences, 2021, 8: 19–24. doi: https://doi.org/10.21272/jes.2021.8(1).f3

82. Payrin. Anatolii N. Anatolii N. Payrin. Cold spray technology. Elsevier. 2007: 22.

83. P. Sirvent, M.A. Garrido, S. Lozano-Pérez, et al., Oscillating and unidirectional sliding wear behaviour of cold sprayed Ti-6Al-4V coating on

Ti-6Al-4V substrate, Surface & Coatings Technology. 2019. doi: https://doi.org/10.1016/j.surfcoat.2019.125152

84. D. MacDonald, R. Fernández, F. Delloro and B. Jodoin.Cold spraying of armstrong process titanium powder for additive manufacturing. Thermal Spray Technol. 2017(26): 598–609. DOI: 10.1007/s11666-016-0489-2.

85. Tan. K, Markovych. S, Hu. W. J, Shorinov. O, Wang. Y. R. Review of Manufacturing and Repair of Aircraft and Engine Parts Based on Cold Spraying Technology and Additive Manufacturing Technology. Aerospace technic and technology. 2020, 3(163): 53–70. DOI: https://doi.org/10.32620/aktt.2020.3.06.

86. R. N. Raoelison, Y. Xie, et al. Cold gas dynamic spray technology: a comprehensive review of processing conditions for various technological developments till to date. Addit. Manuf. 2018, (19): 134–159.

87. H. Singh, T. S. Sidhu, S. S. Kalsi. Cold spraying technology: future of coating deposition processes. Frat. Ed. Integrita Strutt. 2012, (22): 69-84.

88. T. F. Li, Wang. K, Wu. J. Development on Cold Spray Apparatus. Thermal Spray Technology. 2011, 3(2): 15-34. DOI：CNKI:SUN:RPTJ.0.2011-02-006.

89. Cai. J. Q. Study on the micro-cracks in fretting wear of Ti-6Al-4V titanium alloy, Lanzhou university of technology. 2017.

90. ZHANG. W. Y. Titanium alloy surface wear-resisting processing engineering research present situation, Total corrosion control. 2017, 2(31): 25–29. DOI: 10.13726/j.cnki.11-2706/tq.2017.02.025.05.

91. Li. Y, Cao. C. C, Yin. S. Solid-state cold spraying of Ti and its alloys: A literature review, Progress in Materials Science. 2020, 110: 1–53. Available at:https://doi.org/10.1016/j.pmatsci.2019.100633

92. N. W. Khun, A. W. Y. Tan, E. Liu. Mechanical and tribological properties of cold-sprayed Ti coatings on Ti-6Al-4V substrates, Journal of thermal spray technology. 2016, 25(4): 715-724.

93. Khun NW, Tan AWY, Sun W, Liu E. Wear and corrosion resistance of thick Ti6Al4V coating deposited on Ti6Al4V substrate via high-pressure cold spray, Therm Spray Techn. 2017, 26(6): 1393–407. DOI: 10.1007/s11666-017-0588-8

94. Ning. X. J. Cold-sprayed Ni-cBN coating and its friction and wear properties, New technology & new technology. 2018, 4: 11–14.

95. H. X. Zhang. A preparation method of wear-resistant insulating coating of titanium alloy, China patent：CN116084972A. 2020.

96. NW. Khun, AWY. Tan, W. Sun, E. Liu. Effects of Nd YAG laser surface treatment on tribological properties of cold sprayed Ti-6Al-4V coatings tested against 100Cr6 steel under dry condition, Tribol Trans. 2019, 3(62): 391–402. Available at: https://doi.org/10.1080/10402004.2018.1563258.

97. Preparation method of high hardness wear-resisting coating on titanium alloy substrate surface / Y. X. Li – China patent: CN108642488A. 2018.

98. Khun N W, Tan A W Y, Bi K J W, Liu E. Effects of working gas on wear and corrosion resistances of cold sprayed Ti6Al4V coatings, Surface Coat Technology. 2016, 302: 1–12. DOI:10.1016/j.surfcoat.2016.05.052.

99. Wang. H. T, Chen. X, Bai. X. B, Ji. G. C. Research on the microstructure and properties of multiple - dimensioned cold sprayed WC - Co cermet coatings, ACTA ARMAMENTARII. 2013, 34(7): 876-882.

100. Wang. H. T, Chen. X, Ji. G. C, Bai. X. B. Study on the microstructure and properties of cold sprayed wc-co coating. materials engineering, materials engineering. 2013. (10): 29–35. DOI: 10.3969/j.issn.1001 4381.2013.10.005.

101. Zhong, L., Wang, Z. Y., Zhang, H. D. Research progress of precipitation mechanism and apparatus of cold spray. Surface technology. 2015, 4(44): 15–22.

102. Lei J. Patent CN109207988A China, Cold spraying powder for surface damage repair of thin walled titanium alloy parts and a method for repair. 2019.

103. Ogawa, K. Repairing of Degraded Hot Section Parts of Gas Turbines by Cold Spraying, Key Engineering Materials. 2010, 417–418: 545–548. DOI: 10.4028/www.scientific.net/KEM.417-418.545.

104. Champagne, V. K. The repair of magnesium rotorcraft components by cold spray, Journal of failure analysis and prevention. 2008, 8(2): 164–175.

105. Pelletier, J. L. Development of Ti-6Al-4V coating onto Ti-6Al-4V substrate using Low Pressure Cold Spray and Pulse Gas Dynamic Spray, University

of Ottawa, Ottawa, Canada. 2013.

106. Dibakor, B. Evaluation of residual stresses induced by cold spraying of Ti-6Al-4V on Ti-6Al-4V substrates, Surface & Coating Technology. 2019, (374): 591–602.

107. Cao, C. C. Influence of substrate hardness and thermal characteristics on microstructure and mechanical properties of cold sprayed TC4 titanium alloy coating, Materials Reports. 2019, 1(33): 277–282.

108. Yin, S. A systematic investigation on the acceleration behavior and deposition mechanism of cold sprayed particles, Dalian University of Technology, 2012.

109. SMITH M F, BROCKMANN J E, DYKHUIZEN R C, et al. Cold Spray Direct Fabrication-high Rate, Solid State, Material Consolidation[J]. Materials Research Society Symposium Proceedings. 1999, 542: 65–76.

110. JAHEDI M, ZAHIRI S, GULIZIA S, et al. Direct Manufacturing of Titanium Parts by Cold Spray. Light Metals Technology, 2009, 618–619: 505–508.

111. PATTISON J, CELOTTO S, MORGAN R, et al. Cold Gas Dynamic Manufacturing: A Non-thermal Approach to Freeform Fabrication[J]. International Journal of Machine Tools and Manufacture. 2007, 47(3-4): 627–634.

112. Wu J, Jin H. Z, Wu M. J, et al. Research progress of cooling power spraying technology. Material review. 2003(1): 59–62.

113.Yifei Wang, Xiaofang Wang. Numerical simulation of jet flow in cold spraying process. Surface technology. 2003, 32(1):28–30.

114. Li, Q. (2008). Structure design and optimization of cold spray gun, Shenyang University of Technology. 2008.

115. Li Wenya, Li Changjiu. (2005). Optimal design of a novel cold spray gun nozzle at a limited space. Journal of thermal spray technology. 2005, 14: 391–396. doi: 10.1361/105996305X59404

116. Wenjie Hu, O. Shorinov. Optimization of Cold Spraying 90° Rectangular Nozzle Technological Parameter via Response Surface Method. Journal of Engineering sciences. 2024, 11(2): F1-F8.

117. Abdulaziz S. Alhulaifi, Gregory A. Buck. (2014). A simplified approach for the determination of critical velocity for cold spray processes. Journal of thermal spray technology. 2014, 23: 1259–1269, doi:10.1007/s11666-014-0128-8.

118. Cao Congcong, Li Wenya, Han Tianpeng et al. (2019). Simulation study on effect of cold spray nozzle material on particle. Journal of netshape forming engineering. 2019, 6: 149–53.

119. Zhang, Y. J, Liang, Y. L, Zhang J. B. (2011). Numerical simulation of particle tracks in the cold gas dynamic spraying process. Baosteel technology. 2011, 5: 12–16. doi: 10.3969/j.issn.1008-0716.2011.05.003

120. Sunday, T. O. and Jen, T. C. A comparative review on cold gas dynamic spraying processes and technologies, Manufacturing Rev, 2019, 25: 1–20, doi: https://doi.org/10.1051/mfreview/2019023

121. Pelletier, J. L. Development of Ti-6Al-4V coating onto Ti-6Al-4V substrate using low pressure cold spray and pulse gas dynamic spray. University of Ottawa. 2013. DOI: http://dx.doi.org/10.20381/ruor-4265

122. V.N.V. Munagala, V. Akinyi, P. Vo, R.R. Chromik, Influence of powder morphology and microstructure on the cold spray and mechanical properties of Ti6Al4V coatings, J. Therm. Spray Technol. 2018, 27: 827–842.

123. Kun T., Wenjie Hu, Oleksandr Shorinov, Yurong W. Muti-parameter coupled optimization of AL6061 coating porosity based on the RSM. Aerospace technic and technology, 2024, 3:59-67.

124. Wenjie Hu, Kun Tan, Sergii Markovych, Tingting Cao. Structural optimization of the special cold spraying nozzle via response surface method. Conference on Integrated Computer Technologies in Mechanical Engineering – Synergetic Engineering (ICTM’2021), Lecture Notes in Networks and Systems. 2022, (367): 110 ‑ 122. Kharkiv, Ukraine. DOI: 10.1007/978-3-030-94259-5_11.

125. Y. J. Zhang, Y. L. Liang, J. B. Zhang. Baosteel technology, 2011, 5:12. doi: 10.3969/j.issn.1008-0716.2011.05.003.

126. H. R. Karami, M. Keyhani, D. Mowla. Journal of Petroleum Science & Engineering, 2016, 138(2): 104.

127. M. Kumar, A. K Jain, M. Ghosh et al. Biotechnology & Bioprocess Engineering. 2012, 17(3):606.

128. Zho, X. L., Zhang, J. S., Wu, X. K.: “Advanced Cold Spray Technology and Application,” China Machinery Industry Press. 2011.

129. Kun Tan, Wenjie Hu, et al. Dimet Laval Nozzle Expansion Section Analysis and Optimization. Journal of Engineering Sciences, 2021, Vol. 8(2): F6-F10.DOI: https://doi.org/10.21272/jes.2021.8(2).f2.

130. Yin, S., Meyer, M., Li, W. Y., Liao, H. L., and Lupoi, R.: “Gas flow, particle acceleration, and heat transfer in cold spray: a review”, Journal of thermal spray technology. 2016, 2, 874–896. https://doi.org/10.1007/s11666-016-0406-8.

131. Zhou, X. H., Wang, Y., Song, D. P., Bai, G., Li, A, Dong, Q.: “Analysis and prediction on thermal conductivity of coal based on Box Behnken design,” Journal of safety science and technology. 2017, 13(9), 109–115.

132. Karthikeyan, J. The Advantages and disadvantages of the cold spray coating process, in the cold spray materials deposition process: fundamentals and applications, Wood head; CRC Press. 2007:62–71.

133. Meyer, M. (2015). An analysis of the particulate flow in cold spray nozzles. Mechanical sciences. 2015, 2(6): 127–136. doi: 10.5194/ms-6-127-2015

134. Cavaliere P, Silvello, A. Mechanical properties of cold sprayed Titanium and Nickel based coatings. Surface Engineering. 2016, 32: 60–67. doi: https://doi.org/10.1179/1743294415Y.0000000080

135. Chen, Y. Q., Zou, Y. L., Chen X., Bai X. B. Morphological, structural and mechanical characterization of cold sprayed hydroxyapatite coating. Surface and Coatings Technology. 2019, 1(357): 910–923.

136. Jochen Tewes. (2013). Advancements in cold Spray. CSAT Summer Meeting. doi: https://docplayer.net/39787940-Advancements-in-cold-spray.html

137. Tan K. Development of supersonic nozzles for cold spraying, National Aerospace University “Kharkiv Aviation Institute”. 2024.

138. Gruicjic, M., Zhao, C. L., Tong, C., DeRosset W. S., Helfritch. Analysis of the impact velocity of powder particles in the cold-gas dynamic-spraying

processes. Mater. Sci. Eng. A, 2004, 368: 222–230.

139. Li, C. J., Li, W. Y., Liao H. L. Examination of the critical velocity for deposition of particles in cold spraying. Journal of Thermal Spray Technology. 2006, 2(15): 212-222. doi: 10.1361/105996306X108093

140. Steenkiste, T.H.V., Smith, J.R., Teets, R.E. Aluminum coatings via kinetic spray with relatively large powder particles. Surf. Coatings Technol. 2002, 154: 237–252.

141. Liu Jian, Meng fanjun, Yin fengliang, Chen yongxiong, Liang Xiubing. Progress in research on bonding interface between thermal sparying coating and substrate. Journal of materials engineering. 2017, 45(1): 101–110.

142. Li G, Zhou Y, Xue F, et al. Cold spraying technology [J]. Heat treatment technology and equipment. 2009, 30(4): 11–14+21.

143. Bu H. Y, Lu C. Research status and development of cold spraying technology. materials engineering. 2010(1): 94–98.

144. DAS S K, PUTRA N, ROETZEL W. Pool Boiling Characteristics of Nano-Fluids. Int J Heat Mass Trans. 2003, 46: 85.

145. LI Chang-jiu, LI Wen-ya, WANG Yu-yue, et al. A Theoretical Model for Prediction of Deposition Efficiency in Cold Spraying. Thin Solid Films. 2005, 489(1-2): 79–85.

146. KROEMMER W. Cold spraying – a potential new application concept, Proceedings of the International Thermal Spraying Conference 2006.Thermal Spraying Professional Committee of China Surface Engineering Association, 2006.

147. Li W. Y, Li C. J. Cold spraying characteristic. China Surface Engineering, 2002(1): 12–16+2.

148. M. Yu, W.-Y. Li, F.F. Wang, and H.L. Liao. Finite Element Simulation of Impacting Behavior of Particles in Cold Spraying by Eulerian Approach, Journal of Thermal Spray Technology, 2012, 21(3–4):745‑752.

149. G. R. Johnson, and W. H. Cook. A Constitutive Model and Data for Metals Subjected to Large Strains, High Strain Rates, and High Temperatures. 7th International Symposium on Ballistics. Hague: [s. n.], 1983, 541–547.

150. X. K. Wu, X. L. Zhou, H. Cui, and J. S. Zhang, Morphology Prediction of Cold sprayed Cu and Al Coatings through Multi-particles Deposition Simulation. Journal of University of Science and Technology Beijing. 2012, 34: 1391–1399. (in Chinese)

151. G. Bae, Y. Xiong, S. Kumar, and C. Lee, General aspects of interface bonding in kinetic sprayed coatings. Acta Mater. 2008, 56: 4858–4868.

152. W.Y. Li, 3-D FEM analysis of impacting behavior of cold sprayed particles. China surface engineering, 2009, 22: 31–37.

153. A. P. Alkhimov, V. F. Kosarev, A. N. Papyrin. A method of cold gas-dynamic deposition. Doklady Akademii Nauk SSSR, 1990, 315(5): 1062–1065.

154. A. P. Alkhimov, V. F. Kosarev, A. N. Papyrin. Gas-dynamic spraying. An experimental study of the spraying process. Journal of Applied Mechanics and Technical Physics. 1998, 39(2): 318–323.

155. J. Tewes, M. Hotter, H. Vogganreiter. Investigation and comparison of particle parameters determined with spraywatch and LDA (laser Doppler anemometry) during the cold gas spraying process, Proceeding of ITSC 2011, Hamburg, Germany, (2011).

156. J. Wu, H, Fang, S. Yoon et al. Measurement of particle velocity and characterization of deposition in aluminum alloy kinetic spraying process. Applied Surface Science. 2005, 252: 1368–137.

157. H. Assadi, F, Gärtner, T, Stoltenhoff et al. Bonding mechanism in cold gas spraying. Acta Materialia. 2003, 51(15): 4379–4394.

158. Moridi A， Hassani-Gangaraj S M， Guagliano M. A hybrid approach to determine critical and erosion velocities in the cold spray process. Applied Surface Science, 2013, 273:617–624.

159. S. Rahmati, A. Ghaei. The Use of Particle/Substrate Material Models in Simulation of Cold-Gas Dynamic- Spray Process. Journal of Thermal Spray Technology. 2014, 23(3): 530–540.

160. A. Manap, O. Nooririnah, H. Misran, et al. Experimental and SPH study of cold spray impact between similar and dissimilar metals. Surface Engineering. 2014, 30(5): 335–341.

161. X. K. Wu, X. L. Zhou, J. G. Wang, J. S. Zhang. Numerical investigation on energy balance and deposition behavior during cold spraying. ACAT METALLURGICA SINICA. 2010, 46(4): 385–389.

162. Y. Yang, Y. Hao, L. Y. Kong et al. Research on Critical Velocity of Particle during Cold Spray Process. Thermal spray technology. 2015, 7(4): 1–16.

163. R. C. Dykhuizen, M. F. Smith. Gas dynamic principles of cold spray. Journal of Thermal Spray Technology. 1998,7(2): 05–212.

164. L. Han et al. Critical deposition velocity calculations and properties investigations of TC4 cold spray coatings. Surface Technology. 2017,46(8): 96–101.

165. T. Schmidt, H. Assadi, F. Gärtner et al. From Particle Acceleration to Impact and Bonding in Cold Spraying. Journal of Thermal Spray Technology. 2009, 18, No. 5/6: 794–808.

166. Wenjie Hu. Effects of different metal particles on cold spray deposition onto Ti-6Al-4V alloy via abaqus/explicit. Journal of Engineering Sciences. 2020, 7:19-25. DOI: 10.21272/jes.2020.7(2).e4.

167. Wenjie Hu, K. Tan, S. Markovych, T. T. Cao. A simple method for determining the critical velocity value of cold spraying via SPH, International Conference on Artificial Intelligence and Advanced Manufacturing (AIAM 2021). Manchester, England, 2021, 23-25 oct. pp. 215-221.

168. Wenjie Hu, K. Tan, S. Markovych, T. T. Cao, X. L. Liu. Research on the adhesive property of Al+Ti mixed powder deposited on Ti6Al4V substrate by CS using Abaqus/Explicit, Metallophysics and Advanced Technologies. 2022, 44(5):613-621.

169. Wenjie Hu, S. Markovych, Kun Tan, O. Shorinov. Deposition of protective and restorative cold spraying coating on aircraft parts made of titanium alloys. 2021 (Topic: The modern problems of engine building, energy and

intellectual mechanics - 2021, The open scientific-practical student conference of the Faculty of Aircraft engines (FAE) in National N.E. Zhukovsky Aerospace University "KhAI")

170. Wenjie Hu, O. Shorinov. Optimization of particle acceleration parameters of special cold spray nozzles via neural network and genetic algorithm. Aerospace technic and technology. 2024,4:64-70. DOI: 10.32620/aktt.2024.4.08

171. Wenjie Hu, K. Tan, O. Shorinov. Study on Multi-parameter of Cold Spraying Technology via RSM and BP+GA Methods. International Conference on Artificial Intelligence and Advanced Manufacturing, Belgium, Brussels, 2023, 272-278.

APPENDIX A

THE KEY STEPS TO THE MIX POWDER MODELING OF ABAQUS

Through ABAQUS analysis, the key steps of the cold spraying deposition process are shown as follows; the time interval is 50 ns (Fig. 1).

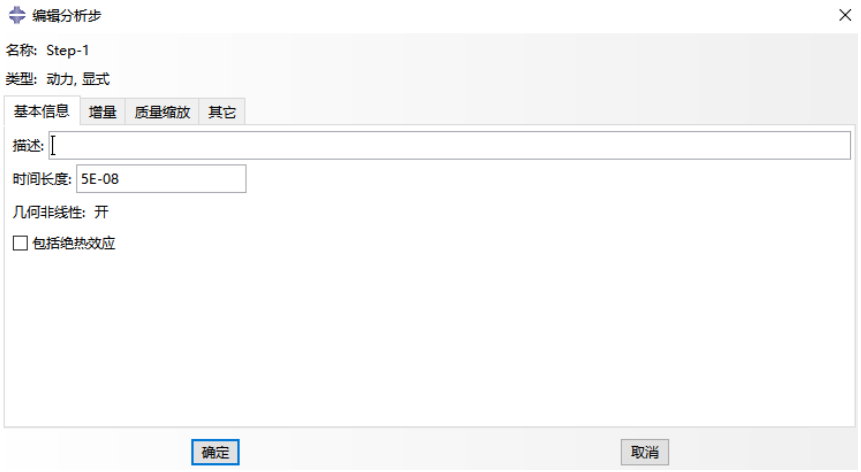

Fig. 1. Analysis step parameters

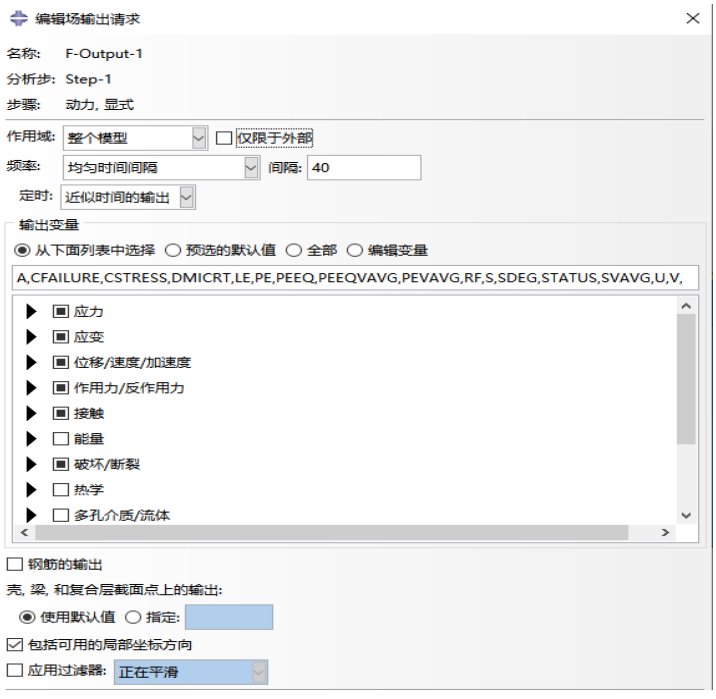

Fig. 2. Field output parameters

Field output takes into account stress, strain, failure and other parameters (Fig. 2). According to the final goal parameter, energy variation is considered, so the path output considers all energy options (Fig. 3)

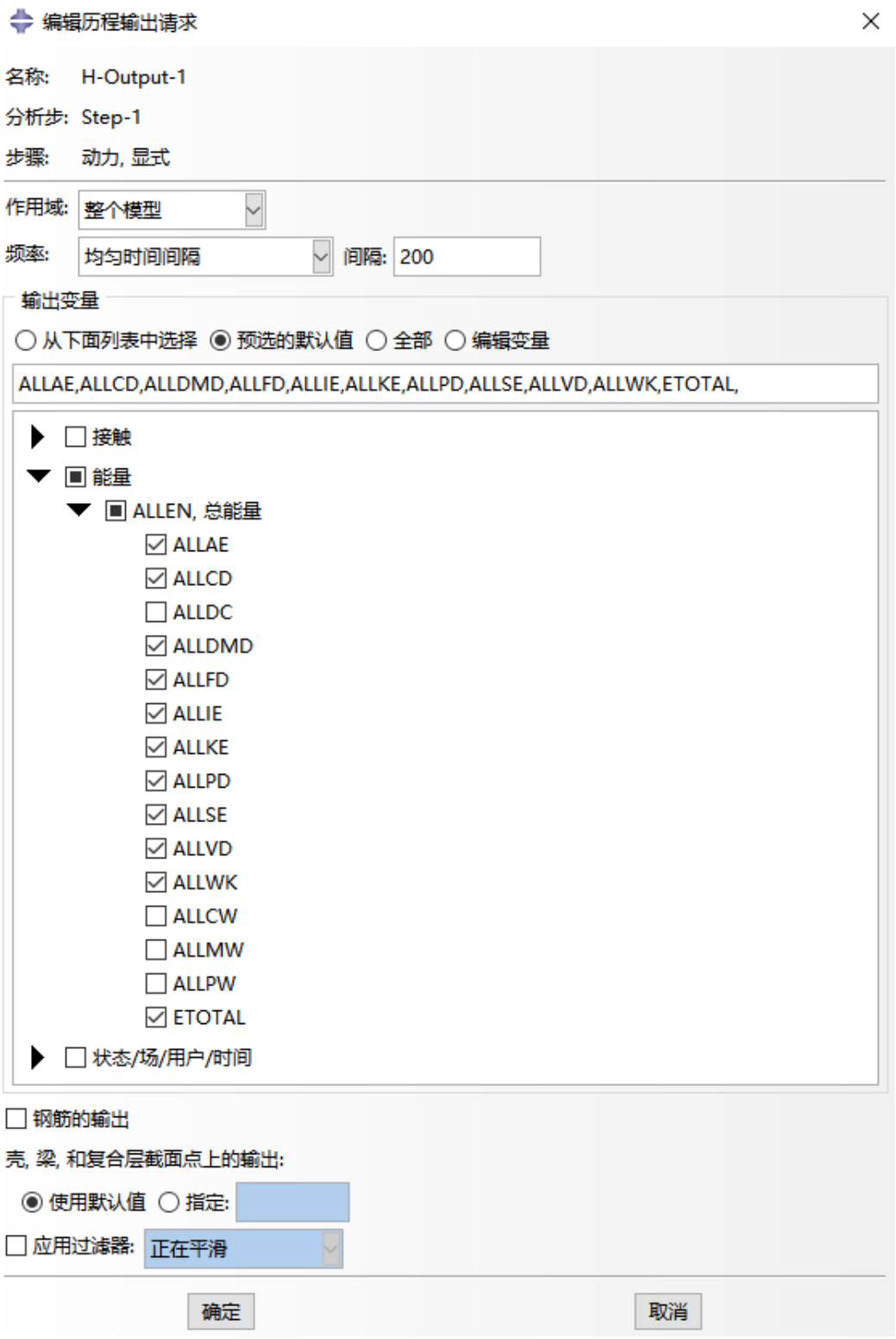

Fig. 3. Process output parameters

After the analysis step is designed, the interaction is also a key step, and both internal and external surfaces of particles must be selected (Fig. 4). In order to save calculation time, the substrate surface in contact with particles is selected as the

contact surface, and the substrate depth is 3 times the particle diameter (as shown in Fig5).

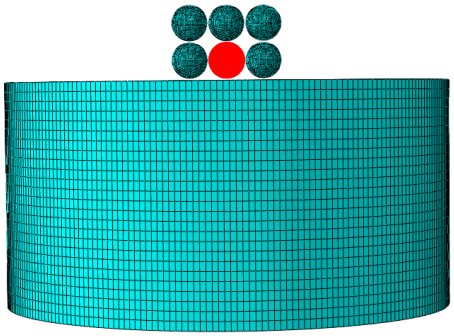

Fig. 4. Particle surface Settings

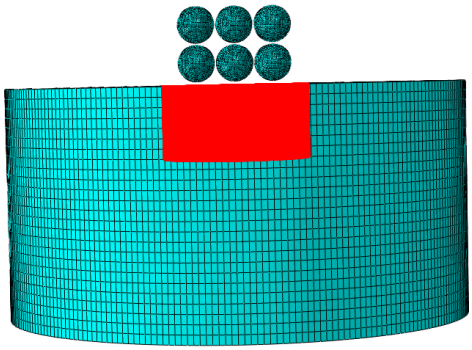

a

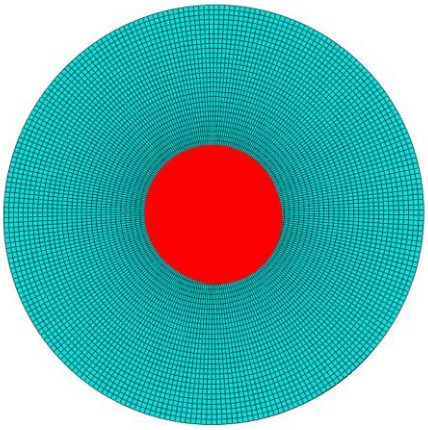

b

a – Front view; *b* – Top view

Fig. 5. Setting of substrate surface

The interaction surfaces that contact with particles are set respectively, as shown in Table 1.

Table 1 – Setting of the interaction surface

The first surface	The second surface
Surface-1	Surface-2
Surface-1	Surface-4
Surface-2	Surface-3
Surface-2	Surface-4
Surface-2	Surface-5
Surface-2	Surface-6
Surface-3	Surface-5
Surface-3	Surface-6
Surface-4	Surface5
Surface-4	Surface-7
Surface-5	Surface-6
Surface-5	Surface-7
Surface-6	Surface-7

The base surface of the matrix is fixed, and the initial velocity of six particles is set respectively.

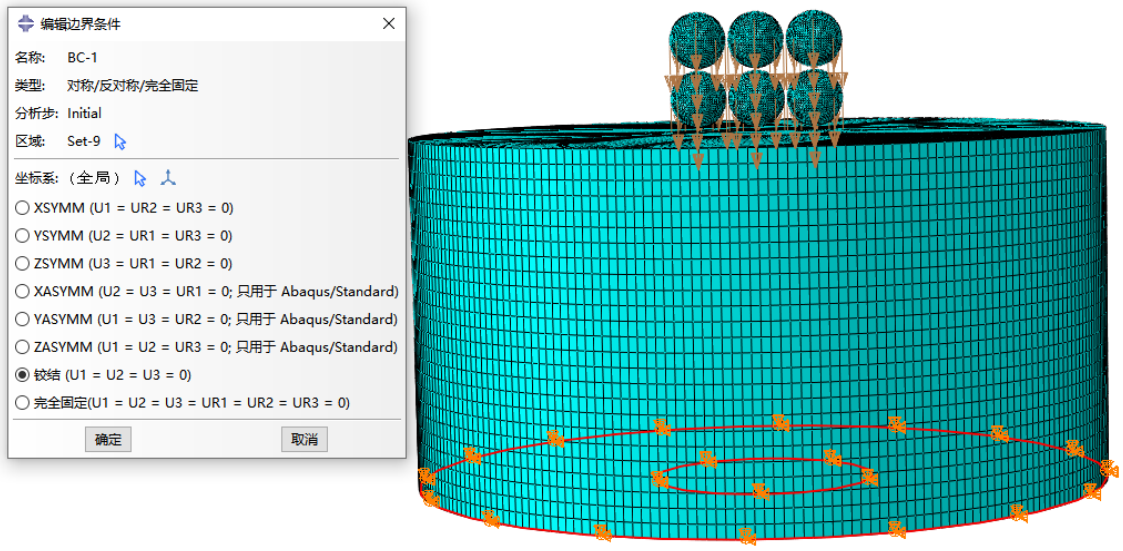

Fig. 6. Fixed setting of matrix

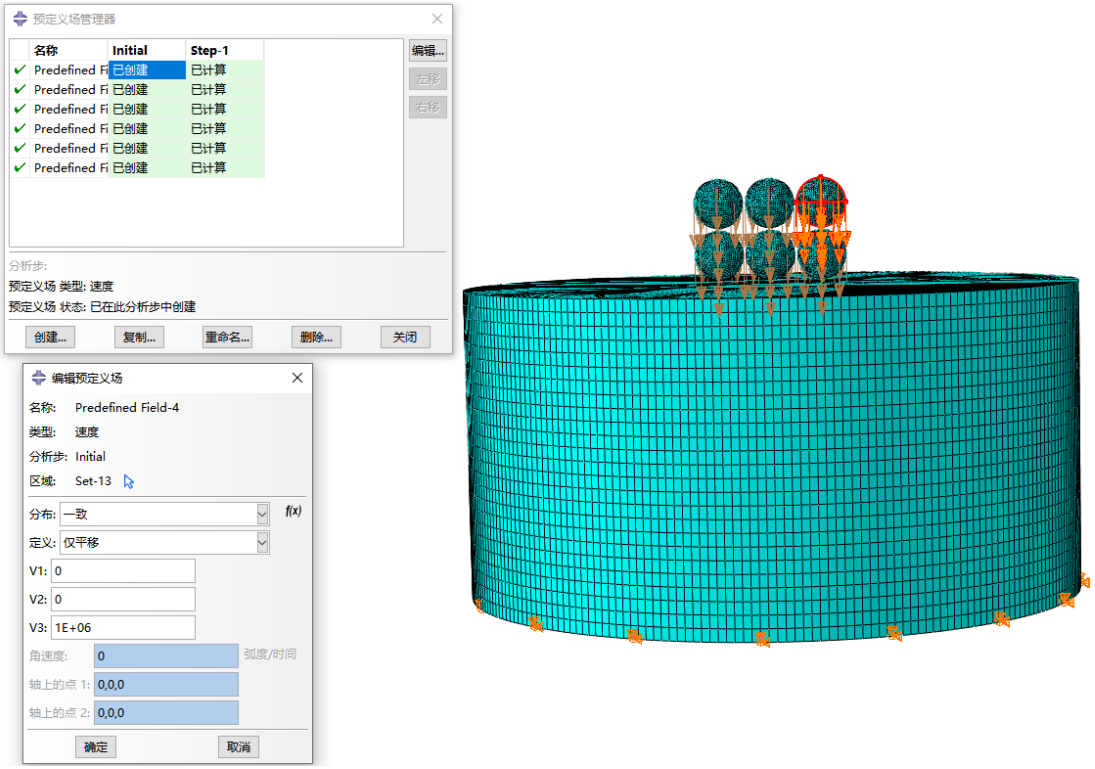

Fig. 7. Speed setting of particles

Select 3d stress for element type option, linear for geometric order, and use C3D8R method (Fig. 8 and Fig. 9)

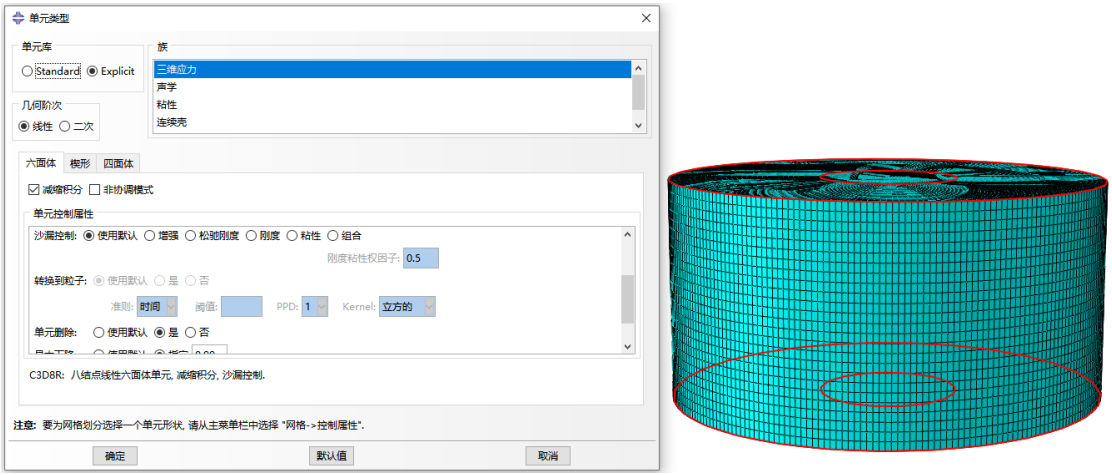

Fig. 8. Element type of substrate

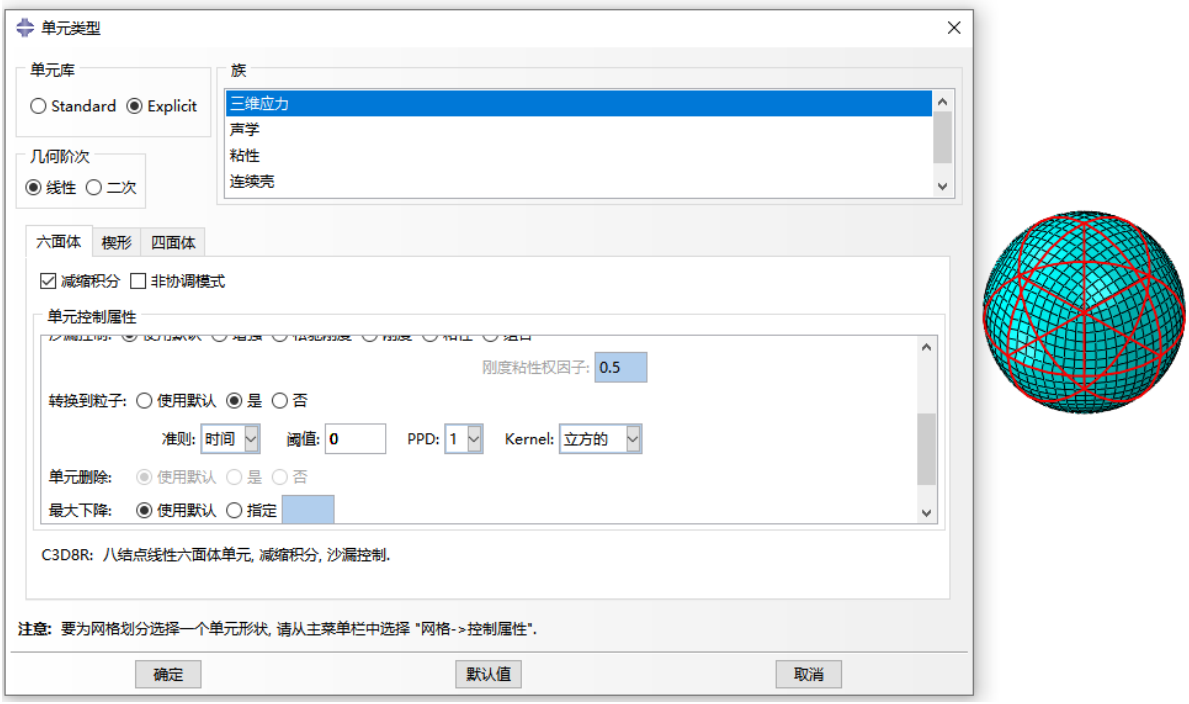

Fig. 9. Unit types of particles

APPENDIX B
LIST OF THE APPLICANT'S PUBLICATIONS ON THE TOPIC OF THE DISSERTATION

Articles in scientific periodical publications included in category «A» of the List of scientific specialized publications of Ukraine, or in foreign publications indexed in the Web of Science Core Collection and/or Scopus databases:

1.**Wenjie Hu,** O. Shorinov. Optimization of Cold Spraying 90° Rectangu lar Nozzle Technological Parameter via Response Surface Method. Journal of Engineering sciences, 2024, 11(2): F1-F8. DOI: https://doi.org/10.21272/jes.2024.11(2).f1. (**Scopus, Q4**)

2. **Wenjie Hu**, K. Tan, S. Markovych, T. T. Cao, X. L. Liu. Research on the adhesive property of Al+Ti mixed powder deposited on Ti-6Al-4V substrate by CS using Abaqus/Explicit, Metallophysics and Advanced Technologies. 202244(5):613-621. DOI: https://doi.org/10.15407/mfint.44.05.0613.(**Scopus, Q3**)

3. **Wenjie Hu**, Kun Tan, Sergii Markovych, Tingting Cao. Study on structure and technological parameters of multi-channel cold spraying nozzle, Eastern-European Journal of Enterprise Technologies,2021, 5 (113), 6-14. DOI: https://doi.org/10.15587/1729-4061.2021.242707. (**Scopus, Q3**)

4. **Wenjie Hu**, Tan K., S. Markovych, Liu X. L. Study of a Cold Spray Nozzle Throat on Acceleration Characteristics via CFD. Journal of Engineering Sciences, 2021, 8: 19-24. DOI: https://doi.org/10.21272/jes.2021.8(1).f3. (**Scopus, Q4**)

5. **Wenjie Hu**. Effects of different metal particles on cold spray deposition onto Ti-6Al-4V alloy via abaqus/explicit. Journal of Engineering Sciences. 2020, 7:19-25. DOI: 10.21272/jes.2020.7(2).e4. (**Scopus, Q4**)

6. Kun T., **Wenjie Hu**., Yurong W. Optimization of cold spray nozzles based on the response surface methodology. Journal of Engineering Sciences, 2024, 11(1), pp. F1–F11. DOI: https://doi.org/10.21272/jes.2024.11(1).f1. (**Scopus, Q4**)

7. Kun Tan, **Wenjie Hu**, et al. Dimet Laval Nozzle Expansion Section Analysis and Optimization. Journal of Engineering Sciences, 2021, Vol. 8(2): F6-F10.DOI: https://doi.org/10.21272/jes.2021.8(2).f2. (**Scopus, Q4**)

Articles in scientific periodical publications included in the List of scientific specialized publications of Ukraine (category «Б»):

8. **Wenjie Hu**, S. Markovych, Kun Tan, O. Shorinov, Tingting Cao. Research on Wear Resistance Coating of Aircraft Titanium Alloy Parts by Cold Spraying Technology. Aerospace technic and technology. 2020, 6:61-71. DOI: https://doi.org/10.32620/aktt.2020.6.07.

9. **Wenjie Hu,** S. Markovych, Kun Tan, O. Shorinov, Tingting Cao. Surface repair of aircraft titanium alloys by cold spray technology. Aerospace technic and technology. 2020, 3:30-42. DOI:https://doi.org/10.32620/aktt.2020.3.04.

10. **Wenjie Hu**, O. Shorinov. Optimization of particle acceleration parameters of special cold spray nozzles via neural network and genetic algorithm. Aerospace technic and technology. 2024,4:64-70. DOI: 10.32620/aktt.2024.4.08

11. Kun Tan, S. Markovych, **Wenjie Hu**, O. Shorinov, Yurong Wang. Review of manufacturing and repair aircraft and engine parts based on cold spraying technology and additive manufacturing technology. Aerospace technic and technology, 2020, 3:53-70. DOI: https://doi.org/10.32620/aktt.2020.3.06.

12. Kun Tan, S. Markovych, **Wenjie Hu**, O. Shorinov, Yurong Wang. Review of application and research based on cold spray coating materials. Aerospace technic and technology, 2021, 1:47-59. DOI: 10.32620/aktt.2021.1.05.

13. Kun T., **Wenjie Hu**, Oleksandr Shorinov, Yurong W. Muti-paramete coupled optimization of AL6061 coating porosity based on the RSM. Aerosp ace technic and technology, 2024, 3:59-67. DOI: https://doi.org/10.32620/aktt.2 024.3.05.

Scientific works are certified for the approbation of dissertation materials:

14. **Wenjie Hu**, K. Tan, O. Shorinov. Study on Multi-parameter of Cold Spraying Technology via RSM and BP+GA Methods. International Conference on

Artificial Intelligence and Advanced Manufacturing, Belgium, Brussels, 2023, pp. 272-278. DOI: https://doi.org/10.1049/icp.2023.2950. (**EI, Scopus**)

15. **Wenjie Hu**, Kun Tan, Sergii Markovych, Tingting Cao. Structural optimization of the special cold spraying nozzle via response surface method. Conference on Integrated Computer Technologies in Mechanical Engineering – Synergetic Engineering (ICTM'2021), Lecture Notes in Networks and Systems, vol. 367, pp. 110 – 122, 2022, Kharkiv, Ukraine. DOI: https://doi.org /10.1007/978-3-030-94259-5_11. (**Scopus**)

16. **Wenjie Hu**, K. Tan, S. Markovych, T. T. Cao. A simple method for determining the critical velocity value of cold spraying via SPH, International Conference on Artificial Intelligence and Advanced Manufacturing (AIAM 2021). Manchester, England, 2021, 23-25 oct. pp. 215-221. DOI: https://doi.org/10.1109/AIAM54119.2021.00052.(**Scopus, Engineering Index**)

17. Kun Tan, S. Markovych, **Wenjie Hu**, Yun Wang, O. Shorinov and Yurong Wang. On the Characteristics of Cold Spray Technology and Its Application in Aerospace Industries, IOP Conference Series: Earth and Environmental Science, 2021,719(3), p. 032023. DOI: https://doi.org/10.1088/1755-1315/719/3/032023. (**Scopus**)

18. **Wenjie Hu**, S. Markovych, Kun Tan, O. Shorinov. Deposition of protective and restorative cold spraying coating on aircraft parts made of titanium alloys. 2021 (Topic: The modern problems of engine building, energy and intellectual mechanics - 2021, The open scientific-practical student conference of the Faculty of Aircraft engines (FAE) in National N.E. Zhukovsky Aerospace University "KhAI") https://drive.google.com/file/d/1trS11rljWf1ylXnAkefWSohV8rkH5p28/view

Scientific works that additionally represent the scientific results of the dissertation:

19. Cao Tingting, **Wenjie Hu**. A piston type cold spray device, 2020. (Chinese patent: CN211756622U).
https://xueshu.baidu.com/usercenter/paper/show?paperid=1v0b06y0kv5g06c0e20a0200uy018632&site=xueshu_se